Analysis and numerics for a thermomechanical phase transition model in steel

vorgelegt von
Diplom-Mathematikerin
Daniela Stefanie Kern
aus Wuppertal

Von der Fakultät II – Mathematik und Naturwissenschaften
der Technischen Universität Berlin
zur Erlangung des akademischen Grades
Doktor der Naturwissenschaften
Dr. rer. nat.

genehmigte Dissertation

Promotionsausschuss:

Vorsitzender:	Prof. Dr. Martin Skutella
Betreuer / Gutachter:	Prof. Dr. Dietmar Hömberg
Gutachter:	Prof. Dr. Alfred Schmidt (Universität Bremen)

Tag der wissenschaftlichen Aussprache:
26. Mai 2011

Berlin, 2011

D83

Eidesstattliche Versicherung

Hiermit versichere ich an Eides statt, dass die vorliegende Dissertationsschrift mit dem Titel *Analysis and numerics for a thermomechanical phase transition model in steel* von mir selbständig und ohne Verwendung anderer als der angegebenen Hilfsmittel angefertigt wurde. Ferner versichere ich, dass alle Stellen, die im Wortlaut oder dem Sinn nach aus wissenschaftlichen Publikationen oder anderen Quellen entnommen sind, von mir als solche kenntlich gemacht wurden.

Datum	Unterschrift

Abstract

This thesis is concerned with the thermomechanical modeling and numerical treatment of metallurgical phase transitions in steel during quenching.

Based on the fundamental principles of thermodynamics, a coupled model consisting of partial and ordinary differential equations is derived. The constitutive equations are adapted to the focus of interest which is deformation induced by phase transitions considered on the macroscale. For the modeling of phase transitions a mixture approach is chosen leading to a system of ordinary differential equations. The deformation caused by phase transitions is included into the model by different expansion coefficients of the respective steel phases and an integral term accumulating deviatoric stresses during transformation, which accounts for transformation induced plasticity (trip).

Existence and uniqueness results are obtained utilizing fixed point arguments applied for a series of subproblems until finally the complete original equation system is solved. The fixed point iterations take place in an L^p-setting, $p > 4$, to achieve the self-mapping property of the operator by embedding theorems.

With respect to the numerical treatment, a scheme for a reduced model, which still captures major effects and includes transformation induced plasticity, is set up. The implementation is done within the finite element framework provided by the toolbox WIAS-pdelib. The single equations are solved sequentially for each time discretization point, the time stepping is carried out by a semi-implicit approach.

The resulting code is applied to an experimental setup investigated within the collaborative research center SFB 570 *Distortion Engineering* in Bremen. The effect of inhomogenous quenching strategies on the so-called "out-of-roundness" of roller bearing rings is investigated and the outcome of the numerical computations is compared to experimental observations. Motivated by the correspondence of locally varying heat transfer coefficients and shape alteration of the workpiece, a strategy for distortion compensation by means of a gradient method obtained from optimal control theory is introduced.

Zusammenfassung

Das Thema dieser Arbeit ist die thermomechanische Modellierung und numerische Behandlung von metallurgischen Phasenumwandlungen in Stahl beim Abkühlen.

Auf Grundlage der Hauptsätze der Thermodynamik wird ein gekoppeltes Modell aus partiellen und gewöhnlichen Differentialgleichungen hergeleitet. Die Materialgleichungen werden mit Hinblick auf makroskopische Verformungen, die von Phasenübergängen rühren, formuliert. Für die Modellierung der Phasenübergänge wird ein Mischungsansatz gewählt, der zu einem System von gewöhnlichen Differentialgleichungen führt. Die Berücksichtigung der transformationsbedingten Verformungen geschieht durch verschiedene Ausdehnungskoeffizienten der jeweiligen Phasen und durch einen Integralterm, der während Phasenübergängen auftretende Scherspannungen akkumuliert. Dadurch wird umwandlungsbedingter Plastizität (*up* oder Englisch *trip*) Rechnung getragen.

Durch Verwendung von Fixpunktargumenten wird Existenz und Eindeutigkeit für eine Reihe von ansteigend komplexen Teilproblemen gezeigt bis schließlich die Lösbarkeit des ursprünglichen Systems resultiert. Die Fixpunktiterationen werden in Unterräumen von L^p, $p > 4$, betrachtet, um die Selbstabbildungseigenschaft durch Einbettungssätze gewährleisten zu können.

Für die numerischen Berechnungen wird ein iteratives Schema zu einem reduzierten Modell aufgestellt und mit Hilfe der Finite-Elemente-Werkzeuge des Softwarepakets WIAS-*pdelib* implementiert. Simulationen zu einem Experiment des Bremer Sonderforschungsbereichs SFB 570 *Distortion Engineering* zur "Unrundheit" bei Kugellagerringen zeigen die Korrespondenz von lokal variierenden Wärmeübergangskoeffizienten und Formveränderungen des Werkstücks. Motiviert durch diese Ergebnisse wird eine Strategie für die Verzugskompensation im Sinne eines Abstiegsverfahrens mit Mitteln der Theorie optimaler Steuerprozesse entworfen.

Acknowledgments

The research presented in thesis was supported by the outstanding research conditions given at the Weierstrass Institute for Applied Analysis and Stochastics, at the DFG research center MATHEON, and by the research environment for applied mathematics in Berlin as a whole.

My gratitude belongs to numerous colleagues who helped and motivated me completing this work. I am indebted to Prof. Dr. Dietmar Hömberg who supervised this thesis and taught me on mathematical techniques for coupled partial differential equations. Apart from sharing his mathematical expertise, he encouraged the attendance at international conferences and collaborations with different experts in the field of steel treatments and gave me the opportunity to fully participate in scientific life. Cordial thanks go to Prof. Dr. Alfred Schmidt, who did not hesitate to be a referee for this thesis. I enjoyed the stays at the ZeTeM in Bremen very much and received valuable hints from him and various colleagues, in particular Dr. Michael Wolff, Dr. Bettina Suhr, and Sören Boettcher. Moreover, I am grateful to Dr. Thomas Lübben and Dr. Friedhelm Frerichs from IWT Bremen for explanations regarding experimental setups, the supply with material data, and interesting discussions regarding engineering aspects of steel treatments. Further, I am obliged to Prof. Dr. Krzysztof Chełmiński from the Technical University of Warsaw for his good ideas on solving thermomechanical systems for phase transitions.

I am particularly indebted to my colleagues at WIAS who were always available for discussions. I thank Dr. Wolf Weiss and Oliver Rott, who introduced me into the world of thermomechanics and its simulation, for their interest and their valuable thoughts; Prof. Dr. Christian Meyer for sharing his broad mathematical knowledge of existence and regularity theory, numerical treatment and optimal control of PDEs, and the willingness and time to give concise and comprehensible explanations; Timo Streckenbach for providing his expertise regarding pdelib, his practical help, and his valuable remarks; Dr. Dorothee Knees and Dr. Johannes Elschner for their hints on elasticity theory. Furthermore, I like to express my sincere gratitude to Thomas Arnold, Anke Giese, Dr. Guanghui Hu, Norbert Kleemann, Dr. Chantal Landry, Dr. Lucia Panizzi, Thomas Petzold, Dr. Andreas Steinbrecher, Nataliya Togobytska, and all the other friendly fish in the pond for their help, fruitful discussions, and the pleasant time.

Finally, my thanks belong to Heinz-Josef Kurschilgen and Thomas Brücher, who encouraged me to learn and study, to my father Bernhard Kern for his trust, and to my mother Ulrike Kern for the freedom and continuous support of my aims.

Contents

Chapter 1

Introduction

[...] or arm th' obdurèd breast with stubborn patience as with triple steel.
John Milton, Paradise Lost

Discoveries of daggers in Anatolia and Mesopotamia (today Turkey and Iraq) provide us with information about the early use of iron, in particular for the production of weapons. One can deduce that the processing of iron dates back at least to 4000 B.C., where the material stemmed probably from meteorite impacts as the high nickel concentration of about 10 percent suggests. Other findings in Egypt indicate that the winning of iron from its ore was already known before 2000 B.C., followed by the Early Iron Age when iron gained from ore was utilized to great extent.

Asia also has a long history of iron and steel production. For instance, Asian (in particular Japanese) swords are legendary. While early swords were straight and had double edged blades, later the typical bent shape (e.g. Katanas) evolved and the swords became something like cult objects, in particular during the martial Kamakura period (1185-1333 A.D.), and were traditionally worn by samurai from the 15th century onwards. The popularity of these swords lies in their extreme hardness which is the result of a hardening process. Hardness comes with the disadvantage of an increased brittleness, therefore not both blade edges are hardened but only one, leaving the blade core and the other side resilient to avoid the risk of breaking. This differential hardening evokes (or at least supports) the typical bent shape as the hard zone possesses a larger volume. This is an early example of a heat treatment as considered in this thesis.

In the European Middle Ages, mining became ever more important and metal refining and processing, e.g. by building larger bloomeries and improving cementation techniques, advanced with giant leaps. Finally, in the course of Industrialization

steel was a major driving force of innovation as it enabled the building of large production machinery and transportation devices. Also nowadays, steel has not lost its vital importance to society. Despite the fact that ever new materials are being developped, the toughness, the good recycability, and the excellent processing properties of steel let it remain one of the most commonly used construction materials. For instance, the mainstay of mass-produced automobile is still steel.

The great importance of steel to production processes makes it desirable to understand the physics of steel as well as possible.

1.1 Subject of this thesis

This dissertation thesis came into being during the author's occupation in research group *Nonlinear Optimization and Inverse Problems* at the *Weierstrass Institute for Applied Analysis and Stochastics*, *Leibniz Institute in Forschungsverbund Berlin e.V.*, located in Berlin, Germany. The presented results were obtained by research carried out within project *C11 – Modeling and optimization of phase transitions in steel* supported by the DFG research center MATHEON – *Mathematics for key technologies*. The work benefitted from the circumstance that both institutions, WIAS and MATHEON, provide excellent opportunities for interdisciplinary research. Accordingly, this application-driven thesis combines mathematical analysis with numerical treatment of a hands-on practical task from engineering. The work is motivated by a problem that is investigated within the collaborative research center SFB 570 *Distortion Engineering* in Bremen, Germany. Among the institutions contributing to SFB 570 is the *IWT – Institute for Materials Science* which provides outstanding expertise in the field of metalworking. In SFB 570 the reasons for distortion of steel components during heat treatment are explored. It has the aim of optimizing the manufacturing process as a whole under a system-oriented view. Their investigations bear most valuable insights which helped a great deal in understanding effects caused by inhomogenous quenching procedures.

In this thesis, phase transitions in steel and their effect on workpiece deformation are investigated. In particular, the ultimate goal is the derivation of systematic inhomogenous quenching strategies to obtain desired deformation profiles. For this purpose a thermomechanical model is derived based on the fundamental laws of thermodynamics. Based on the process in mind, i.e., quenching applied to steel workpieces in the range of millimetres to centimetres, phenomenological equations which suit experimental observations supplement the model. The obtained model contains a number of non-standard terms and is challenging with respect to mathematical analysis. Existence of a unique solution for the full coupled system is achieved by

means of fixed point argumentation. Regarding numerical computations, a finite element code is implemented which can be applied to 2D or 3D settings. It reproduces the experimentally observed behaviour of roller bearing rings during quenching well. Furthermore, it allows for flexible variation of parameters and equation parts, and thereby for an extensive investigation of the model behaviour. For a concerted determination of optimal parameters for desired deformations, an optimization algorithm is set up. To this end, in addition to the code for the state system, one for a complex system of adjoint equations is implemented as well. First results are encouraging and motivate future work.

Also a group of mathematicians at the university of Bremen, among them M. Wolff, M. Böhm, and A. Schmidt, investigates phase transitions in steel and heat treatment applications from a mathematical point of view. They are well connected to the SFB 570 and possess expert knowledge which has refined in many years of dedicated work. A recent outcome is the dissertation [77] by Bettina Suhr supervised by Alfred Schmidt, which focusses on the simulation of classical plasticity and transformation induced plasticity. In this work numerical methods are developped and different models are compared. In particular, different types of plastic effects including classical plasticity are included into the investigations.

In comparison, the focus of interest in the thesis at hand is shifted. Regarding plasticity, only transformation induced plasticity is included but both, mathematical analysis and numerical treatment, play an important role. Further emphasis lies on an optimal control problem to compensate distortion by means of inhomogenous quenching.

1.2 Outline

In the beginning of chapter 2 well-known distinctive properties of steel are introduced and explained, among them the notion of metallurgical phases. In further course, a thermomechanical model including phase transitions is derived based on the fundamental principles of thermodynamics manifested in the Clausius-Duhem inequality.

The resulting challenging system of partial and ordinary differential equations is analyzed in the course of of chapter 3. Finally, different specifications of boundary terms are compared and checked with respect to representing the physical reality and being mathematically manageable.

In chapter 4 the method for the numerical solution of the model equations is explained. The single state quantities are sequentially updated by their time increment, where a a (linear) finite element scheme is set up for the computation of the

increment of the heat and of the mechanical quantities. Considerations about a reduction of the computations to 2D systems and about the exploitation of symmetries is given at the end of the chapter.

In chapter 5 an application from the collaborative research center SFB 570, the processing of roller bearing rings crafted from steel 100Cr6, is described. Numerous experimental data exists for this steel, in particular there has been done a lot of research regarding distortion. This well-established experimental basis gives reason to compare own numerical results to the observed phenomena. In the end, an optimal control problem is formulated for this application to provide controlling parameters which could be used to improve the steel processing in the future.

In the appendix at the end of this thesis, an overview on the notation and utilized theorems are given.

Remarks on the notation throughout this thesis

Variables c with or without index usually denote generic constants. This is the case especially for inequality chains. They do not give a single fixed constant value but have to be regarded as a new variable for each occurence.

Additional to subscripts, also superscript variables and superscript natural numbers usually denote indices and determine the considered component. Superscript 2 and e.g. p, q could also denote squaring or taking the respective power, but this will be clear from the context.

Chapter 2

Modeling

2.1 Basics about steel

Iron itself is a rather soft material, e.g., one can bend a nail easily just by hitting it with a hammer in an improper angle; at a temperature of about 700 degrees Celsius iron gets red hot and is ready for forming. Furthermore, iron workpieces are unlikely to keep sharp edges as they do not stand abrasion well. At room temperature, iron atoms are ordered in a body centered cubic (bcc) crystal structure, see figure (2.1). To increase the strength of iron, alloying elements are added which influence the lattice. One distinguishes between interstitial and substitutional alloying, see figure (2.2). In the case of substitutional alloying, iron atoms are replaced by other (large) metal atoms, e.g. nickel. In the case of interstitial alloying, small non-metal atoms, in particular carbon, fill empty spaces in the iron matrix, where the suitable configuration of neighbouring atoms is provided. Iron with a large amount of carbon of about 2.1 to 4 weight percent (cast iron) is very resistant, but has bad forming properties, it can not be shaped and is prone to damages by breaking. Regarding strength and workability, steel combines the best of two worlds. It is a compound of iron with a small carbon content between 0.2 and 2.1 weight percent with the

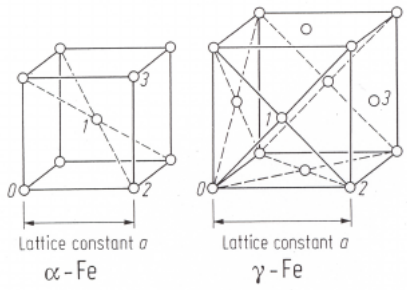

Figure 2.1: Lattice structures of α-iron (bcc) and γ-iron (fcc), from [82].

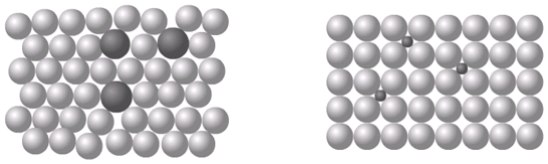

Figure 2.2: Schematic representation of a substitutional (left) and an interstitional (right) alloy, from esa.

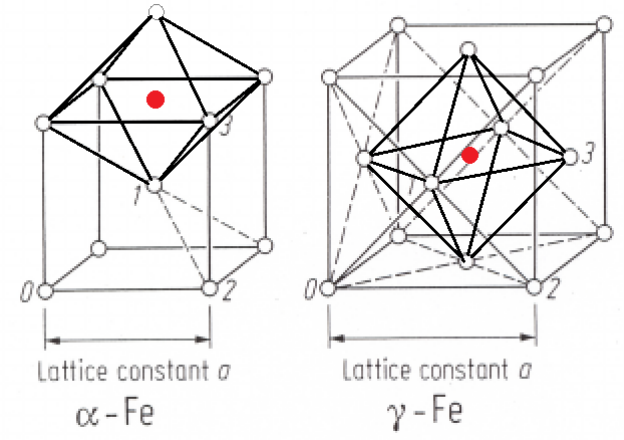

Figure 2.3: Lattice structures of α-iron (bcc) and γ-iron (fcc) with interstitial carbon.

characteristic trait that its mechanical properties can by manipulated by thermal interference.

Heat treatments, i.e. processes of controlled heating and cooling, influence the grid structure in which iron and carbon atoms are arranged. To understand this better, first the lattice structure of iron is considered in more detail. Depending on temperature and pressure, iron exists in a number of molecular forms (allotropes), where the atoms are bonded together differently. There are at least four of those, called α-, γ-, δ-, and ε-iron. Some experiments lead to the assumption that there possibly exists another phase β which is only stable at very high pressures and temperatures. The ε phase also only forms at very high pressures and is not of interest here. During a cooling process at moderate pressure, δ-iron crystallizes when the temperature of molten iron falls below 1538 degree Celsius. Further cooling leads to first γ-iron (between 1394 and 912 degree Celsius) and later α-iron (below 912 degrees Celsius). Both δ- and α-iron exhibit the body centered cubic (bcc) crystal structure. This structure dissolves only little amounts of carbon, as there are fewer appropriate interstices to take the carbon in. γ-iron has a face centered cubic (fcc) structure (see (2.1)), where the iron atoms are packed differently and carbon has more opportunities to dissolve, see figure (2.3). When pure iron is cooled

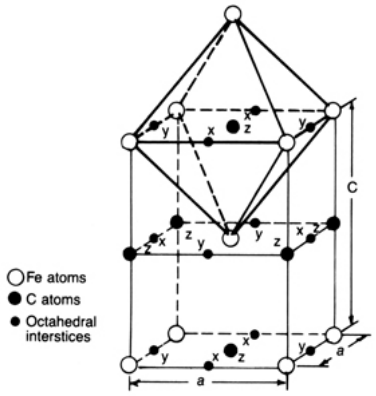

Figure 2.4: Body centred tetragonal lattice structure of martensite, from TU Delft, the Netherlands.

from higher temperatures below 912 degrees Celsius, it simply switches from the γ-state to the α-state. However, if there is a sufficient amount of carbon dissolved in the lattice, different processes may happen. If the material is cooled down rapidly (quenched), carbon has no time to diffuse and is trapped inbetween the reconfiguring lattice. This results in shifted body centered tetragonal cubic crystals (Martensite) (see figure (2.4)) and in high internal stresses, making the material harder and more brittle. (It should be pointed out that the shifted lattice structure is only possible because of the alloying element, pure iron can not be hardened.) Low cooling rates in contrast give time for diffusion and thereby the iron lattice switches from the γ- to the α-state like it does for pure iron and the carbon partly dissolves. Accordingly, by slower cooling one achieves compositions of ferrite (virtually pure iron) and cementite (i.e., iron carbide, Fe_3C), e.g. a lamellar structure (pearlite) or a non-lamellar structure with many dislocations in the ferrite grid (bainite). Those mixtures vary in proportion and composition structure. In all, steel may occur (locally) in one of the following phases or phase mixtures: in the high temperature phase Austenite (γ-iron), in one of the possible product phases martensite (body centered tetragonal crystal, hard and brittle), ferrite (α-iron with smallest amounts of carbon), cementite, pearlite (lamellar composition of 88 percent ferrite and 12 percent cementite), bainite (fine, non-lamellar composition of dislocation-rich ferrite and bainite), or ledeburite (mixture of austenite and cementite). All of these possess different mechanical properties. In this thesis, considerations are usually restricted to steels and respective treatments where only the high-temperature phase austenite, the very hard, brittle, and voluminous martensite, and the softer and more ductile pearlite occur.

The correspondence of temperature and carbon concentration to metastable steel phases can be seen in the iron - iron carbide diagram (2.5). Martensite is not included

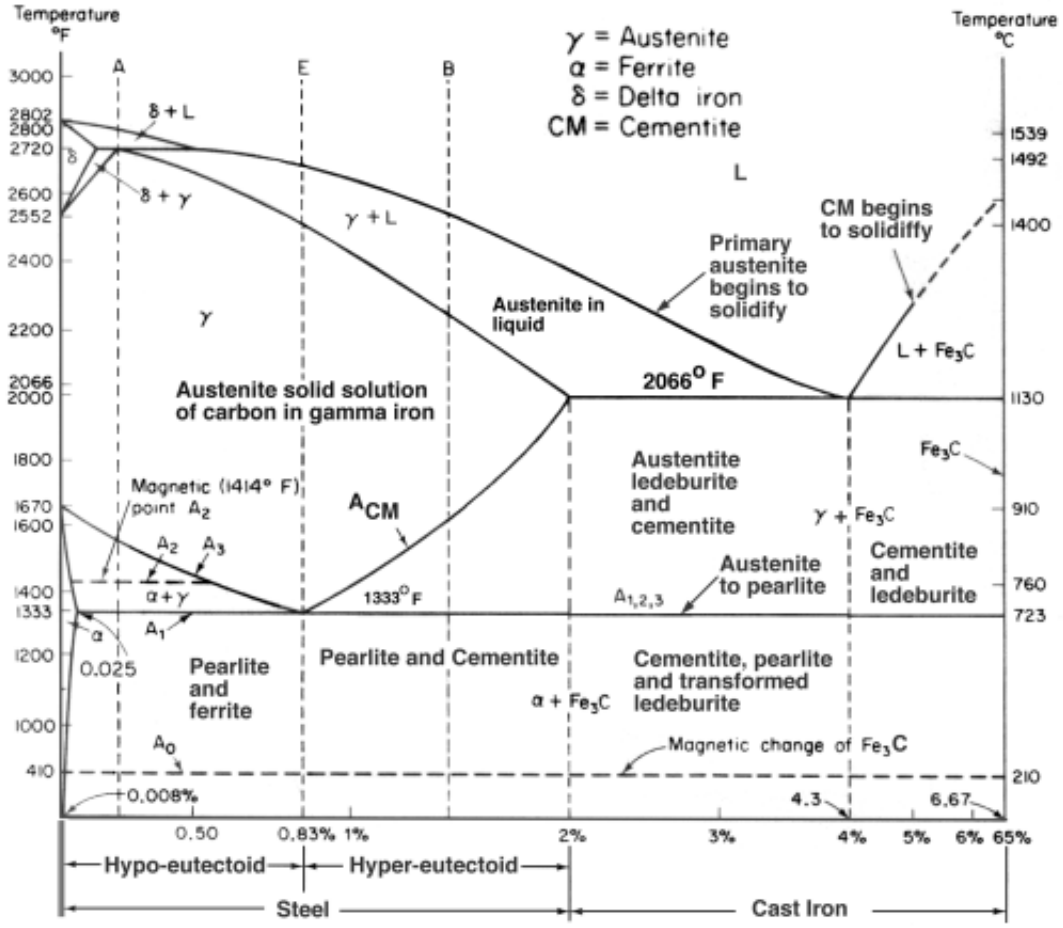

Figure 2.5: Fe-Fe_3C phase diagram. *Materials Science and Metallurgy*, 4th ed., Pollack, Prentice-Hall, 1988.

in this diagram as it is a unstable configuration which is formed only for very high cooling rates.

In heat treatment processes, the cooling velocity is of great importance as it determines the time for the carbon atoms to diffuse and thereby which steel phase can be formed. Information about the connection of the cooling rate and phase evolution can be gathered from Continuous-Cooling-Transformation (CCT) or Time-Temperature-Transformation (TTT) diagrams. CCT diagrams (e.g. the bottom part of figure (2.6)) display temperature trajectories and the according phase fractions and hardness values along this curve. Those diagrams are convenient for real heat treatments as the temperature curves are well attainable. For the sake of modeling parameters, TTT diagrams (as in figure (2.7)) are also handy. Here, areas indicate start and end time (x-axis) of transformation from austenite to the respective product phases if temperature is held constant at the value given by the y-axis. Solving simple integral equations one obtains interpolation data for the evolution of phases, see e.g. [72], p. 8, or later in this chapter at the end of (2.2.1).

2.1.1 Heat treatments and distortion

When talking about steel, one has to distinguish different scales. On a microscopic level, steel is considered as a lattice structure, consisting mainly of iron and carbon atoms. There are various configurations for these lattices, i.e. steel phases, which yield different material properties observable on the macroscopic level. The equilibrium lattice structure depends on the system's energy, that is, the distribution of metallurgical phases can be influenced by temperature and pressure. The dependence on temperature is utilized in the heat treatment of steel where one seeks to produce a desired phase distribution by controlled heating and cooling. Usually, one tries to achieve a hardened workpiece boundary layer which is given by a high distribution of the metastable steel phase martensite. This is achieved by quenching, i.e. rapid cooling, from high temperature as martensite is a polymorphic form obtained by "freezing" atoms in place. For simplicity, in the following only three phases will be considered: the high-temperature phase austenite, the strong martensite, and the ductile pearlite.

The standard lab test to investigate the hardenability of steels is the Jominy end quench test. A hot, austenitized steel cylinder is clamped on the one end and cooled by spray water on the other end. The soaked end is cooled rapidly, the cooling rate decreases with growing distance from the quenched end. In figure 2.6, the cooling is applied to the left side of the steel cylinder depicted on top of the picture. This is represented by the temperature curves A to D. Being very steep, curve A circumvents the zone (nose) where pearlite is formed, whereas slow cooling

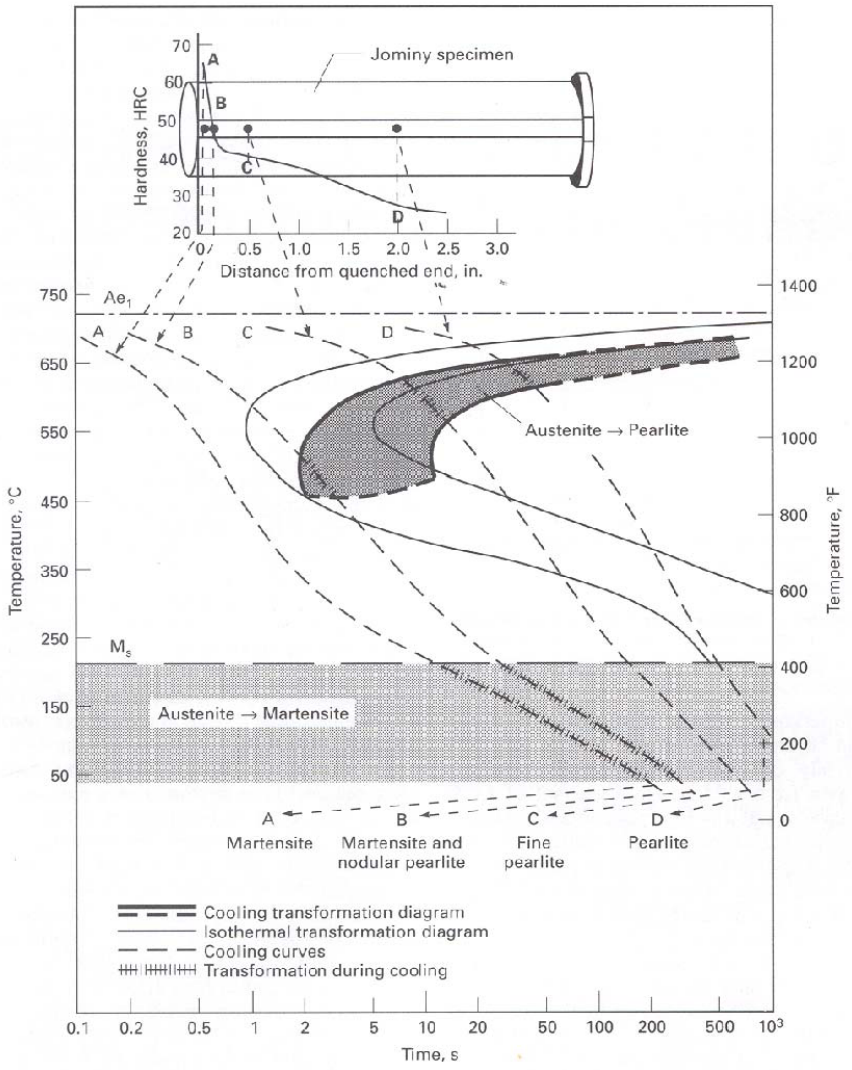

Figure 2.6: Jominy end quench test and Continuous-Cooling-Transformation(CCT)-diagram, from [9]

(curve D) leads to a large pearlite fraction. After the quenching, when the steel specimen is completely cooled down, the quenched end possesses a high martensite concentration and is therefore very hard and brittle. The farther one moves away from this end, the softer and more ductile the steel gets. This the first important effect of the heat treatment quenching: the hardness and ductility properties are controlled. The second effect concerns the volume of the specimen: the formation of the low-density phase martensite causes an expansion of the quenched end. This results in a shape alteration (i.e. distortion) of the quenched steel specimen.

Distortion in steel is not only caused by heat treatments. Any process that brings internal stresses into the workpiece, e.g., clamping, milling, drilling, or mere transportation, can result in distortion. Distortion phenomena mean severe trouble and and its correction can cost a lot of money. Therefore its investigation is of vital importance in engineering.

2.2 Model derivation

The material properties of steel are determined by its microstructural formation. For a modeling of steel treatments in engineering, which are observed on a macroscale, a phenomenological macroscopic description of the metallurgical phases is reasonable.

The models considered in this thesis give a description of the physical processes taking place in the steel workpiece which is given by a bounded set $\Omega \subset \mathbb{R}^3$ with boundary $\Gamma = \partial\Omega$. Mainly three quantities will be taken into account: temperature θ, displacement u, and phase fractions z_i.

The application in chapter 5 deals with cooling, it is assumed that the workpiece is sufficiently heated at initial time. Workpiece geometry, reference data, and the terms included in the equations correspond to this high-temperature initial state.

A nice survey of the general ideas of linear and nonlinear thermomechanical modeling is given in the introduction of [5], more detailed further reading by the references therein. In this paper one can also find information about the modeling of phase transformations using set-valued differential equations, which will not be subject of this thesis.

2.2.1 Phase transitions

A model is always formulated with respect to the underlying application, in particular with what is actually *observed*. The focus of our interest lies on engineering applications on large scales in the range of tenth of millimetres. Thus, phenomena observable only under strong microscopes are neglected, only their *effects* on larger scales are included phenomenologically. As there are often misunderstandings due

to different conceptions of the notion *steel phase* and the according modeling on different scales and under different objectives, the phase concept utilized throughout this thesis will be briefly distinguished from others. In this thesis, the term phase is used in a sense where at each point in space one or more phases simultaneously coexist. A phase is rather a state (which could be fully or just partly achieved) than a material zone as in some engineering works (e.g. [57] as cited in [87]). Accordingly, sharp interface approaches, e.g. Stefan problems, where each point in space is assigned to a uniquely determined metallurgical phase, do not come into play, not even by convergence. One could say, that a degenerated phase field model is utilized, which is lacking direct spatial interdependence (having spatial derivatives with coefficient zero). A transition to a sharp interface model by convergence is not considered. (Information about phase field models can be gathered from [14], [66], and [68]. A thermodynamically consistent sharp interface model to describe the austenite-ferrite phase transition can be found in [24].) An exhausting introduction into different frameworks and models for (general and steel) phase transformations is presented in [84] or [14]. In this thesis, the phase transition description is given by a phase mixture approach, phase evolution occurs at each point independently from the neighbouring points and phase diffusion is omitted (we do not consider spatial derivatives). In mathematical terms, the occurence of the i-th phase at point $x \in \Omega$ is given as a fraction $z_i(x) \in [0, 1]$. An overview on the modeling of phase transitions in steel based on the phase mixture approach can be found in numerous books and articles, e.g. Hömberg [43], [41], Hömberg and Weiss [47], Wolff, Boettcher, Böhm [90], and the references therein. A very pleasant and complete summary is given by [12].

One has to distinguish isothermal and non-isothermal processes, i.e., processes where the temperature is held constant and where temperature may vary.

In the isothermal case, the fraction $p(t)$ of pearlite transformed from austenite for randomly distributed, spherical nuclei with constant nucleation rate N_v and growth rate G is described by the classical law of Johnson and Mehl, [51],

$$p(t) = 1 - \exp(-\frac{\pi}{3} N_v G^3 t^4). \tag{2.1}$$

Utilizing approaches by Scheil, Avrami, and Cahn, rules for non-isothermal processes can be obtained, see [43]. A comparison of models for the austenite-pearlite transition in steel 100Cr6 is found in [91].

The martensite formation works differently. It forms very quickly from the remaining austenite. A common rule for martensite formation below some start temperature M_s is given by the Koistinen-Marburger formula

$$m(\theta) = 1 - \exp(-c(M_s - \theta)). \tag{2.2}$$

This formula does not account for the fact that the austenite–martensite formation is irreversible. To overcome this problem, there are different modifications (see e.g. [43], [47], [92]), among them embedding it into a Leblond-Devaux evolution law [55].

We use a reduced, semilinear version of these phase equation system presented in [47], which is more convenient for mathematical analysis and the numerical application, but is still capable of representing the physical reality of the applications of interest well enough. In particular, an explicit computation of austenite is omitted as stated in the following. The sum of all phase fractions z_i, $1, .., n$ at any point x fulfills

$$z_i(x) \in [0,1], \qquad \sum_i z_i(x) = 1. \tag{2.3}$$

As this leads to one dependent variable $z_k = 1 - \sum_{i \neq k} z_i$, depending on the context sometimes a reduced representation $\{z_i \ ; \ i \neq k\}$ is used. In particular, in the case of cooling processes, only transitions from the high-temperature phase austenite to the low-temperature product phases are considered. Starting with full austenization, the austenite fraction at initial time is 1 and the fractions of the product phases are 0. Then, only the explicit description of the fractions of the product phases is required.

In the following, only the evolution of the hard and brittle phase martensite ($i = 1$) and soft and ductile pearlite ($i = 2$) will be considered. The phase vector $z(x)$ consists only of two components. The evolution of phases in each point of space is given by ordinary differential equations, which depend on the time variant, spatially inhomogeneous quantities temperature, stress, and displacement. The transition from austenite to pearlite is driven by carbon diffusion, the growth rate is influenced by temperature and stress. Temperature does not only influence the velocity of martensite evolution but its possible total amount, under isothermal conditions the martensite fraction is limited. As mentioned before, the formation of martensite needs very little time. A possible approach is to treat the martensite fraction as a direct result of temperature and remaining austenite and give a simple algebraic rule to compute its fraction. An ordinary differential equation is canonically derived by taking the time derivative of formula (2.2) (and extend it by corrective terms to account for the irreversibility of the martensite transformation). The resulting equation contains the time derivative of the temperature and its solution is for monotonically decreasing temperature again equal to the fraction given by the Koistinen-Marburger formula, where there is no time gap (see [12]). If the Koistinen-Marburger expression is taken as a kind of equilibrium function within a Leblond type differential equation (again extended by correcting terms),

$$\dot{m} = \frac{c}{\tau} \max\{\min\{\bar{m}(\theta), 1 - z_1\} - z_2, 0\} \tag{2.4}$$

the solution suffers from a deceleration compared to the (corrected) result of the Koistinen-Marburger formula. This time delay can be eliminated by ever smaller relaxation parameters τ, but this leads to numerical problems. For the mathematical analysis on the other hand, it is more pleasant not to have temperature's time derivative on the right hand side.

In all, the phase transformations are described by the following rate laws, where z_1 and z_2 denote the phase fractions of pearlite and martensite.

$$\dot{z}_1 = f_1(\theta, z, \sigma) = (1 - z_1 - z_2) g_{11}(\theta) g_{12}(\sigma) \tag{2.5a}$$

$$\dot{z}_2 = f_2(\theta, z, \sigma) = [\min\{\bar{m}(\theta), 1 - z_1\} - z_2]_+ g_{21}(\theta) g_{22}(\sigma) \tag{2.5b}$$

$$z_i(0) = 0 \quad i = 1, 2\,. \tag{2.5c}$$

Both phase fractions evolve from austenite, the growth rate depends on the non-transformed fraction $1 - z_1 - z_2$ and temperature. The function g_{11} describes the temperature dependency of pearlite's growth rate, g_{12} the stress dependency. As the total amount of martensite is limited under isothermal conditions, the rate law for martensite requires an additional term. The bracket $[\cdot]_+$ denotes the positive part function $[\cdot]_+ = \max\{\cdot, 0\}$, $\bar{m}(\theta)$ is the fraction of martensite which can be attained at temperature θ. The term $\min\{\bar{m}(\theta), 1 - z_1\}$ represents the maximal fraction that can be transformed to martensite. All g_{ij} are non-negative functions.
Note that these rate laws only allow irreversible phase transitions from austenite to pearlite or martensite, respectively. $z_{i,t} \geq 0$ holds for all temperatures θ during the cooling process. For convenience, the ordinary differential equation will be formulated in vector notation

$$z_t = f(\theta, z, \sigma), \qquad z(0) = 0. \tag{2.6}$$

Remark 2.7 *Actually, according to Noll's principle of material frame-indifference, [79], here and in the following, one has no dependence of material functions on the full stress tensor σ but on its invariant parts, i.e.,*

$$\sigma_v(\sigma) = \left(\frac{3}{2}\sigma^* : \sigma^*\right)^{\frac{1}{2}} \quad \textit{(von Mises stress)}, \tag{2.8}$$

$$\sigma_m(\sigma) = \frac{1}{3} tr(\sigma) \quad \textit{(mean (principal) value)}. \tag{2.9}$$

For simplicity, as in [84], we stay with the notational dependence on full σ, but never exploit frame dependent values.

How to obtain material data from TTT diagrams

Descriptions of how the parameters of phase equations are derived from TTT diagrams, are given in e.g. [72] and [43]. Assume that phase z^i can be described by an

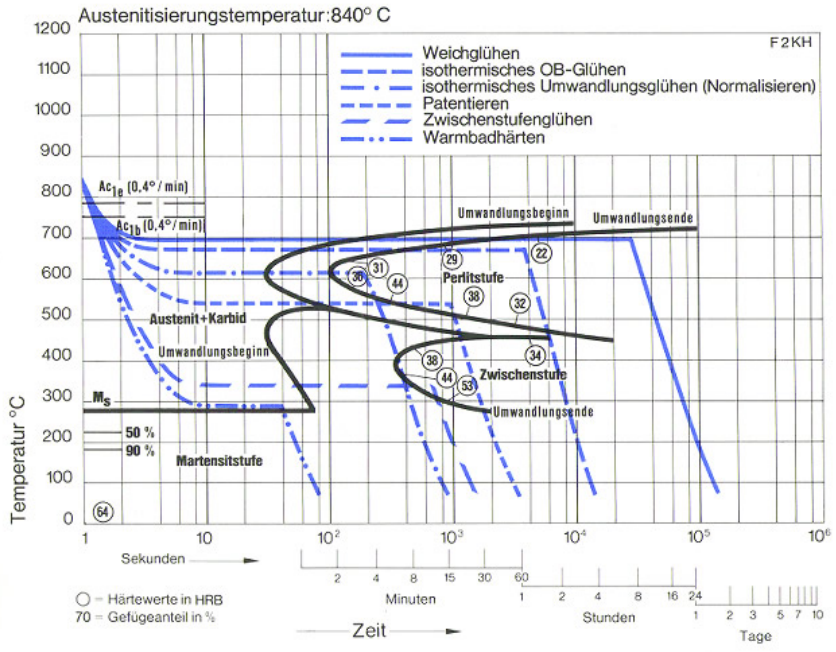

Figure 2.7: Time-Temperature-Transformation(TTT)-diagram, from Saarstahl

ordinary differential equation

$$z_t^i(t) = f(\theta(t), z(t), \sigma(t)) = (1 - \sum_i z^i) g(\theta) h(\sigma).$$

Considering a stress-free, isothermal process (temperature is held constant), in a diagram such as (2.7) one follows a horizontal line according to a fixed temperature. Only the evolution of a single phase is considered. Thus, the phase equation reduces to a formula

$$z_t^i(t) = (c - z^i) g(\theta),$$

where $c = 1$ for the case, that phase z^i evolves completely from austenite or $c < 1$ if austenite is already partly consumed for the transformation into other phases z^j, θ is considered as a constant. Coming from the left (the initial time), when a line of the phase area is crossed, the transformation into the respective phase starts, one can read t_0 (the time when approximately 1% of the phase is formed) from the x-axis. When again a line is crossed, the phase evolution zone of the considered phase is left and one can read the transformation end time t_f (the time when approximately 99% of the phase is formed) from the x-axis. Possible additional percentage numbers indicate fractions of product phases build so far. Simple computations yield

$$\int_{t_0}^{t_f} g(\theta) = \int_{t_0}^{t_f} \frac{z_t^i}{c - z^i} dt = \int_{c - z^i(t_f)}^{c - z^i(t_0)} \frac{1}{\varphi} d\varphi = \ln \left(\frac{c - z^i(t_0)}{c - z^i(t_f)} \right),$$

using furthermore $(t_f - t_0)g_1(\theta) = \int_{t_0}^{t_f} g(\theta)$, one achieves for $g(\theta)$ for a single fixed value θ:

$$g(\theta) = \frac{1}{t_f - t_0} \ln\left(\frac{c - z^i(t_0)}{c - z^i(t_f)}\right).$$

Usually, one determines the t_0^k and t_f^k for a couple of values θ^k from the TTT-diagram and does an interpolation for the discrete $g(\theta^k)$ achieved by the above formula to obtain the mapping $\theta \mapsto g(\theta)$.

As presented in section (2.2.1), the rule for martensite formation reads differently. Also the diagram has to be read in another way: For a given temperature θ, one obtains almost immediately the maximal possible amount of martensite fraction ("equilibrium fraction"), it does not change over time. Therefore, one has no delimiting curved borders (that are crossed if a horizontal line is drawn) for the onset and the finish of transformation according to time, but merely a kind of rectangular area at the bottom of the diagram in the low temperature zone. Its upper boundary gives the temperature when martensite formation starts M_s (**m**artensite **s**tart, i.e. the highest temperature where any martensite is formed), possibly there is also a lower boundary M_f (**m**artensite **f**inish) noted where the martensite formation is complete. (For some steels, the martensite finish temperature is far below zero degrees Celsius and can therefore not be obtained by experiments properly – at least not without exceeding costs. In this case it makes sense to content oneself with the more relevant value of martensite at room temperature.) Percent numbers (if specified) give the amount of the virtually instantaneously formed martensite fraction at this temperature – if austenite was not already consumed by the formation of other phases in the case of slow cooling. One sees the expectable fact that the "equilibrium" fraction grows for ever lower temperatures until 100 percent is reached. (It is not a real equilibrium as martensite is in itself a unstable phase but rather an expectation value.) This justifies the approach of anti-sigmoidal function $\bar{m}(\theta)$ in (2.5b) and determines its values, e.g. for given percentage values m_i^{eq} for a descending sequence of temperatures θ_i, $i = 1, .., n$, by a linear interpolation

$$\bar{m}(\theta) = \begin{cases} 0\ , & \theta \geq M_s \\ m_{i+1}^{eq} + \frac{\theta - \theta_{i+1}}{\theta_i - \theta_{i+1}}(m_i^{eq} - m_{i+1}^{eq})\ , & \theta \in [\theta_{k+1}, \theta_k] \\ 1\ , & \theta \geq M_f \end{cases} \tag{2.10}$$

Both, CCT and TTT diagrams may only deliver reference points for the phase evolution modeling. They contain only restricted information according to certain experimental setups. CCT diagrams give good values for specific heat treatments that are charted as temperature trajectories in them. This can be utilized for data fitting procedures where some qualitative behaviour is assumed from experience and represented by a parametrized function. The same holds true for TTT diagrams

which give information about isothermal processes that are utilized – as explained above – to determine terms in a non-isothermal model by considering the special case of constant temperature. In a way, this is also a kind of fitting a model to a restricted set of experimental values. Therefore, one should remain skeptical of the reliability of the achieved parameters and review them if the application changes (e.g. if additional carburizing comes into play).

2.2.2 Mechanical quantities

Among the main quantities of interest for heat treatments are (Cauchy) stress and strain during the treatment and the shape at end time. The strain is determined by the displacement vector u that assigns to each point x of the reference workpiece geometry a new position by $x + u(x)$. u defines the strain tensor by

$$\frac{1}{2}\left(\frac{\partial u_i}{\partial x_j} + \frac{\partial u_j}{\partial x_i} + \sum_k \frac{\partial u_k}{\partial x_i}\frac{\partial u_k}{\partial x_j}\right). \tag{2.11}$$

For small deformations it is sufficient to consider the symmetric part of the strain rate tensor,

$$\varepsilon_{ij}(u) = \frac{1}{2}\left(\frac{\partial u_i}{\partial x_j} + \frac{\partial u_j}{\partial x_i}\right). \tag{2.12}$$

Unfortunately, this linearized representation of strain is not invariant to rigid body motions (see e.g [13]). Therefore, a thorough fixing of boundary conditions in the numerical examples and the resulting stresses is inevitable.

Furthermore, we suppose small stresses and neglect effects from classical plasticity.

We assume that the strain may be additively decomposed into an elastic, a thermal, and a plastic part,

$$\varepsilon = \varepsilon^{el} + \varepsilon^{th} + \varepsilon^{tp}, \tag{2.13}$$

where the plastic effects are merely given by transformation induced plasticity, yield is neglected. This additive ansatz is widely accepted but not the only one. See Bertram [11], for a nice overview of modeling approaches for strain decomposition and plasticity.

Now, we want to investigate the single additive components in more detail.

Thermal strain

Dilatometer measurements show an almost linear correspondence of thermal expansion and temperature for each phase (see figure 2.8), the occurence of phase

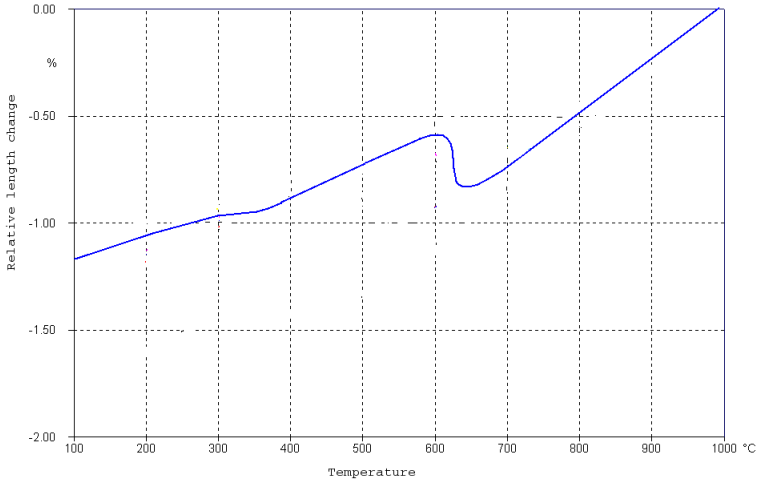

Figure 2.8: Dilatometer curve with 2 product phases (Courtesy of IEHK, Aachen).

transitions results in a change of rate such that a piecewise linear curve is observed. This suggests describing the thermal expansion of each single phase z_i by

$$\varepsilon_i^{th} = q_i(\theta - \theta_{i,ref})I \tag{2.14}$$

with constant reference temperatures $\theta_{i,ref}$ and unit tensor $I \in \mathbb{R}^{3\times3}$. The overall thermal strain ε^{th} is then computed from the mixture ansatz

$$\varepsilon^{th} = z_1\varepsilon_1^{th} + z_2\varepsilon_2^{th} + (1-z_1-z_2)\varepsilon_0^{th}. \tag{2.15}$$

By reconfiguration of the single parts of the sum we achieve

$$\varepsilon^{th} = q(z)\theta I + q_{ref}(z)I =: \beta(\theta, z)I \tag{2.16}$$

with

$$q(z) = z_1q_1 + z_2q_2 + (1-z_1-z_2)q_0, \tag{2.17}$$

$$q_{ref}(z) = z_1q_1\theta_{1,ref} + z_2q_2\theta_{2,ref} + (1-z_1-z_2)q_0\theta_{0,ref}. \tag{2.18}$$

Remark 2.19 *We will use the abbreviations*

$$\bar{q} = (q_1 - q_0, q_2 - q_0), \tag{2.20}$$

$$\bar{q}_r = (q_1\theta_{1,ref} - q_0\theta_{0,ref}, q_2\theta_{2,ref} - q_0\theta_{0,ref}), \tag{2.21}$$

$$q^* = \max\{q_1, q_2, q_3\}. \tag{2.22}$$

Actually, one has to distinguish in the phase mixture approach if mass or volume fractions are meant, see [87]. Fortunately, the discrepancy of these values is small as the density differences of the phases are. Therefore, this distinction is not made here.

TrIP strain

Transformation induced plasticity occurs during phase transition even for small stresses far below yield stress. As for classical plasticity, it accounts for stresses that lead to shear, volumetric changes are irrelevant. This behaviour is modelled by the following standard formula.

$$\varepsilon_{i,t}^{tp} = \Phi_{i1}(\theta)\,\frac{\partial \Phi_{i2}(z_i)}{\partial z_i}\,z_{i,t}\sigma^*\,, \tag{2.23}$$

where $\cdot^*$ denotes the deviatoric part of a second-order tensor, i.e. $\sigma^* = \sigma - \frac{1}{3}tr(\sigma)I$, $tr(\sigma) = \sigma_{11} + \sigma_{22} + \sigma_{33}$. The resulting flow is volume preserving and grows proportionally to the growth rate $z_{i,t}$ of phase z_i. Typical choices for $\Phi_{i1}(\theta)$ and $\Phi_{i2}(z_i)$ can be found in works of Tanaka, e.g. [32]. For brevity, in the following the modeling ODE for the trip contribution will be written as

$$\varepsilon_t^{tp} = \gamma(\theta, z, z_t)\sigma^*\,. \tag{2.24}$$

Elastic strain

The remaining elastic part of the strain tensor results as the difference

$$\varepsilon^{el} = \varepsilon(u) - \varepsilon^{th} - \varepsilon^{tp} \tag{2.25}$$

and can be inserted in Hooke's law,

$$\sigma = K\varepsilon^{el} = K(\varepsilon(u) - \varepsilon^{th} - \varepsilon^{tp}), \tag{2.26}$$

with a fourth order tensor K. In our case we assume K to be constant (see e.g. the results of Elschner, [26], [27], or [39] and the references therein for L^p-regularity problems arising even for smooth boundaries and Dirichlet boundary conditions if $K_{ijke} \in L^\infty$). (Further details on regularity issues will be given later on in this thesis.) More precisely, as we consider steel on the macroscopic scale as an isotropic material, the stiffness tensor K possesses the form

$$K_{ijke} = \lambda\delta_{ij}\delta_{ke} + 2\mu\delta_{ik}\delta_{je} \tag{2.27}$$

and the product $K\varepsilon^{el}$ reads as

$$\sigma = 2\mu\varepsilon(u) + \lambda tr(\varepsilon(u))I - (2\mu + 3\lambda)\beta(\theta, z)I - 2\mu\varepsilon^{tp}. \tag{2.28}$$

Remark 2.29 *K is a symmetric tensor fulfilling*

$$K_{ijkl} = K_{ijlk} = K_{jikl} = K_{klij}. \tag{2.30}$$

Sometimes in literature, it is written rather $K\nabla u$ than $K\varepsilon(u)$. Due to the symmetry conditions of K these two expressions denote the same.

Note that the trip contribution effects solely the shear, i.e. is trace free.

Remark 2.31 *The Lamé coefficients λ and μ of steel are positive, here assumed to be constants, K is positive definite. The coefficient of the thermal part divided by 3, $b = \frac{1}{3}(2\mu + 3\lambda)$, is called bulk modulus.*

2.2.3 Derivation of coupled system

Adopting the approach presented in e.g. [61], [64], [63], we derive parameters for a coupled system of heat equation and momentum balance. The main idea is to utilize the first and second principle of thermodynamics, balance laws, and the positivity of the entropy time derivative to obtain identities for the occuring coupling parameters. We consider cooling processes or more precisely processes with only minor heating where the rate laws (2.6) and $z_{i,t} \geq 0$ hold.

The displacement u (or velocity $v = u_t$), the stress σ, and temperature θ are governed by the quasistatic momentum balance and the balance law of internal energy e. We give a formulation in the undeformed reference domain Ω and for the linear strain tensor ε (2.12) assuming that only small deformations occur.

$$-\operatorname{div}\sigma = F \tag{2.32}$$

$$\varrho e_t + \operatorname{div}\Lambda = \sigma : \varepsilon(v) + h\,. \tag{2.33}$$

':' denotes the scalar product in $\mathbb{R}^{3,3}$, $A : B = \sum_{i,j=1}^{3} A_{ij}B_{ij}$.

To derive a constitutive relation for the internal energy, the Helmholtz free energy ψ and entropy s are introduced. They fulfill the thermodynamic identity

$$e = \psi + \theta s\,. \tag{2.34}$$

Following the approach presented in Petryk, [64], we consider a twice continuously differentiable thermodynamic potential $\psi = \hat{\psi}(\varepsilon^{el}, \theta, z)$ where phase fractions z are treated as internal variables. For small deformations, the first and second law of thermodynamics result in the Clausius-Duhem inequality in the following form.

$$\sigma : \varepsilon(v) - \varrho(\psi_t + s\theta_t) - \frac{1}{\theta}\,\Lambda \cdot \nabla\theta \quad \geq \quad 0\,. \tag{2.35}$$

Exploiting the law of Fourier,

$$\Lambda = -k\nabla\theta, \tag{2.36}$$

inserting the additive decomposition of ε, (2.13), and applying the chain rule for $\hat{\psi}$ the inequality reads

$$\begin{aligned}\left(\sigma - \varrho\frac{\partial\hat{\psi}}{\partial\varepsilon^{el}}(\varepsilon^{el},\theta,z)\right) : \varepsilon_t^{el} - \varrho\left(s + \frac{\partial\hat{\psi}}{\partial\theta}(\varepsilon^{el},\theta,z)\right)\theta_t \\ + \sigma : (\varepsilon_t^{th} + \varepsilon_t^{tp}) - \varrho\frac{\partial\hat{\psi}}{\partial z}(\varepsilon^{el},\theta,z)\cdot z_t + \frac{1}{\theta}\,k|\nabla\theta|^2 \quad \geq \quad 0. \end{aligned} \tag{2.37}$$

This inequality holds for all admissible solutions to the field equations, in particular for purely elastic deformations with θ constant in time and space and z constant in time. Recalling (2.24) and (2.16), $z_t = 0$ delivers $\varepsilon_t^{tp} = 0$, whereas the additional condition $\theta_t = 0$ yields $\varepsilon_t^{th} = 0$. Altogether, (2.37) then reduces to

$$\left(\sigma - \varrho\frac{\partial\hat{\psi}}{\partial\varepsilon^{el}}(\varepsilon^{el},\theta,z)\right) : \varepsilon_t^{el} \geq 0. \tag{2.38}$$

ε is defined as a symmetric tensor. It therefore makes sense to require $\frac{\partial\hat{\psi}}{\partial\varepsilon^{el}}$ to be symmetric as well, that is

$$\frac{\partial\hat{\psi}}{\partial\varepsilon_{ij}^{el}} = \frac{\partial\hat{\psi}}{\partial\varepsilon_{ji}^{el}}. \tag{2.39}$$

We then achieve by pointwise discussion

$$\sigma = \varrho\frac{\partial\hat{\psi}}{\partial\varepsilon^{el}}(\varepsilon^{el},\theta,z) \tag{2.40}$$

as inequality (2.38) holds for all admissible elastic strain rates. By similar reasoning we obtain

$$s = -\frac{\partial\hat{\psi}}{\partial\theta}(\varepsilon^{el},\theta,z)\,. \tag{2.41}$$

Here we vary the sign of θ_t for uniform θ (that is $\nabla\theta = 0$), $z_t = 0$, and $\sigma = 0$ (e.g. by choosing $u_k(x,t) = -(q(z)\theta + q_0(z))(x_1 + x_2 + x_3)$, $k = 1,2,3$; for $z_t = 0$ this yields $\varepsilon^{el} = \varepsilon - \varepsilon^{th} - \varepsilon^{tp} = 0$).

For consistency, we assume the remaining addends of (2.37) to be non-negative each, see e.g. ([64]). Since $z_{i,t} \geq 0$, we define the latent heat of z_i (actually the latent heat of the transition from austenite to z_i) as

$$L_i(\varepsilon^{el},\theta,z) = -\frac{\partial\hat{\psi}}{\partial z_i}(\varepsilon^{el},\theta,z) \tag{2.42}$$

and assume $L_i > 0$. Finally, the inequality

$$\sigma : (\varepsilon_t^{th} + \varepsilon_t^{tp}) \geq 0 \tag{2.43}$$

describes non-negative intrinsic dissipation. Inserting

$$\varepsilon_t^{th} = (\beta(\theta, z))_t I, \tag{2.44}$$

$$\frac{\partial \beta}{\partial \theta} = q(z), \tag{2.45}$$

$$\frac{\partial \beta}{\partial z_i} = (q_i - q_0)\theta + q_i\theta_{i,ref} - q_0\theta_{0,ref}, \tag{2.46}$$

$$\begin{aligned}(\beta(\theta, z))_t &= \frac{\partial \beta}{\partial \theta}\theta_t + \frac{\partial \beta}{\partial z} z_t \\ &= q(z)\theta_t + (q(z))_t\theta + (q_{ref}(z))_t \\ &= q(z)\theta_t + (z_{1,t}(q_1 - q_0) + z_{2,t}(q_2 - q_0))\theta \\ &\quad + z_{1,t}(q_1\theta_{1,ref} - q_0\theta_{0,ref}) + z_{2,t}(q_2\theta_{2,ref} - q_0\theta_{0,ref})\end{aligned} \tag{2.47}$$

and 2.24 the addends of (2.43) read in more detail

$$\sigma : \varepsilon_t^{th} = \sigma : (\beta(\theta, z))_t I = (\beta(\theta, z))_t \; tr(\sigma), \tag{2.48}$$

$$\begin{aligned}\sigma : \varepsilon_t^{tp} &= \sigma : \varepsilon_t^{tp} = \sigma : \gamma(\theta, z, z_t)\sigma^* \\ &= \gamma(\theta, z, z_t)|\sigma^*|^2.\end{aligned} \tag{2.49}$$

To compute a constitutive relation for the internal energy e, we differentiate (2.41) and then (2.34) with respect to time.

$$\begin{aligned}s_t &= (-\frac{\partial \hat{\psi}}{\partial \theta})_t \\ &= -\left(\frac{\partial}{\partial \theta}(\frac{\partial \hat{\psi}}{\partial \varepsilon^{el}} : \varepsilon_t^{el}) + \frac{\partial}{\partial \theta}(\frac{\partial \hat{\psi}}{\partial \theta}\theta_t) + \frac{\partial}{\partial \theta}(\frac{\partial \hat{\psi}}{\partial z} z_t)\right) \\ &= -\frac{1}{\varrho}\frac{\partial \sigma}{\partial \theta} : \varepsilon_t^{el} + \frac{\partial s}{\partial \theta}\theta_t + \frac{\partial L}{\partial \theta} z_t.\end{aligned} \tag{2.50}$$

We now assume $\frac{\partial L}{\partial \theta} = 0$ and denote by $c_p = \theta\frac{\partial s}{\partial \theta}$ the specific heat capacity at constant pressure and evaluate the time derivative of (2.34).

$$\begin{aligned}e_t &= \psi_t + \theta_t s + \theta s_t \\ &= \frac{\partial \hat{\psi}}{\partial \theta}\theta_t + \frac{\partial \hat{\psi}}{\partial \varepsilon^{el}} : \varepsilon_t^{el} + \frac{\partial \hat{\psi}}{\partial z} z_t + \theta_t s + \theta(-\frac{1}{\varrho}\frac{\partial \sigma}{\partial \theta} : \varepsilon_t^{el} + \frac{\partial s}{\partial \theta}\theta_t) \\ &= -s\theta_t + \frac{1}{\varrho}\sigma : \varepsilon_t^{el} - Lz_t + \theta_t s - \frac{1}{\varrho}\theta\frac{\partial \sigma}{\partial \theta} : \varepsilon_t^{el} + c_p\theta_t \\ &= \frac{1}{\varrho}\sigma : \varepsilon_t^{el} - Lz_t - \frac{1}{\varrho}\theta\frac{\partial \sigma}{\partial \theta} : \varepsilon_t^{el} + c_p\theta_t.\end{aligned} \tag{2.51}$$

For simplification, we assume that the temperature dependency of ε^{tp} can be neglected, i.e. $\frac{\partial \varepsilon^{tp}}{\partial \theta} = 0$. (Actually, under this assumption it would be consistent to

assume that also γ does not depend on θ. In practice, this is the case for many models of transformation induced plasticity.)

$$\begin{aligned}\frac{\partial \sigma}{\partial \theta} &= \frac{\partial}{\partial \theta}(K(\varepsilon(u) - \varepsilon^{th} - \varepsilon^{tp})) \\ &= -\frac{\partial}{\partial \theta}(K\varepsilon^{th}) = -\frac{\partial}{\partial \theta}(3b(q(z)\theta - q_{ref}(z)))I \\ &= -3bq(z)I. \end{aligned} \tag{2.52}$$

(2.51) then reads

$$e_t = \frac{1}{\varrho}\sigma : \varepsilon_t^{el} - Lz_t + \frac{1}{\varrho}\theta 3bq(z)I : \varepsilon_t^{el} + c_p\theta_t. \tag{2.53}$$

We continue with inserting the last identity and Fourier's law into the balance law of internal energy (2.33).

$$\begin{aligned}\sigma : \varepsilon(v) + h &= \sigma : \varepsilon_t^{el} - \varrho L z_t + 3bq(z)\theta I : \varepsilon_t^{el} + \varrho c_p\theta_t - \operatorname{div}(k\nabla\theta) \\ &= \sigma : \varepsilon_t^{el} - \varrho L z_t + 3bq(z)\theta I : (\varepsilon(v) - \varepsilon_t^{th} - \varepsilon_t^{tp}) + \varrho c_p\theta_t - \operatorname{div}(k\nabla\theta) \\ &= \sigma : \varepsilon_t^{el} - \varrho L z_t + 3bq(z)\theta \operatorname{div}(v) - 9bq(z)\theta(\beta(\theta, z))_t + \varrho c_p\theta_t - \operatorname{div}(k\nabla\theta)\end{aligned} \tag{2.54}$$

Remember that ε_t^{tp} is defined as a trace-free tensor. After rearranging of terms and using (2.48) and (2.49) we achieve

$$\begin{aligned}&\left(\varrho c_p - 9bq(z)\theta\frac{\partial \beta}{\partial \theta}\right)\theta_t - \operatorname{div}(k\nabla\theta) + 3bq(z)\theta\operatorname{div}(v) \\ &= \left(\varrho L + 9bq(z)\theta\frac{\partial \beta}{\partial z}\right)z_t + \sigma : (\varepsilon(v) - \varepsilon_t^{el}) + h \\ &= \left(\varrho L + 9bq(z)\theta\frac{\partial \beta}{\partial z}\right)z_t + \sigma : (\varepsilon_t^{th} + \varepsilon_t^{tp}) + h \\ &= \left(\varrho L + 9bq(z)\theta\frac{\partial \beta}{\partial z}\right)z_t + (\beta(\theta, z))_t tr(\sigma) + \gamma(\theta, z, z_t)|\sigma^*|^2 + h.\end{aligned} \tag{2.55}$$

Finally, the following nonlinear parabolic equation is obtained:

$$\alpha^\theta(\theta, \sigma, z)\theta_t - \operatorname{div}(k\nabla\theta) + 3bq(z)\theta\operatorname{div}(v) = \alpha^z(\theta, \sigma, z)z_t + \gamma(\theta, z, z_t)|\sigma^*|^2 + h. \tag{2.56}$$

where the α are defined by

$$\alpha^\theta(\theta, \sigma, z) = \varrho c_p - 9b\theta q(z)^2 - q(z)tr(\sigma) \tag{2.57}$$

$$\begin{aligned}\alpha_i^z(\theta, \sigma, z) = {}& \varrho L_i + 9bq(z)(q_i - q_0)\theta^2 + 9bq(z)(q_i\theta_{i,ref} - q_0\theta_{0,ref})\theta \\ &+ ((q_i - q_0)\theta + q_i\theta_{i,ref} - q_0\theta_{0,ref})\ tr(\sigma)\end{aligned} \tag{2.58}$$

Hence, an equation for the heat is obtained.

In the next chapter, all derived model equations will be summarized to the complete coupled model and analyzed.

Chapter 3

Analysis of the model

The considerations in the foregoing chapter 2 condense into the following model.

3.1 Coupled system

Let $\Omega \subset \mathbb{R}^3$ bounded with smooth boundary $\partial\Omega$ and $Q = \Omega \times (0,T)$ the corresponding time cylinder. Summarizing the prior model equations, we consider the following boundary value problem:

Problem 3.1

$$-\operatorname{div}\sigma = F \quad in \quad Q \tag{3.2a}$$

$$\sigma = K\Big(\varepsilon(u) - \beta(\theta,z)I - \int_0^t \gamma(\theta,z,z_s)\sigma^* ds\Big) \quad in \quad Q \tag{3.2b}$$

$$u = 0 \quad on \quad \partial\Omega \times (0,T) \tag{3.2c}$$

$$z_t = f(\theta,z,\sigma) \quad in \quad Q \tag{3.2d}$$

$$z(0) = 0 \quad in \quad \Omega \tag{3.2e}$$

$$\begin{aligned}\alpha^\theta(\theta,\sigma,z)\theta_t - k\Delta\theta + 3bq(z)\theta\operatorname{div}u_t \\ = h + \alpha^z(\theta,\sigma,z)\cdot z_t + \gamma(\theta,z,z_t)|\sigma^*|^2 \quad in \quad Q\end{aligned} \tag{3.2f}$$

$$-k\frac{\partial\theta}{\partial n} = 0 \quad on \quad \partial\Omega\times(0,T) \tag{3.2g}$$

$$\theta(0) = \theta_0 \quad in \ \Omega\,. \tag{3.2h}$$

The functions α^θ and α^z are given by

$$\alpha^\theta(\theta,\sigma,z) = \varrho c_p - 9b\theta q(z)^2 - q(z)tr(\sigma) \tag{3.3}$$

$$\begin{aligned}\alpha_i^z(\theta,\sigma,z) = \varrho L_i + 9bq(z)(q_i-q_0)\theta^2 + 9bq(z)(q_i\theta_{i,ref} - q_0\theta_{0,ref})\theta \\ + ((q_i-q_0)\theta + q_i\theta_{i,ref} - q_0\theta_{0,ref})\ tr(\sigma)\end{aligned} \tag{3.4}$$

where ϱ denotes mass density, c_p the specific heat capacity. $f = (f_1, f_2)^T$ is the right-hand side of (2.5a), (2.5b).

The chosen boundary conditions convene the mathematical analysis but do not reflect the physical reality. Without further difficulties, the boundary conditions for the heat equation could be extended to the more reasonable Newton type. For the sake of simplicity, we restrict ourselves to the case of pure Neumann conditions in the proofs. Unfortunately, the matter is more complicated for the elasticity equations. Here, the theory relies on pure Dirichlet boundary conditions. Other boundary conditions bring partially irremediable disadvantages. The choice of boundary conditions, possible modifications, and resulting challenges will be addressed at the end of this chapter again in more detail.

Remark 3.5 *We require $q*$ to be sufficiently small – on the one hand to have $\alpha^\theta(\theta, \sigma, z)$ positive and on the other hand to achieve existence of a solution by the forthcoming fixed point argumentations.*

3.2 Preparations and assumptions

Remark 3.6 (Notation) *We will use the following standard notations:*
Let $v \in \mathbb{R}^n$ be a vector, $v = (v_1, .., v_n)^T$. $|v|$ denotes the euclidean vector norm,

$$|v| = \sqrt{\sum_{i=1}^{n} v_i^2}. \tag{3.7}$$

For $0 < p < \infty$ and a measure space E, $\mathcal{L}^p(E)$ denotes the set of all measurable functions $f : E \to \mathbb{R}$ where

$$\int_E |f|^p dx < \infty. \tag{3.8}$$

$\mathcal{L}^p$ is equipped with the seminorm $\|\cdot\|_p$ defined by $\|f\|_p = \left(\int_E |f|^p dx\right)^{\frac{1}{p}}$.

For $p = \infty$, $\mathcal{L}^p(E)$ denotes the set of all measurable functions $f : E \to \mathbb{R}$ where

$$ess\sup_{x\in E} |f(x)| = \inf_{|\mathcal{N}|=0} \sup_{x\in\Omega\setminus\mathcal{N}} |f(x)| = \inf\{c \geq 0 \ : \ |\{x \in \Omega \ : \ |y(x)| > c\}| = 0\} < \infty \tag{3.9}$$

and the seminorm $\|\cdot\|_\infty$ is given by $\|f\|_\infty = ess\sup_{x\in E} |f(x)|$.
The null sets $\mathcal{N}^p$ are then defined by

$$\mathcal{N}^p = \{f \in \mathcal{L}^p \ ; \ \|f\|_p = 0\}, \quad 0 < p \leq \infty \tag{3.10}$$

and the normed vector (Banach) spaces $L^p(E)$ by

$$L^p(E) = \mathcal{L}^p \setminus \mathcal{N}^p. \tag{3.11}$$

We use the notation $\|f\|_{L^p(E)}$ *for both scalar valued functions* $f : E \to \mathbb{R}$ *and tensor valued functions* $f : E \to \mathbb{R}^{n_1 \times .. \times n_m}$, $2 \leq n_1, .., n_m \in \mathbb{N}$ *with tensor values of arbitrary order* m. *In particular, for* $m = 1$ *the function* f *is vector valued and for* $m = 2$ *it possesses matrix values. The norm is induced by the respective scalar product of* f*'s image space, that is,*

$$\|f\|_{L^p(E)} = \left(\int_E |f(x)|^p dx \right)^{\frac{1}{p}} = \left(\int_E \langle f(x), f(x) \rangle^{\frac{p}{2}} dx \right)^{\frac{1}{p}}, \tag{3.12}$$

$$\langle v, w \rangle = \begin{cases} vw \ , & v, w \in \mathbb{R} \\ \sum_{i_1=1}^{n_1} .. \sum_{i_m=1}^{n_m} v_{i_1..i_m} w_{i_1..i_m} \ , & v, w \in \mathbb{R}^{n_1 \times .. \times n_m} \end{cases} \tag{3.13}$$

To be more precise, one could write $\|f\|_{[L_p(E)]^{n_1 \times .. \times n_m}}$ *or* $\|\|f\|\|_{L_p(E)}$ *for tensors of order 1 or higher.*
$W^{k,p}(E)$ *denotes the set of all functions* $f \in L^p(E)$ *possessing weak derivatives up to the order* k.

Remark 3.14 *Triangle inequality and Young's inequality yield for vectors* $\xi \in \mathbb{R}^k$ *the equivalence of the 1-norm (Manhattan) and the 2-norm (Euclidean)*

$$\exists \ c > 0 \ : \ |\xi| \leq \sum_{i=1}^{k} |\xi_i| \leq c|\xi|. \tag{3.15}$$

Utilizing this inequality chain in the definition of the L^p*-norm,*

$$\|u\|_{L^p(E)} \leq \sum_i \|u\|_{L^p(E)} \leq c\|u\|_{L^p(E)}, \tag{3.16}$$

it is easily verified that Lipschitz continuity of all components $u_i : E \to \mathbb{R}$, $i = 1, .., n$, *of* u *is equivalent to the Lipschitz-continuity of the whole vector-valued function* $u : E \to \mathbb{R}^n$. *Furthermore, utilizing the Cauchy-Schwarz inequality and Hölder's inequality for scalar-valued functions, we obtain Hölder's inequality for vector-valued functions,*

$$\begin{aligned} \|uv\|_{L^1(E)} = \int_E |\langle u, v \rangle| dx \leq \int_E |u||v| dx = \|\|u||v|\|_{L^1(E)} \\ \leq \|\|u|\|_{L^p(E)} \|\|v|\|_{L^q(E)} = \|u\|_{L^p(E)} \|v\|_{L^q(E)} \end{aligned}$$

Assumption 3.17 *The following assumptions are imposed on the occuring data functions:*

(A1) k, κ, c_p, $L_{1,2}$ *are positive constants*

(A2) γ *is bounded and Lipschitz-continuous*

(A3) q_1, q_2, q_3 *are positive constants such that* $q^* := \max\{q_1, q_2, q_3\}$ *is sufficiently small*

(A4) $\bar{m}$ *is Lipschitz-continuous satisfying* $\bar{m}(\vartheta) \in [0,1]$ *for all* $\vartheta \in \mathbb{R}$

(A5) $g_{ij}, \quad i,j = 1,2,$ *are non-negative, bounded, and Lipschitz-continuous*

(A6) $F_i \in W^{1,p}(0,T;L^p(\Omega)) \cap L^{2p}(Q), \quad i = 1,2,3,$

(A7) $\theta_0 \in W^{1,p}(\Omega)$

(A8) $h \in L^p(Q)$, $p > 4$

3.3 Existence and uniqueness

To prove the existence of a unique weak solution to the problem (3.1) we first analyze smaller subproblems, i.e., problems with less variables and treat the other variables as data. The subproblems will be extended sequentially by the other variables until the whole problem is considered. The course of action is reflected in the section structure and as follows:

- we start with phase equations treating u and θ as data,
- then consider the subsystem in z and σ with data θ,
- then consider the almost complete subsystem but replace the term $\gamma(\theta, z, z_t)|\sigma^*|^2$ in the heat equation by variable H,
- and finally achieve existence for the complete system based on the foregoing lemmas.

3.3.1 Phase equations

We start with the solvability of the boundary value problem (3.2d), (3.2e) for θ, σ considered as data.

Lemma 3.18 *Assume that* $\theta, \sigma_{ij} \in L^p(0,T;L^p(\Omega))$ *with* $p \in [1,\infty]$ *for* $i,j \in \{1,2,3\}$. *a) Then the ordinary differential equation (3.2d), (3.2e) has a unique solution satisfying*

$$\|z\|_{W^{1,\infty}(0,T;L^\infty(\Omega))} \le C \tag{3.19}$$

where the constant C *does not depend on* θ *and* σ. *Moreover,* $z_1 + z_2 \in [0,1]$ *for a.e.* $(x,t) \in Q$.

b) If additionally $\nabla\theta, \nabla\sigma_{i,j} \in L^p(0,T;L^p(\Omega))$ *then* $\nabla z \in L^\infty(0,T;L^p(\Omega))$.
c) Let z^i *be the solution from a) corresponding to* θ^i, σ^i, $i = 1, 2$, *then exist* Λ_1 *and* Λ_2 *such that*

$$\|z^1 - z^2\|_{W^{1,p}(0,T;L^p(\Omega))} \leq \Lambda_1 \|\theta^1 - \theta^2\|_{L^p(0,T;L^p(\Omega))} + \Lambda_2 \|\sigma^1 - \sigma^2\|_{L^p(0,T;L^p(\Omega))}. \quad (3.20)$$

Regarding $\|\cdot\|_{W^{1,p}(\Omega)}$ *we achieve*

$$\|z^1(t) - z^2(t)\|_{W^{1,p}(\Omega)} \leq c(t)(\|\theta^1 - \theta^2\|_{W^{1,p}(\Omega)} + \|\sigma^1 - \sigma^2\|_{W^{1,p}(\Omega)}). \quad (3.21)$$

Proof:
a) Consider representatives $\tilde{\theta} \in \mathcal{L}^p((0,T)\times\Omega)$ of θ and $\tilde{\sigma} \in \mathcal{L}^p((0,T)\times\Omega)$ of σ. Fix arbitrary $x \in \Omega$ and consider the ordinary differential equation given by

$$\dot{\zeta}(t) = \hat{f}(t,\zeta), \qquad \zeta(0) = 0, \quad (3.22)$$

where $\hat{f}(t,\zeta) = f(\tilde{\theta}(t,x), \zeta, \tilde{\sigma}(t,x))$. As g and $\bar{m}$ are continuous ((A4), (A5)), $t \to \hat{f}(t,\zeta)$ is an algebraic composition of measurable functions and therefore measurable for all $\zeta \in \mathbb{R}^2$. The continuity of $\zeta \to \hat{f}(t,\zeta)$ for almost all $t \in [0,T]$ is seen immediately. In all, the Carathéodory conditions are fulfilled. The growth condition in (A.2.24) is also easily satisfied:

$$|\hat{f}_1(t,\zeta)| = |(1-\zeta_1-\zeta_2)g_{11}(\theta)g_{12}(\sigma)| \leq M(1+\sqrt{2}|\zeta|) = M + M\sqrt{2}|\zeta|, \quad (3.23)$$

$$\begin{aligned}|\hat{f}_2(t,\zeta)| &= |[\min\{\bar{m}(\theta), 1-\zeta_1\} - \zeta_2]_+ g_{21}(\theta)g_{22}(\sigma)| \\ &\leq (|\bar{m}(\theta)| + 1 + |\zeta_1| + |\zeta_2|)|g_{21}(\theta)||g_{22}(\sigma)| \leq 2M + \sqrt{2}M|\zeta| \end{aligned} \quad (3.24)$$

utilizing (A4) and (A5) where M is given by the boundedness of the g_{ij}. The existence of a solution $\zeta \in W^{1,1}(0,T;\mathbb{R}^2)$ to (3.22) then follows from the theorem of Carathéodory [67], (A.2.24). In a similar fashion the Lipschitz condition in (A.2.24) and therefore the uniqueness of solutions is obtained due to the boundedness of the g_{ij}.

The solutions to the ordinary differential equations for each x then define a function

$$\tilde{z} : [0,T]\times\Omega \to \mathbb{R}^2 \quad (3.25)$$

Due to

$$0 \leq (z_1+z_2)_t \leq (1-z_1-z_2)(g_{11}(\theta)g_{12}(\sigma) + g_{21}(\theta)g_{22}(\sigma)), \quad (3.26)$$

$z_1 + z_2 \in [0,1]$ almost everywhere and $z \in W^{1,\infty}(0,T;L^\infty(\Omega))$ bounded independently from θ and σ.
b) Consider the differential equation

$$\nabla z_t = f_\theta(\theta,z,\sigma)\nabla\theta + f_\sigma(\theta,z,\sigma)\nabla\sigma + f_z(\theta,z,\sigma)\nabla z \quad (3.27)$$

$$\nabla z(0) = 0 \quad (3.28)$$

for ∇z. The occuring terms exist according to assumption (A5) and Rademacher's theorem. Again we use Carathéodory's theorem to achieve a unique solution $\nabla z \in W^{1,1}(0,T;L^p(\Omega))$ to this ordinary differential equation. By Sobolev's embedding theorem we obtain the regularity $z \in L^\infty(0,T;L^p(\Omega))$.
c) Consider the difference

$$z_t^1 - z_t^2 = f(\theta^1, z^1, \sigma^1) - f(\theta^2, z^2, \sigma^2), \qquad (z^1 - z^2)(0) = 0. \tag{3.29}$$

By the Lipschitz continuity of f we have

$$|z^1 - z^2|_t \leq \Lambda_1|\theta^1 - \theta^2| + \Lambda_2|\sigma^1 - \sigma^2| + \Lambda_3|z^1 - z^2| \tag{3.30}$$

for some $\Lambda_1, \Lambda_2, \Lambda_3 \in \mathbb{R}$. After integration in time the requirements for Gronwall's lemma (e.g. in [14], (A.2.30)) are fulfilled and the proof is complete. □

Remark 3.31 *The statements in the foregoing Lemma 3.18 hold true also for non-zero initial value functions $x \mapsto z_0(x)$ satisfying*

$$z_0 \in L^\infty(\Omega), \qquad \nabla z_0 \in L^p(\Omega) \tag{3.32}$$

$$(z_0)_1 + (z_0)_2 \in [0,1] \quad \textit{for a.e. } (x,t) \in Q \tag{3.33}$$

and the occuring constants C, Λ_1, and Λ_2 do not depend on z_0.
This will be utilized in bootstrapping arguments (i.e. continuation on larger time intervals).

Remark 3.34 *∇z in Lemma 3.18 can be estimated by $\nabla\theta$ and $\nabla\sigma$ using Gronwall's lemma. Consider the pointwise boundary value problem for almost every $x \in \Omega$,*

$$\nabla z = \nabla z_0 + \int_0^t \nabla f(\theta, z, \sigma)ds = \nabla z_0 + \int_0^t (f_\theta \nabla\theta + f_z \nabla z + f_\sigma \nabla\sigma)ds. \tag{3.35}$$

Then

$$\begin{aligned} 0 \leq |\nabla z| &= |\nabla z_0 + \int_0^t \nabla f(\theta, z, \sigma)ds| \\ &\leq |\nabla z_0 + \int_0^t (f_\theta(\theta, z, \sigma)\nabla\theta + f_\sigma(\theta, z, \sigma)\nabla\sigma)ds| + |\int_0^t f_z(\theta, z, \sigma)\nabla z|ds \\ &\leq |\nabla z_0| + c_1 \int_0^T |\nabla\theta|ds + c_2 \int_0^T |\nabla\sigma|ds + c_3 \int_0^t |\nabla z| \end{aligned}$$

and application of Gronwall's lemma yields for almost every $x \in \Omega$

$$|\nabla z(x,t)| \leq c(x)\exp(c_3 t), \tag{3.36}$$

where $c(x) = |\nabla z_0| + c_1 \int_0^T |\nabla\theta| ds + c_2 \int_0^T |\nabla\sigma| ds$ *and* c_3 *is determined by the Lipschitz constant of* f*. Then*

$$\begin{aligned}
\|\nabla z\|_{L^\infty(0,T;L^p(\Omega))} &= ess\ \sup_t \left(\int_\Omega |\nabla z|^p dx \right)^{\frac{1}{p}} \\
&\leq ess\ \sup_t \left(\int_\Omega c^p(x) \exp(pc_3 t) dx \right)^{\frac{1}{p}} \\
&= ess\ \sup_t \exp(at) \left(\int_\Omega c^p(x) dx \right)^{\frac{1}{p}} \\
&\leq exp(c_3 T) \left(\|\nabla z_0\|_{L^p(\Omega)} + c_1 \| \int_0^T |\nabla\theta| ds \|_{L^p(\Omega)} + c_2 \| \int_0^T |\nabla\sigma| ds \|_{L^p(\Omega)} \right) \\
&\leq exp(c_3 T) \left(\|\nabla z_0\|_{L^p(\Omega)} + \tilde{c}_1 \|\nabla\theta\|_{L^p(Q)} + \tilde{c}_2 \|\nabla\sigma\|_{L^p(Q)} \right)
\end{aligned}$$

3.3.2 Elasticity equations with phase transformation

Elliptic systems have been analyzed to great extent under ever weaker assumptions. An introduction to common methods and an overview of existing theory is given for example in [30], [67], but also in many other books. Regarding linear elasticity, i.e. systems for non-scalar valued displacement functions, there exists a lot of literature for the case $p = 2$ for pure Dirichlet and also for mixed boundary conditions, a compehensive survey is given e.g. in [58].

The more recent research results deal with mixed boundary conditions, low assumptions regarding regularity of data functions and domain, and p in a neighbourhood of 2 or even $p = 3 + \delta$ for some small δ, where δ results from data and can not be chosen freely, see e.g. [39], [26], [3], [4], [60], [40] and the references therein. Unfortunately, to the author's knowledge, some useful results from scalar-valued elliptic theory for arbitrary, self-chosen $p > 1$ have not been transferred to tensor-valued theory, yet, see e.g. remark (3.43). Nevertheless, following the ways of other authors, as the general validity of such a theory is well-believed, it is not doubted here.

We continue with studying the solvability of (3.2a), (3.2b), and (3.2c). For this purpose, the following definition is given:

Definition 3.37

$$W_p^{k,r}(Q) := L^p(0,T; W^{k,p}(\Omega)) \cap W^{r,p}(0,T; L^p(\Omega)). \tag{3.38}$$

Recalling Remark 2.31, K is positive definite. Furthermore, Ω was introduced with C^∞-boundary. Therefore the following regularity results will be useful:

Lemma 3.39 *Let Ω be C^1 and let K be a positive definite tensor of fourth order. Then*

$$-div(K\varepsilon(u) - \tau) = \eta \quad \text{in } \Omega \tag{3.40}$$

$$u = 0 \quad \text{on } \partial\Omega \tag{3.41}$$

possesses a unique solution $u \in W^{1,p}(\Omega)$ and

$$\|u\|_{W^{1,p}(\Omega)} \leq c_1 \ \|\tau\|_{L^p(\Omega)} + c_2 \ \|\eta\|_{L^p(\Omega)} \tag{3.42}$$

with c_1 and c_2 independent from u, τ, and η.

Proof:
$(u, v) \mapsto \int_\Omega K\varepsilon(u) : \varepsilon(v)dx$ defines a coercive bilinear form on $W_0^{1,2}(\Omega)$ using Korn's inequality. By Valent [80], p. 66, we achieve that $u \mapsto div(K\varepsilon(u))$ is a homeomorphism of $W_0^{1,p}(\Omega)$ onto $W^{-1,p}(\Omega) \simeq W_0^{1,q}(\Omega)$ with any $1 < p < \infty$ and $\frac{1}{p} + \frac{1}{q} = 1$. This yields the existence of a unique solution u to (3.40), (3.41) and of a $c > 0$ independent from u, τ, and η, such that

$$\begin{aligned}
\|u\|_{W^{1,p}(\Omega)} &\leq c \ \|div \ \tau - \eta\|_{W^{-1,p}(\Omega)} \\
&= c \sup_{\substack{\zeta \in W_0^{1,q} \\ \|\zeta\|_{W^{1,q}(\Omega)} \leq 1}} |\langle div \ \tau - \eta, \zeta\rangle| \\
&\leq \sup_{\substack{\zeta \in W_0^{1,q} \\ \|\zeta\|_{W^{1,q}(\Omega)} \leq 1}} \left(c_1 \ \|\tau\|_{L^p(\Omega)}\|\varepsilon(\zeta)\|_{L^q(\Omega)} + c_2 \ \|\eta\|_{L^p(\Omega)}\|\zeta\|_{L^q(\Omega)}\right) \\
&\leq c_1 \ \|\tau\|_{L^p(\Omega)} + c_2 \ \|\eta\|_{L^p(\Omega)}
\end{aligned}$$

with c_1 and c_2 independent from u, τ, and η. □

Remark 3.43 *Unfortunately, the foregoing statement relies on a widely believed argument (see [80], A.2.34) which seems to be not completely proven up to now. In [80], it is shown that given an ellipticity condition of the bilinear form associated to the differential operator, a homeomorphism of $W_0^{1,2}(\Omega)$ and $W^{-1,2}(\Omega)$ and thereby unique solvability of system (3.40), (3.41) is given in a weak L^2 setting. Simader's methods allow a transfer of such results to L^p settings for $1 < p < \infty$ for scalar-valued functions u and it is quite possible but yet unproven that this is also possible for non-scalar-valued functions u or elliptic systems, respectively. See also [6], p.6, for a description of the available results. Like in this reference, we will act on the assumption that it is admissible to generalize the L^2 results to L^p as in the scalar-valued case.*

Lemma 3.44 *Let Ω be C^∞, K be a positive definite tensor of fourth order (with real-valued coefficients), and u be the solution of*

$$\begin{aligned} -div(K\varepsilon(u) - \tau) &= \eta \quad && \text{in } \Omega \\ u &= 0 && \text{on } \partial\Omega \end{aligned}$$

Then

$$\|u\|_{W^{k,p}(\Omega)} \leq c_1 \|\tau\|_{W^{k-1,p}(\Omega)} + c_2 \|\eta\|_{W^{k-2,p}(\Omega)} \tag{3.45}$$

holds for any $k \geq 2$ with constants c_1, c_2 independent from u. This is a conclusion of theorem 3.1.1 in [60].

Furthermore, we need the following standard result on convergence in different settings.

Lemma 3.46 *Let $1 \leq p \leq \infty$, $f_n, f \in L^\infty(E)$, $\|f_n\|_{L^\infty} \leq M$ for all $n \in \mathbb{N}$ with fixed $M \in \mathbb{R}$, and $\|f_n - f\|_{L^p(E)} \xrightarrow{n\to\infty} 0$. Then*

$$\|f_n - f\|_{L^q(E)} \xrightarrow{n\to\infty} 0 \qquad \text{for any } \ 1 \leq q < \infty.$$

Proof:
As $\|f_n - f\|_{L^p(E)} \xrightarrow{n\to\infty} 0$ we have $\|f_{n_k} - f\|_{L^p(E)} \xrightarrow{k\to\infty} 0$ for any subsequence $(f_{n_k})_{k\in\mathbb{N}}$ of $(f_n)_{n\in\mathbb{N}}$. Consider such a subsequence. By Weyl's lemma (A.2.4) there exists a subsubsequence $(f_{n_{k_r}})_{r\in\mathbb{N}}$ such that

$$f_{n_{k_r}} - f \xrightarrow{r\to\infty} 0 \quad a.e.$$

Furthermore, by $f_n \in L^\infty(E)$, $\|f_n\|_{L^\infty} \leq M$ for all $n \in \mathbb{N}$, we have

$$|f_n| \leq M \quad a.e., \qquad \text{in particular } \ |f_{n_{k_r}}| \leq M \quad a.e.$$

Lebesgue's Dominated Convergence Theorem A.2.42 then yields

$$\|f_{n_{k_r}} - f\|_{L^q(E)} \xrightarrow{r\to\infty} 0$$

for any $1 \leq q < \infty$. As the subsequence $(f_{n_k})_{k\in\mathbb{N}}$ was chosen arbitrarily, we have that for any $1 \leq q < \infty$ any subsequence of $(f_n)_{n\in\mathbb{N}}$ possesses itself a subsequence that converges towards f in $L^q(E)$. Therefore, also $(f_n)_{n\in\mathbb{N}}$ converges towards f in $L^q(E)$. □

Now we have the tools at hand to treat (3.2a), (3.2b), and (3.2c).

Lemma 3.47 *Let $\hat{\theta} \in W_p^{2,1}(Q)$, $4 < p < \infty$. Then the system of equations*

$$
\begin{aligned}
-\operatorname{div}\sigma &= F \quad \text{in } Q && \text{(3.48a)}\\
\sigma &= K\left(\varepsilon(u) - \beta(\hat{\theta}, z)I - \int_0^t \gamma(\hat{\theta}, z, z_s)\sigma^* ds\right) \quad \text{in } Q && \text{(3.48b)}\\
u &= 0 \quad \text{on } \partial\Omega \times (0,T) && \text{(3.48c)}\\
z_t &= f(\hat{\theta}, z, \sigma) \quad \text{in } Q && \text{(3.48d)}\\
z(0) &= 0 \quad \text{in } \Omega && \text{(3.48e)}
\end{aligned}
$$

has a unique solution (u, z) satisfying the estimates in (3.18) and

$$
\|u\|_{L^p(0,T;W^{2,p}(\Omega))} + \|u_t\|_{L^p(0,T;W^{1,p}(\Omega))} \le C_1 + C_2\|\hat{\theta}\|_{W_p^{2,1}(Q)}\,. \tag{3.49}
$$

Proof:
We will employ Schauder's fixed point theorem in terms of ([93], A.2.41). For this purpose we introduce the operator

$$
\mathcal{P} : L^p(Q) \longrightarrow L^p(Q)), \quad \hat{\sigma} \mapsto \sigma = \mathcal{P}(\hat{\sigma})\,, \tag{3.50}
$$

which maps right-hand side data $\hat{\sigma}$ to the weak solution σ of the linear problem

$$
\begin{aligned}
-\operatorname{div}\sigma &= F \quad \text{in } Q && \text{(3.51a)}\\
\sigma &= K\left(\varepsilon(u) - \beta(\hat{\theta}, z)I - \int_0^t \gamma(\hat{\theta}, z, z_s)\hat{\sigma}^* ds\right) \quad \text{in } Q && \text{(3.51b)}\\
u &= 0 \quad \text{on } \partial\Omega \times (0,T)\,, && \text{(3.51c)}
\end{aligned}
$$

where the function z is the solution of the ordinary differential equation

$$
z_t = f(\hat{\theta}, z, \hat{\sigma}) \quad \text{in } Q\,, \qquad z(0) = z_0 \quad \text{in } \Omega, \qquad z_0 \in L^p(\Omega). \tag{3.52}
$$

We want to find an appropriate nonempty, convex, and compact subset $\mathcal{M} \subset L^p(Q)$ such that $\mathcal{P}$ is continuous on $\mathcal{M}$ and $\mathcal{P}(\mathcal{M}) \subset \mathcal{M}$. To this end we consider data $\hat{\sigma} \in W_p^{1,1}(Q) \le M < \infty$, M will be specified later on. By definition of σ we have

$$
\begin{aligned}
\int_\Omega K\varepsilon(u) : \varepsilon(w)dx = \int_\Omega Fw dx + 3\kappa \int_\Omega \beta(\hat{\theta}, z)I : \varepsilon(w)dx\\
+ 2\mu \int_\Omega \int_0^t \gamma(\hat{\theta}, z, z_s)\hat{\sigma}^* ds : \varepsilon(w)dx\,.
\end{aligned} \tag{3.53}
$$

Now we want to utilize Lemma 3.44 with $\tau = 3b\beta(\hat{\theta}, z)I + 2\mu\int_0^t \gamma(\hat{\theta}, z, z_s)\hat{\sigma}^* ds$ and $\eta = F$. Due to (A6), the regularity condition for η is immediately given.

$\|\tau\|_{L^p(0,T;W^{1,p}(\Omega))}$ is finite because γ is Lipschitz continuous (therefore its partial derivatives are bounded a.e.). Further, the embedding

$$W_p^{1,1}(Q) \hookrightarrow L^\infty(Q) \tag{3.54}$$

holds for $p > 4$ due to Sobolev's embedding theorem (A.2.7) for dimension 4, where the weak derivative is given in terms of an augmented gradient which contains as fourth component the time derivative. In more detail, the single terms can be bounded by the given data as in the following. To estimate the $L^p(0,T;W^{1,p}(\Omega))$-norm of a function τ it suffices to evaluate the $L^p(Q)$-norms of τ and its spatial gradient $\nabla\tau$. This is the case due to

$$\begin{aligned}\|\tau\|^p_{L^p(0,T;W^{1,p}(\Omega))} &= \int_0^T \|\tau(t)\|^p_{W^{1,p}(\Omega)} dt \\ &= \int_0^T \left(\left(\int_\Omega |\tau(x,t)|^p + |\nabla\tau(x,t)|^p dx \right)^{\frac{1}{p}} \right)^p dt = \|\tau\|^p_{L^p(Q)} + \|\nabla\tau\|^p_{L^p(Q)},\end{aligned}$$

and therefore

$$\|\tau\|_{L^p(0,T;W^{1,p}(\Omega))} \leq c\ (\|\tau\|_{L^p(Q)} + \|\nabla\tau\|_{L^p(Q)}). \tag{3.55}$$

To exploit this estimate, the right hand side terms for the elasticity equation under considerations are analyzed. The expansion part is L^p-bounded by

$$\begin{aligned}&\|\beta(\hat\theta, z)\|_{L^p(Q)} = \|q(z)\hat\theta + q_0(z)\|_{L^p(Q)} \\ &\leq \|q(z)\hat\theta\|_{L^p(Q)} + \|q_0(z)\|_{L^p(Q)} \\ &\leq \|\hat\theta\|_{L^\infty(Q)} \|q(z)\|_{L^p(Q)} + \|q_0(z)\|_{L^p(Q)} \\ &= \|\hat\theta\|_{L^\infty(Q)} \left(\int_0^T \|q(z)\|_{L^p(\Omega)} dt \right)^{\frac{1}{p}} + \left(\int_0^T \|q_0(z)\|^p_{L^p(\Omega)} dt \right)^{\frac{1}{p}} \\ &\leq T^{\frac{1}{p}} \|\hat\theta\|_{L^\infty(Q)} \|q(z)\|_{L^\infty(0,T;L^p(\Omega))} + T^{\frac{1}{p}} \|q_0(z)\|_{L^\infty(0,T;L^p(\Omega))} < \infty.\end{aligned} \tag{3.56}$$

For its spatial derivative it holds,

$$\begin{aligned}&\|\nabla\beta(\hat\theta, z)\|_{L^p(Q)} = \|\nabla q(z)\hat\theta + q(z)\nabla\hat\theta + \nabla q_0(z)\|_{L^p(Q)} \\ &\leq \|\nabla q(z)\|_{L^p(Q)} \|\hat\theta\|_{L^\infty(Q)} + \|q(z)\|_{L^p(Q)} \|\nabla\hat\theta\|_{L^\infty(Q)} + \|\nabla q_0(z)\|_{L^p(Q)} \\ &\leq T^{\frac{1}{p}} \|\nabla q(z)\|_{L^\infty(0,T;L^p(\Omega))} \|\hat\theta\|_{L^\infty(Q)} + T^{\frac{1}{p}} \|q(z)\|_{L^\infty(0,T;L^p(\Omega))} \|\nabla\hat\theta\|_{L^\infty(Q)} \\ &\quad + T^{\frac{1}{p}} \|\nabla q_0(z)\|_{L^\infty(0,T;L^p(\Omega))} \qquad < \infty.\end{aligned}$$

Regarding the TrIP term we achieve

$$\begin{aligned}
&\|\int_0^t \gamma(\hat{\theta}, z, z_s)\hat{\sigma}^* ds\|_{L^p(Q)} = \left(\int_0^T \int_\Omega \left|\int_0^t \gamma(\hat{\theta}, z, z_s)\hat{\sigma}^* ds\right|^p dxdt\right)^{\frac{1}{p}} \\
&\leq \left(\int_0^T \int_\Omega \int_0^T \left|\gamma(\hat{\theta}, z, z_s)\hat{\sigma}^*\right|^p ds\ dx\ dt\right)^{\frac{1}{p}} \\
&= T^{\frac{1}{p}} \|\gamma(\hat{\theta}, z, z_s)\hat{\sigma}^*\|_{L^p(Q)} \leq c\ T^{\frac{1}{p}} \|\hat{\sigma}^*\|_{L^p(Q)} < \infty.
\end{aligned}$$

(Recall that γ is bounded on Q.)

∇z_s can be estimated by

$$\begin{aligned}
\|\nabla z_s\|_{L^p(Q)} &= \|\nabla f(\theta, z, \sigma)\|_{L^p(Q)} \\
&= \|f_\theta(\theta, z, \sigma)\nabla\theta + f_z(\theta, z, \sigma)\nabla z + f_\sigma(\theta, z, \sigma)\nabla\sigma\|_{L^p(Q)} \\
&\leq c_1\|\nabla\theta\|_{L^p(Q)} + c_2\|\nabla z\|_{L^p(Q)} + c_3\|\nabla\sigma\|_{L^p(Q)}. \qquad (3.57)
\end{aligned}$$

Using that γ is bounded and Lipschitz continuous and by Lemma 3.18 we then achieve

$$\begin{aligned}
&\|\nabla \int_0^t \gamma(\hat{\theta}, z, z_s)\hat{\sigma}^* ds\|_{L^p(Q)} \\
&= \|\int_0^t \left(\gamma_\theta(\hat{\theta}, z, z_s)\nabla\hat{\theta} + \gamma_z(\hat{\theta}, z, z_s)\nabla z + \gamma_{z_s}(\hat{\theta}, z, z_s)\nabla z_s\right)\hat{\sigma}^* ds \\
&\qquad + \int_0^t \gamma(\hat{\theta}, z, z_s)\nabla\hat{\sigma}^* ds\|_{L^p(Q)} \\
&\leq \|\int_0^t \gamma_\theta(\hat{\theta}, z, z_s)\nabla\hat{\theta}\ \hat{\sigma}^* ds\|_{L^p(Q)} + \|\gamma_z(\hat{\theta}, z, z_s)\nabla z\ \hat{\sigma}^* ds\|_{L^p(Q)} \\
&\qquad + \|\gamma_{z_s}(\hat{\theta}, z, z_s)\nabla z_s\ \hat{\sigma}^* ds\|_{L^p(Q)} + \|\int_0^t \gamma(\hat{\theta}, z, z_s)\ \nabla\hat{\sigma}^* ds\|_{L^p(Q)} \\
&\leq c_1 T^{\frac{1}{p}} \|\nabla\hat{\theta}\|_{L^p(Q)}\|\hat{\sigma}^*\|_{L^\infty(Q)} + c_2 T^{\frac{1}{p}} \|\nabla z\|_{L^p(Q)}\|\hat{\sigma}^*\|_{L^\infty(Q)} \\
&\qquad + c_3 T^{\frac{1}{p}} \|\nabla z_s\|_{L^p(Q)}\|\hat{\sigma}^*\|_{L^\infty(Q)} + c_4 T^{\frac{1}{p}} \|\nabla\hat{\sigma}^*\|_{L^p(Q)} \qquad < \infty.
\end{aligned}$$

In all, recalling Remark 3.31 the data $\tau = 3b\beta(\hat{\theta}, z)I + 2\mu\int_0^t \gamma(\hat{\theta}, z, z_s)\hat{\sigma}^* ds$ is

bounded in $L^p(0,T;W^{1,p}(\Omega))$ by

$$\begin{aligned}
&\|\tau\|_{L^p(0,T;W^{1,p}(\Omega))} = c\|\tau\|_{L^p(Q)} + c\|\nabla\tau\|_{L^p(Q)}\\
&\leq c_1 T^{\frac{1}{p}}\Big(\|\hat{\theta}\|_{L^\infty(Q)}\|q(z)\|_{L^\infty(0,T;L^p(\Omega))} + \|q_0(z)\|_{L^\infty(0,T;L^p(\Omega))}\Big)\\
&+ c_2 T^{\frac{1}{p}}\Big(\|\nabla q(z)\|_{L^\infty(0,T;L^p(\Omega))}\|\hat{\theta}\|_{L^\infty(Q)}\\
&\qquad + \|q(z)\|_{L^\infty(0,T;L^p(\Omega))}\|\nabla\hat{\theta}\|_{L^\infty(Q)} + \|\nabla q_0(z)\|_{L^\infty(0,T;L^p(\Omega))}\Big)\\
&+ c_3\ T\|\hat{\sigma}^*\|_{L^p(Q)} + c_4 T^{\frac{1}{p}}\|\nabla\hat{\theta}\|_{L^p(Q)}\|\hat{\sigma}^*\|_{L^\infty(Q)} + c_5 T^{\frac{1}{p}}\|\nabla z\|_{L^p(Q)}\|\hat{\sigma}^*\|_{L^\infty(Q)}\\
&+ c_6 T^{\frac{1}{p}}\|\nabla z_s\|_{L^p(Q)}\|\hat{\sigma}^*\|_{L^\infty(Q)} + c_7 T^{\frac{1}{p}}\|\nabla\hat{\sigma}^*\|_{L^p(Q)}\\
&\leq c_1 T^{\frac{1}{p}} q^*\|\hat{\theta}\|_{L^\infty(Q)} + c_2 T^{\frac{1}{p}} q^*\\
&+ c_3 T^{\frac{1}{p}}\|\hat{\theta}\|_{L^\infty(Q)} q^* exp(c_4 T)\Big(\|\nabla z_0\|_{L^p(\Omega)} + \|\nabla\hat{\theta}\|_{L^p(Q)} + \tilde{c}_5\|\nabla\hat{\sigma}\|_{L^p(Q)}\Big)\\
&+ c_6 T^{\frac{1}{p}} q^*\|\nabla\hat{\theta}\|_{L^\infty(Q)} + c_7 T^{\frac{1}{p}} q^* + c_8\ T\|\hat{\sigma}^*\|_{L^p(Q)} + c_9 T^{\frac{1}{p}}\|\nabla\hat{\theta}\|_{L^p(Q)}\|\hat{\sigma}^*\|_{L^\infty(Q)}\\
&+ c_{10} T^{\frac{1}{p}} exp(c_4 T)\Big(\|\nabla z_0\|_{L^p(\Omega)} + \|\nabla\hat{\theta}\|_{L^p(Q)} + \tilde{c}_{11}\|\nabla\hat{\sigma}\|_{L^p(Q)}\Big)\|\hat{\sigma}^*\|_{L^\infty(Q)}\\
&+ c_{12} T^{\frac{1}{p}}\Big(\|\nabla\hat{\theta}\|_{L^p(Q)} + \Big(\|\nabla z_0\|_{L^p(\Omega)} + \|\nabla\hat{\theta}\|_{L^p(Q)} + \tilde{c}_{13}\|\nabla\hat{\sigma}\|_{L^p(Q)}\Big)\\
&\qquad + \|\nabla\hat{\sigma}\|_{L^p(Q)}\Big)\|\hat{\sigma}^*\|_{L^\infty(Q)} + c_{14} T^{\frac{1}{p}}\|\nabla\hat{\sigma}^*\|_{L^p(Q)}\\
&\leq \tilde{c}_1(T) + \tilde{c}_2(T)\|\hat{\sigma}\|_{W_p^{1,1}(Q)} + \tilde{c}_3(T)\|\hat{\sigma}\|^2_{W_p^{1,1}(Q)},
\end{aligned} \tag{3.58}$$

where the $\tilde{c}_i(T)$ are continuous and strictly monotonic increasing with respect to T with bounded derivative, $\tilde{c}_i(0) = 0$, and depend only on fixed data (including Ω) and on $\hat{\theta}$ and ∇z_0. By Lemma 3.44 we achieve

$$\begin{aligned}
\|u\|_{L^p(0,T;W^{2,p}(\Omega))} \leq C_1\|F\|_{L^p(0,T;L^p(\Omega))} + C_2\Big(&\|\beta(\hat{\theta},z)\|_{L^p(0,T;W^{1,p}(\Omega))}\\
&+ \Big\|\int_0^t \gamma(\hat{\theta},z,z_s)\hat{\sigma}^* ds\Big\|_{L^p(0,T;W^{1,p}(\Omega))}\Big)
\end{aligned} \tag{3.59}$$

with independent, positive constants C_1 and C_2.
That is,

$$\|u\|_{L^p(0,T;W^{2,p}(\Omega))} \leq c_1\|F\|_{L^p(0,T;L^p(\Omega))} + \tilde{c}_2(T) + \tilde{c}_3(T)M + \tilde{c}_4(T)M^2. \tag{3.60}$$

We continue with an estimation of the time derivative u_t. It fulfills

$$\begin{aligned}
\int_\Omega K\varepsilon(u_t) : \varepsilon(w)dx = &\int_\Omega F_t w dx + 3\kappa\int_\Omega \beta_t(\hat{\theta},z) I : \varepsilon(w)dx\\
&+ 2\mu\int_\Omega \gamma(\hat{\theta},z,z_s)\hat{\sigma}^* ds : \varepsilon(w)dx\,.
\end{aligned} \tag{3.61}$$

Now we want to utilize Lemma 3.39 with $\tilde{\tau} = \tau_t = 3b\beta_t(\hat{\theta}, z)I + 2\mu\gamma(\hat{\theta}, z, z_s)\hat{\sigma}^*$ and $\tilde{\eta} = \eta_t = F_t$. The regularity condition for η is again satisfied by (A6). The addends of $\|\tau_t\|_{L^p(0,T;L^p(\Omega))}$ can be estimated in the following way.

$$\begin{aligned}
&\|\beta_t(\hat{\theta}, z)\|_{L^p(Q)} = \|\bar{q}z_t\hat{\theta} + q(z)\hat{\theta}_t + \bar{q}_r z_t\|_{L^p(Q)} \\
&= \|\bar{q}f(\hat{\theta}, z, \sigma)\hat{\theta} + q(z)\hat{\theta}_t + \bar{q}_r f(\hat{\theta}, z, \sigma)\|_{L^p(Q)} \\
&\leq q^* c_1 T^{\frac{1}{p}} \|\hat{\theta}\|_{L^\infty(0,T;L^p(\Omega))} + q^* \|z\|_{L^\infty(Q)} \|\hat{\theta}_t\|_{L^p(Q)} + q^* c_2 T^{\frac{1}{p}} \\
&\leq q^* c_1 T^{\frac{1}{p}} \|\hat{\theta}\|_{L^\infty(0,T;L^p(\Omega))} + q^* T \|z_t\|_{L^\infty(Q)} \|\hat{\theta}_t\|_{L^p(Q)} + q^* c_2 T^{\frac{1}{p}}
\end{aligned}$$

$$\begin{aligned}
&\|\gamma(\hat{\theta}, z, z_s)\hat{\sigma}^*\|_{L^p(Q)} \leq \|\gamma(\hat{\theta}, z, z_s)\|_{L^p(Q)} \|\hat{\sigma}^*\|_{L^\infty(Q)} \\
&\leq c T^{\frac{1}{p}} \|\gamma(\hat{\theta}, z, z_s)\|_{L^\infty(0,T;L^p(\Omega))} \|\hat{\sigma}^*\|_{L^\infty(Q)} \\
&\leq q^* c_1 T^{\frac{1}{p}} \|\hat{\theta}\|_{L^\infty(0,T;L^p(\Omega))} + q^* T \|z_t\|_{L^\infty(Q)} \|\hat{\theta}_t\|_{L^p(Q)} + q^* c_2 T^{\frac{1}{p}} \\
&\quad + c_3 T^{\frac{1}{p}} \|\gamma(\hat{\theta}, z, z_s)\|_{L^\infty(0,T;L^p(\Omega))} \|\hat{\sigma}^*\|_{L^\infty(Q)}.
\end{aligned}$$

Lemma 3.39 then yields

$$\begin{aligned}
\|u_t\|_{L^p(0,T;W^{1,p}(\Omega))} &\leq c_1 \|\beta_t(\hat{\theta}, z)I + \gamma(\hat{\theta}, z, z_t)\hat{\sigma}^*\|_{L^p(Q)} + c_3 \|F_t\|_{L^p(Q)} \\
&\leq \tilde{c}_1(T) q^* + \tilde{c}_2(T) \|\hat{\sigma}^*\|_{L^\infty(Q)} + c_3 \|F_t\|_{L^p(Q)}. \qquad (3.62)
\end{aligned}$$

Adding (3.60) and (3.62) we have

$$\begin{aligned}
\|\varepsilon(u)\|_{W_p^{1,1}(Q)} &\leq c_1 \|\beta(\hat{\theta}, z)I + \int_0^t \gamma(\hat{\theta}, z, z_s)\hat{\sigma}^* ds\|_{W_p^{1,1}(Q)} + c_2 \|F\|_{W^{1,p}(0,T;L^p(\Omega))} \\
&\leq \tilde{c}_1(T) + \tilde{c}_2(T) M + \tilde{c}_3(T) M^2 + \tilde{c}_4(T) q^* + \tilde{c}_5(T) \|\hat{\sigma}^*\|_{L^\infty(Q)} + c_0
\end{aligned}$$

Recalling (3.48b) we achieve

$$\|\sigma\|_{W_p^{1,1}(Q)} \leq c_0 + \tilde{c}_1(T) q^* + \tilde{c}_2(T) \|\hat{\sigma}^*\|_{L^\infty(Q)} \leq c_0 + \tilde{c}_1(T) \|\hat{\sigma}^*\|_{L^\infty(Q)} \qquad (3.63)$$

with a strictly monotonic increasing $\tilde{c}_1(\cdot)$ with bounded derivative, $\tilde{c}_1(0) = 0$, depending only on data.
By choosing M large enough (e.g. $M = 2c_0$) and T sufficiently small (e.g. such that $\tilde{c}_1(T) \leq \frac{1}{2}$) we have shown that the set

$$\mathcal{M} := \left\{ \sigma \in W^{1,1}(Q) \ ; \ \|\sigma\|_{W^{1,1}(Q)} \leq M \right\} \qquad (3.64)$$

is mapped into itself by $\mathcal{P}$. As $\mathcal{M}$ is nonempty, closed, convex and compact in L^p (see Rellich-Kondrachov's compactness theorem (A.2.13)), it only remains to be shown that $\mathcal{P}$ is continuous. Let $\hat{\sigma}^n \to \hat{\sigma}$ in $L^p(Q)$. By part c) of Lemma 3.18 we

obtain immediately that the sequence (z^n) of solutions to the ordinary differential equations

$$z_t^n = f(\hat{\theta}, z^n, \hat{\sigma}^n) \text{ in } Q, \qquad z^n(0) = z_0 \text{ in } \Omega, \tag{3.65}$$

converges in $W^{1,p}(0,T;L^p(\Omega))$ to the solution z of

$$z_t = f(\hat{\theta}, z, \hat{\sigma}) \text{ in } Q, \qquad z(0) = z_0 \text{ in } \Omega. \tag{3.66}$$

Consequently, by Lipschitz continuity of β and γ we have

$$\begin{aligned}\|\beta(\hat{\theta}, z^n) - \beta(\hat{\theta}, z)\|_{L^p(Q)} &= \left(\int_0^T \int_\Omega |\beta(\hat{\theta}, z^n) - \beta(\hat{\theta}, z)|^p dxdt\right)^{\frac{1}{p}} \\ &\leq \left(\int_0^T \int_\Omega \left(c_1|\hat{\theta} - \hat{\theta}| + c_2|z^n - z|\right)^p dxdt\right)^{\frac{1}{p}} = c\|z^n - z\|_{L^p(Q)} \to 0.\end{aligned}$$

Further, any subsequence $(z^{n'})_{n'=n_0'}^\infty$ of $(z^n)_{n=1}^\infty$ converges to z in $W^{1,p}(0,T;L^p(\Omega))$. By Weyl's theorem (A.2.4), the $W^{1,p}$-convergence of $(z^{n'})_{n'=n_0'}^\infty$ yields the existence of a subsequence $(z^{n_k'})_{k=1}^\infty$ such that

$$z^{n_k'} \to z, \quad z_t^{n_k'} \to z_t \quad a.e. \tag{3.67}$$

and thereby, due to the Lipschitz-continuity of γ,

$$\gamma(\hat{\theta}, z^{n_k'}, z_t^{n_k'}) \to \gamma(\hat{\theta}, z, z_t) \quad a.e. \tag{3.68}$$

In particular,

$$\gamma(\hat{\theta}, z^{n_k'}, z_t^{n_k'})\hat{\sigma}^* \to \gamma(\hat{\theta}, z, z_t)\hat{\sigma}^* \quad a.e. \tag{3.69}$$

By Lebesgue's Dominated Convergence Theorem (A.2.42) we then conclude

$$\|(\gamma(\hat{\theta}, z^{n_k'}, z_t^{n_k'}) - \gamma(\hat{\theta}, z, z_t))\hat{\sigma}^*\|_{L^p(Q)} \to 0. \tag{3.70}$$

As we have convergence towards the same limit value independently of the chosen subsequence $z^{n'}$, we achieve $\|(\gamma(\hat{\theta}, z^n, z_t^n) - \gamma(\hat{\theta}, z, z_t))\hat{\sigma}^*\|_{L^p(Q)} \to 0$ for the whole sequence. Hence,

$$\begin{aligned}&\|\gamma(\hat{\theta}, z^n, z_t^n)\hat{\sigma}^{n*} - \gamma(\hat{\theta}, z, z_t)\hat{\sigma}^*\|_{L^p(Q)} \\ &\leq \|(\gamma(\hat{\theta}, z^n, z_t^n) - \gamma(\hat{\theta}, z, z_t))\hat{\sigma}^*\|_{L^p(Q)} + \|\gamma(\hat{\theta}, z^n, z_t^n)(\hat{\sigma}^{n*} - \hat{\sigma}^*)\|_{L^p(Q)} \to 0.\end{aligned}$$

By Lemma 3.39 we then obtain the convergence of $\sigma^n = \mathcal{P}(\hat{\sigma}^n) \to \mathcal{P}(\hat{\sigma}) = \sigma$ in $L^p(Q)$ and thereby the $L^p(Q)$-continuity of $\mathcal{P}$ (actually one obtains convergence in L^q for any $q \geq 1$) and this completes the proof of existence for T small enough.

Due to 3.31 and the boundedness of occuring data, the solution can be continued to larger time intervals by bootstrapping and a solution on the whole time interval $[0,T]$ is achieved.

Uniqueness is obtained utilizing the stability estimates in lemma 3.72.
The inequality

$$\|u\|_{L^p(0,T;W^{2,p}(\Omega))} + \|u_t\|_{L^p(0,T;W^{1,p}(\Omega))} \leq C_1 + C_2\|\hat{\theta}\|_{W_p^{2,1}(Q)}\,. \tag{3.71}$$

is a corollary of the existence proof. □

Lemma 3.72 *Here we give a collection of stability estimates for the forthcoming investigations. If u (and according σ) is the solution of the foregoing problem in lemma 3.47 for bounded $\hat{\theta} \in W_p^{2,1}(Q)$, then*

$$\|\sigma\|_{L^p(Q)} \leq c_1\|F\|_{L^p(Q)} + c_2\|\hat{\theta}\|_{L^p(Q)} \tag{3.73}$$

and

$$\|\sigma\|_{W_p^{1,1}(Q)} \leq c_1 + c_2\|\hat{\theta}\|_{W_p^{1,1}(Q)}. \tag{3.74}$$

Regarding differences, if u^i (and according σ^i) is the solution of the foregoing problem for bounded $\hat{\theta}^i \in W_p^{2,1}(Q)$, $i = 1, 2$, then

$$\|\sigma^1 - \sigma^2\|_{L^p(Q)} \leq c(T)\|\hat{\theta}^1 - \hat{\theta}^2\|_{L^p(Q)} \tag{3.75}$$

*with $c(t)$ strictly monotonic increasing with bounded derivative, $c(0) = 0$.
Furthermore,*

$$\|u^1 - u^2\|_{W_p^{1,1}(Q)} \leq c\|\hat{\theta}^1 - \hat{\theta}^2\|_{L^p(Q)}, \tag{3.76}$$

and

$$\|divu_t^1 - divu_t^2\|_{L^p(Q)} \leq c\|\theta^1 - \theta^2\|_{W^{1,p}(0,T;L^p(\Omega))}. \tag{3.77}$$

Proof:
$\hat{\theta} \in W_p^{2,1}(Q)$ bounded implies the boundedness of σ. According to (A.2.34), we may estimate σ by

$$\begin{aligned}
\|\sigma\|_{L^p(\Omega)}^p &= \|K\varepsilon(u) - \beta(\theta, z)I - \int_0^t \gamma(\theta, z, z_s)\sigma^* ds\|_{L^p(\Omega)}^p \\
&\leq c_1 + c_2\|\beta(\theta, z)I + \int_0^t \gamma(\theta, z, z_s)\sigma^* ds\|_{L^p(\Omega)}^p \\
&\leq c_1 + c_2\|\beta(\theta, z)I\|_{L^p(\Omega)}^p + c_3\|\int_0^t \gamma(\theta, z, z_s)\sigma^* ds\|_{L^p(\Omega)}^p \\
&\leq c_1 + c_2\|\theta\|_{L^p(\Omega)}^p + c_3\int_0^t \|\sigma\|_{L^p(\Omega)}^p \\
&\leq c_1 + c_2\|\theta\|_{L^p(\Omega)}^p
\end{aligned}$$

using Gronwall's lemma. As in Lemma 3.47, it holds for almost every time t

$$\begin{aligned}
&\|\sigma(t)\|_{W^{1,p}(\Omega)} \\
&\quad = \|K\left(\varepsilon(u(t)) - \beta(\theta(t), z(t))I - \int \gamma(\theta(s), z(s), z_s(s))\sigma^*(s)ds\right)\|_{W^{1,p}(\Omega)} \\
&\quad \leq c_0 + c_1\|\varepsilon(u(t))\|_{W^{1,p}(\Omega)} + c_2\|\beta(\theta(t), z(t))\|_{W^{1,p}(\Omega)} \\
&\qquad\qquad + c_3\|\int \gamma(\theta(s), z(s), z_s(s))\sigma^*(s)ds\|_{W^{1,p}(\Omega)} \\
&\quad \leq c_1 + c_2\|\theta(t)\|_{W^{1,p}(\Omega)} + c_3\|\int_0^t \sigma(s)ds\|_{W^{1,p}(\Omega)} \\
&\quad \leq c_1 + c_2\|\theta(t)\|_{W^{1,p}(\Omega)} + c_3\int_0^t \|\sigma(s)\|_{W^{1,p}(\Omega)}ds,
\end{aligned}$$

thus, by Gronwall's lemma,

$$\|\sigma(t)\|_{W^{1,p}(\Omega)} \leq c_1 + c_2\|\theta(t)\|_{W^{1,p}(\Omega)}.$$

Moreover,

$$\begin{aligned}
\|\sigma_t(t)\|_{L_p(\Omega)} &\leq c_1 + c_2\|\theta(t)\|_{L_p(\Omega)} + c_3\|\theta_t(t)\|_{L_p(\Omega)} + c_4\|\sigma(t)\|_{L_p(\Omega)} \\
&\leq c_1 + c_2\|\theta(t)\|_{L_p(\Omega)} + c_3\|\theta_t(t)\|_{L_p(\Omega)} + c_4\|\theta(t)\|_{W^{1,p}(\Omega)}.
\end{aligned}$$

Finally, we achieve

$$\|\sigma\|_{W_p^{1,1}(Q)} \leq c_1 + c_2\|\theta\|_{W_p^{1,1}(Q)}.$$

Again using (A.2.34) and Young's inequality we compute for the difference $\sigma^1 - \sigma^2$:

$$\begin{aligned}
&\|\sigma^1 - \sigma^2\|^p_{L^p(\Omega)} \\
&\leq c\|\beta(\hat{\theta}^1, z^n)I - \beta(\hat{\theta}^2, z^2)I + \int_0^t \gamma(\hat{\theta}^1, z^1, z_s^1)\sigma^{1*}ds - \int_0^t \gamma(\hat{\theta}^2, z^2, z_s^2)\sigma^{2*}ds\|^p_{L^p(\Omega)} \\
&\leq c_1\|\hat{\theta}^1 - \hat{\theta}^2\|^p_{L^p(\Omega)} + c_2\int_0^t \|\sigma^1 - \sigma^2\|_{L^p(\Omega)}.
\end{aligned}$$

Applying Gronwall's lemma we obtain

$$\|\sigma^1 - \sigma^2\|_{L^p(Q)} \leq c(T)\|\hat{\theta}^1 - \theta^2\|_{L^p(Q)} \tag{3.78}$$

with $c(t)$ strictly monotonic increasing with bounded derivative, $c(0) = 0$. With this result at hand we can also make a statement about the time derivative to show the

estimate (3.76).

$$
\begin{aligned}
&\|u_t^1 - u_t^2\|_{W^{1,p}(\Omega)} \\
&\le c_1\|\beta_t(\theta^1, z^1) - \beta_t(\theta^2, z^2)\|_{L^p(\Omega)} + c_2\|\gamma(\theta^1, z^1, z_t^1)\sigma^{1*} - \gamma(\theta^2, z^2, z_t^2)\sigma^{2*}\|_{L^p(\Omega)} \\
&\le c_1 q^*\|f(\theta^1, z^1, \sigma^1)\theta^1 - f(\theta^2, z^2, \sigma^2)\theta^2\|_{L^p(\Omega)} + c_2 q^*\|z^1\theta_t^1 - z^2\theta_t^2\|_{L^p(\Omega)} \\
&\qquad + c_3 q^*\|f(\theta^1, z^1, \sigma^1) - f(\theta^2, z^2, \sigma^2)\|_{L^p(\Omega)} \\
&\qquad + c_4\|\gamma(\theta^1, z^1, z_t^1)\sigma^{1*} - \gamma(\theta^2, z^2, z_t^2)\sigma^{2*}\|_{L^p(\Omega)} \\
&\le c_1 q^*\|\theta^1 - \theta^2\|_{L^p(\Omega)} + c_2 q^*\|f(\theta^1, z^1, \sigma^1) - f(\theta^2, z^2, \sigma^2)\|_{L^p(\Omega)} \\
&\qquad + c_3 q^*\|\theta_t^1 - \theta_t^2\|_{L^p(\Omega)} + c_4 q^*\|(z^1 - z^2)\theta_t^2\|_{L^p(\Omega)} \\
&\qquad + c_5\|\gamma(\theta^1, z^1, z_t^1)\sigma^{1*} - \gamma(\theta^2, z^2, z_t^2)\sigma^{2*}\|_{L^p(\Omega)}
\end{aligned}
$$

With a little help from part c) of lemma 3.18 the estimate can be continued by

$$
q^*\|f(\theta^1, z^1, \sigma^1) - f(\theta^2, z^2, \sigma^2)\|_{L^p(\Omega)} \le q^*(c_1\|\theta^1 - \theta^2\|_{L^p(\Omega)} + c_2\|\sigma^1 - \sigma^2\|_{L^p(\Omega)}),
$$

$$
\begin{aligned}
q^*\|(z^1 - z^2)\theta_t^2\|_{L^p(\Omega)} &\le q^*\|(z^1 - z^2)\|_{L^\infty(\Omega)}\|\theta_t^2\|_{L^p(\Omega)} \\
&\le q^*\|(z^1 - z^2)\|_{W^{1,p}(\Omega)}\|\theta_t^2\|_{L^p(\Omega)} \\
&\le c(t)q^*\|\theta_t^2\|_{L^p(\Omega)}(\|\theta^1 - \theta^2\|_{W^{1,p}(\Omega)} + \|\sigma^1 - \sigma^2\|_{W^{1,p}(\Omega)}),
\end{aligned}
$$

$$
\begin{aligned}
&\|\gamma(\theta^1, z^1, z_t^1)\sigma^{1*} - \gamma(\theta^2, z^2, z_t^2)\sigma^{2*}\|_{L^p(\Omega)} \\
&= \|(\gamma(\theta^1, z^1, z_t^1) - \gamma(\theta^2, z^2, z_t^2))\sigma^{1*} + \gamma(\theta^2, z^2, z_t^2)(\sigma^{1*} - \sigma^{2*})\|_{L^p(\Omega)} \\
&\le \|\gamma(\theta^1, z^1, z_t^1) - \gamma(\theta^2, z^2, z_t^2)\|_{L^p(\Omega)}\|\sigma^{1*}\|_{L^\infty(\Omega)} \\
&\qquad + \|\gamma(\theta^2, z^2, z_t^2)\|_{L^\infty(\Omega)}\|\sigma^{1*} - \sigma^{2*}\|_{L^p(\Omega)} \\
&\le c_1\|\theta^1 - \theta^2\|_{L^p(\Omega)}\|\sigma^{1*}\|_{L^\infty(\Omega)} + c_2\|z^1 - z^2\|_{W^{1,p}(\Omega)}\|\sigma^{1*}\|_{L^\infty(\Omega)} \\
&\qquad + c_3\|\sigma^{1*} - \sigma^{2*}\|_{L^p(\Omega)} \\
&\le c_1\|\theta^1 - \theta^2\|_{L^p(\Omega)}\|\sigma^{1*}\|_{L^\infty(\Omega)} + (c_2 + c_3\|\sigma^{1*}\|_{L^\infty(\Omega)})\ \|\sigma^{1*} - \sigma^{2*}\|_{L^p(\Omega)}.
\end{aligned}
$$

Like above, utilizing lemma 3.39 and Gronwall's lemma, we gain

$$
\|u_t^1 - u_t^2\|_{W^{1,p}(\Omega)} \le c\|\theta^1 - \theta^2\|_{L^p(\Omega)} \tag{3.79}
$$

The estimate

$$
\|divu_t^1 - divu_t^2\|_{L^p(Q)} \le c\|\theta^1 - \theta^2\|_{W^{1,p}(0,T;L^p(\Omega))}.
$$

follows from

$$
\begin{aligned}
&\|u_t^1 - u_t^2\|_{W^{1,p}}(\Omega) \\
&\le c_1\|\beta(\theta^1, z^1)_t - \beta(\theta^2, z^2)_t\|_{L^p(\Omega)} + c_2\|\gamma(\theta^1, z^1, z_t^1)\sigma^{1*} - \gamma(\theta^2, z^2, z_t^2)\sigma^{2*}\|_{L^p(\Omega)} \\
&\le c_1\|q(z^1)_t\theta^1 - q(z^2)_t\theta^2 + q(z^1)\theta_t^1 - q(z_2)\theta_t^2 + z_t^1 - z_t^2\|_{L^p(\Omega)} \\
&\qquad + c_2\|\gamma(\theta^1, z^1, z_t^1)\sigma^{1*} - \gamma(\theta^2, z^2, z_t^2)\sigma^{2*}\|_{L^p(\Omega)} \\
&\le c_1\|\theta^1 - \theta^2\|_{L^p(\Omega)} + c_2\|z_t^1 - z_t^2\|_{L^p(\Omega)} + c_3\|\theta_t^1 - \theta_t^2\|_{L^p(\Omega)} + c_4\|z^1 - z^2\|_{L^p(\Omega)} \\
&\qquad + c_5\|\sigma^1 - \sigma^2\|_{L^p(\Omega)} + c_6\|\theta^1 - \theta^2\|_{L^p(\Omega)} + c_7\|\sigma^1 - \sigma^2\|_{L^p(\Omega)} \\
&\le c_1\|\theta^1 - \theta^2\|_{L^p(\Omega)} + c_2\|\theta_t^1 - \theta_t^2\|_{L^p(\Omega)} + c_3\|\sigma^1 - \sigma^2\|_{L^p(\Omega)} \\
&\le c_1\|\theta^1 - \theta^2\|_{L^p(\Omega)} + c_2\|\theta_t^1 - \theta_t^2\|_{L^p(\Omega)}.
\end{aligned}
$$

□

3.3.3 Complete model

Before we can show existence for the whole coupled system, we consider a slightly simplified model. The only difference to the complete system (3.2a) - (3.2h) is the replacement of $\gamma(\theta, z, z_t)|\sigma^*|^2$ by some fixed $H \in L^p(Q)$ in (3.81f). Afterwards, we have all tools at hand to treat the complete system.

Lemma 3.80 (Existence and uniqueness of a solution to a slightly simplified complete system)
The system

$$
\begin{aligned}
-\operatorname{div}\sigma &= F \quad \text{in } Q && \text{(3.81a)}\\
\sigma &= K\Big(\varepsilon(u) - \beta(\theta, z)I - \int_0^t \gamma(\theta, z, z_s)\sigma^* ds\Big) \quad \text{in } Q && \text{(3.81b)}\\
u &= 0 \quad \text{on } \partial\Omega \times (0,T) && \text{(3.81c)}\\
z_t &= f(\theta, z, \sigma) \quad \text{in } Q && \text{(3.81d)}\\
z(0) &= 0 \quad \text{in } \Omega && \text{(3.81e)}
\end{aligned}
$$

$$
\begin{aligned}
\alpha^\theta(\theta, \sigma, z)\theta_t - k\Delta\theta + 3bq(z)\theta \operatorname{div} u_t& \\
= h + \alpha^z(\theta, \sigma, z)\cdot z_t + H \quad \text{in } Q& && \text{(3.81f)}\\
-k\frac{\partial\theta}{\partial n} &= 0 \quad \text{on } \partial\Omega \times (0,T) && \text{(3.81g)}\\
\theta(0) &= \theta_0 \quad \text{in } \Omega\,. && \text{(3.81h)}
\end{aligned}
$$

with $H \in L^p(Q)$ possesses a unique solution.

The solution depends continuously on H.

Proof:
Again we want to apply a fixed point argument. For that purpose we define an operator $\mathcal{P}$ that maps $\hat{\theta} \in W_p^{2,1}(Q)$ to the solution θ of

$$\begin{aligned}
\rho c_p \theta_t - k\Delta\theta &= h - 3bq(\hat{z})\hat{\theta} div\hat{u}_t + 9b\hat{\theta}q(\hat{z})^2\hat{\theta}_t + q(\hat{z})tr(\hat{\sigma})\hat{\theta}_t \\
&\quad + \sum_i \Big(\rho L_i + 9bq(\hat{z})(q_i - q_0)\hat{\theta}^2 + 9bq(\hat{z})(q_i\theta_{i,ref} - q_0\theta_{0,ref})\hat{\theta} \\
&\qquad + ((q_i - q_0)\hat{\theta} + q_i\theta_{i,ref} - q_0\theta_{0,ref})tr(\hat{\sigma})\Big)\hat{z}_t^i + H \\
&=: B(\hat{\theta}, H) \qquad (3.82) \\
-k\frac{\partial\theta}{\partial n} &= 0 \qquad (3.83) \\
\theta(0) &= \theta_0 \qquad (3.84)
\end{aligned}$$

where $(\hat{\sigma}, \hat{z})$ is the solution to the equation system in Lemma 3.47 for $\hat{\theta}$. Standard regularity theory (see [54], chapter 4) tells that the solution θ of this linear parabolic problem is member of $W_p^{2,1}(Q)$ and satisfies

$$\|\theta_t\|_{L^p(Q)} + \|\theta\|_{L^p(0,T;W^{2,p}(\Omega))} \leq c\|B(\hat{\theta}, H)\|_{L^p(Q)} + \|\theta_0\|_{W^{2-\frac{2}{p},p}(\Omega)}. \qquad (3.85)$$

To show that $\mathcal{P}$ is a self mapping on some

$$\mathcal{M} = \{\eta \in W_p^{2,1}(Q)\ ;\ \|\eta\|_{W_p^{2,1}(Q)} \leq M\}, \qquad M \in \mathbb{R}_+$$

we consider the single right hand side terms of 3.85. The data functions h and H $\in L^p(Q)$ are constants. Furthermore,

$$\begin{aligned}
\|q(\hat{z})\hat{\theta} div\hat{u}_t\|_{L^p(Q)} &\leq \|q(\hat{z})\|_{L^\infty(Q)}\|\hat{\theta}\|_{L^\infty(Q)}\|div\hat{u}_t\|_{L^p(Q)} \\
&\leq cq^*\|\hat{\theta}\|_{W_p^{2,1}(Q)}\|div\hat{u}_t\|_{L^p(Q)} \leq cq^*\|\hat{\theta}\|_{W_p^{2,1}(Q)}(c_1 + c_2\|\hat{\theta}\|_{W_p^{2,1}(Q)}) \\
&\leq \tilde{c}_1 q^* M + \tilde{c}_2 q^* M^2.
\end{aligned}$$

In a similar fashion one obtains

$$\begin{aligned}
\|\hat{\theta}q(\hat{z})^2\hat{\theta}_t\|_{L^p(Q)} &\leq \tilde{c}q^{*2}\|\hat{\theta}\hat{\theta}_t\|_{L^p(Q)} \leq \tilde{c}q^{*2}\|\hat{\theta}\|_{L^\infty(Q)}\|\hat{\theta}_t\|_{L^p(Q)} \\
&\leq \tilde{c}q^{*2}\|\hat{\theta}\|_{W^{2,1}(Q)}\|\hat{\theta}_t\|_{L^p(Q)} \leq cq^{*2}M^2,
\end{aligned}$$

$$\begin{aligned}
\|q(\hat{z})tr(\hat{\sigma})\hat{\theta}_t\|_{L^p(Q)} &\leq \tilde{c}q^*\|tr(\hat{\sigma})\hat{\theta}_t\|_{L^p(Q)} \leq \tilde{c}q^*\|tr(\hat{\sigma})\|_{L^\infty(Q)}\|\hat{\theta}_t\|_{L^p(Q)} \\
&\leq \tilde{c}_1 q^*\|\hat{\theta}_t\|_{L^p(Q)} + \tilde{c}_2 q^*\|\hat{\theta}\|_{W_p^{2,1}(Q)}\|\hat{\theta}_t\|_{L^p(Q)} \leq \tilde{c}_1 q^* M + \tilde{c}_2 q^* M^2,
\end{aligned}$$

and

$$
\begin{aligned}
&\| \sum_i \Big(\rho L_i + 9bq(\hat{z})(q_i - q_0)\hat{\theta}^2 + 9bq(\hat{z})(q_i\theta_{i,ref} - q_0\theta_{0,ref})\hat{\theta} \\
&\qquad +((q_i - q_0)\hat{\theta} + q_i\theta_{i,ref} - q_0\theta_{0,ref})tr(\hat{\sigma})\Big)\, \hat{z}_t^i \|_{L^p(Q)} \\
&\le c_1 + c_2 q^* \|\hat{\theta}^2\|_{L^p(Q)} + c_3 q^* \|\hat{\theta}\|_{L^p(Q)} + c_4 q^* \|\hat{\theta} tr(\hat{\sigma})\|_{L^p(Q)} + c_5 q^* \|tr(\hat{\sigma})\|_{L^p(Q)} \\
&\le c_1 + c_2 q^* \|\hat{\theta}\|_{L^p(Q)} \|\hat{\theta}\|_{L^\infty(Q)} + c_3 q^* \|\hat{\theta}\|_{L^p(Q)} + c_4 q^* \|\hat{\theta}\|_{L^\infty(Q)} \|tr(\hat{\sigma})\|_{L^p(Q)} \\
&\quad + c_5 q^* \|tr(\hat{\sigma})\|_{L^p(Q)} \\
&\le c_1 + c_2 q^* \|\hat{\theta}\|_{L^p(Q)} \|\hat{\theta}\|_{L^\infty(Q)} + c_3 q^* \|\hat{\theta}\|_{L^p(Q)} + c_4 q^* \|\hat{\theta}\|_{L^\infty(Q)} \|tr(\hat{\sigma})\|_{L^p(Q)} \\
&\quad + c_5 q^* \|tr(\hat{\sigma})\|_{L^p(Q)} \\
&\le c_1 + c_2 q^* \|\hat{\theta}\|_{L^p(Q)} \|\hat{\theta}\|_{L^\infty(Q)} + c_3 q^* \|\hat{\theta}\|_{L^p(Q)} + c_4 q^* \|\hat{\theta}\|_{L^\infty(Q)} (c_6 + c_7 \|\hat{\theta}\|_{W_p^{2,1}(Q)}) \\
&\quad + c_5 q^* (c_8 + c_9 \|\hat{\theta}\|_{W_p^{2,1}(Q)}) \\
&\le c_1 + c_2 q^* M + c_3 q^* M^2.
\end{aligned}
$$

Hence, for q^* small and M large enough we have shown the self mapping property of $\mathcal{P}$. To prove contractivity of $\mathcal{P}$, let θ^i be the solution of the investigated problem according to right hand side data $\hat{\theta}^i$. The standard estimate applied on the difference gives

$$
\|\theta_t^1 - \theta_t^2\|_{L^p(Q)} + \|\theta^1 - \theta^2\|_{L^p(0,T;W^{2,p}(\Omega))} \le c \|B(\hat{\theta}^1, H) - B(\hat{\theta}^2, H)\|_{L^p(Q)}. \tag{3.86}
$$

We consider the single right hand side terms.

The constants h and $H \in L^p(Q)$ cancel out.

As the $W_p^{2,1}(Q)$-boundedness of $\hat{\theta}$ implies $W_p^{2,1}(Q)$-boundedness of u, and using (3.49), Lemma 3.72, we have

$$
\begin{aligned}
&\|q(\hat{z}^1)\hat{\theta}^1 div\hat{u}_t^1 - q(\hat{z}^2)\hat{\theta}^2 div\hat{u}_t^2\|_{L^p(Q)} \\
&\le \|q(\hat{z}^1)\hat{\theta}^1(div\hat{u}_t^1 - div\hat{u}_t^2)\|_{L^p(Q)} + \|(q(\hat{z}^1)\hat{\theta}^1 - q(\hat{z}^2)\hat{\theta}^2) div\hat{u}_t^2\|_{L^p(Q)} \\
&\le c_1 \|q(\hat{z}^1)\|_{L^\infty(Q)} \|\hat{\theta}^1\|_{L^\infty(Q)} \|div\hat{u}_t^1 - div\hat{u}_t^2\|_{L^p(Q)} + c_2 \|q(\hat{z}^1)\hat{\theta}^1 - q(\hat{z}^2)\hat{\theta}^2\|_{L^p(Q)} \\
&\le c_1 q^* \|\theta^1 - \theta^2\|_{W^{1,p}(0,T;L^p(\Omega))} + c_2 \|q(\hat{z}^1)\hat{\theta}^1 - q(\hat{z}^2)\hat{\theta}^2\|_{L^p(Q)} \\
&\le c_1 q^* \|\theta^1 - \theta^2\|_{W^{1,p}(0,T;L^p(\Omega))} + c_2 \|(q(\hat{z}^1) - q(\hat{z}^2))\hat{\theta}^1\|_{L^p(Q)} + c_3 \|q(\hat{z}^2)(\hat{\theta}^1 - \hat{\theta}^2)\|_{L^p(Q)} \\
&\le (cq^* + \tilde{c}(T)) \|\theta^1 - \theta^2\|_{W_p^{2,1}(Q)}.
\end{aligned}
$$

In a similar fashion one obtains

$$\begin{aligned}
&\|\hat\theta^1 q(\hat z^1)^2\hat\theta_t^1 - \hat\theta^2 q(\hat z^2)^2\hat\theta_t^2\|_{L^p(Q)}\\
&= \|\hat\theta^1 q(\hat z^1)^2(\hat\theta_t^1 - \hat\theta_t^2)\|_{L^p(Q)} + \|(\hat\theta^1 q(\hat z^1)^2 - \hat\theta^2 q(\hat z^2)^2)\hat\theta_t^2\|_{L^p(Q)}\\
&\le cq^*\|\hat\theta_t^1 - \hat\theta_t^2\|_{L^p(Q)} + \|(\hat\theta^1 q(\hat z^1)^2 - \hat\theta^2 q(\hat z^2)^2)\hat\theta_t^2\|_{L^p(Q)}\\
&\le c_1 q^*\|\hat\theta_t^1 - \hat\theta_t^2\|_{L^p(Q)} + c_2\|(q(\hat z^1)^2 - q(\hat z^2)^2)\hat\theta_t^1\|_{L^p(Q)} + c_3\|q(\hat z^2)^2(\hat\theta^1 - \hat\theta^2)\|_{L^p(Q)}\\
&\le cq^*\|\theta^1 - \theta^2\|_{W_p^{2,1}(Q)}.
\end{aligned}$$

$$\begin{aligned}
&\|q(\hat z^1)tr(\hat\sigma^1)\hat\theta_t^1 - q(\hat z^2)tr(\hat\sigma^2)\hat\theta_t^2\|_{L^p(Q)}\\
&= \|(q(\hat z^1)tr(\hat\sigma^1) - q(\hat z^2)tr(\hat\sigma^2))\hat\theta_t^1\|_{L^p(Q)} + \|q(\hat z^2)tr(\hat\sigma^2)(\hat\theta_t^1 - \hat\theta_t^2)\|_{L^p(Q)}\\
&= \|(q(\hat z^1) - q(\hat z^2))tr(\hat\sigma^1)\|_{L^\infty(Q)}\|\theta_t^1\|_{L^p(Q)} + \|q(\hat z^2)(tr(\hat\sigma^1 - tr(\hat\sigma^2))\|_{L^\infty(Q)}\|\theta_t^1\|_{L^p(Q)}\\
&\qquad + \|q(\hat z^2)tr(\hat\sigma^2)(\hat\theta_t^1 - \hat\theta_t^2)\|_{L^p(Q)}\\
&\le cq^*\|\hat\theta^1 - \hat\theta^2\|_{W_p^{2,1}(Q)}
\end{aligned}$$

And again utilizing similar mechanisms as above and in Lemma 3.72,

$$\begin{aligned}
&\|\sum_i \Big(\rho L_i + 9bq(\hat z^1)(q_i - q_0)(\hat\theta^1)^2 + 9bq(\hat z^1)(q_i\theta_{i,ref} - q_0\theta_{0,ref})\hat\theta^1\\
&\qquad\qquad +((q_i - q_0)\hat\theta^1 + q_i\theta_{i,ref} - q_0\theta_{0,ref})tr(\hat\sigma^1)\Big)\hat z_{i,t}^1\\
&- \sum_i \Big(\rho L_i + 9bq(\hat z^2)(q_i - q_0)(\hat\theta^2)^2 + 9bq(\hat z^2)(q_i\theta_{i,ref} - q_0\theta_{0,ref})\hat\theta^2\\
&\qquad\qquad +((q_i - q_0)\hat\theta^2 + q_i\theta_{i,ref} - q_0\theta_{0,ref})tr(\hat\sigma^2)\Big)\hat z_{i,t}^2\|_{L^p(Q)}\\
&\le c_1\|z_t^1 - z_t^2\|_{L^p(Q)} + c_2\|q(\hat z^1)(\hat\theta^1)^2 z_t^1 - q(\hat z^2)(\hat\theta^2)^2 z_t^2\|_{L^p(Q)}\\
&\qquad + c_3\|q(\hat z^1)\hat\theta^1 z_t^1 - q(\hat z^2)\hat\theta^2 z_t^2\|_{L^p(Q)} + c_4 q^*\|\hat\theta^1 z_t^1 - \hat\theta^2 z_t^2\|_{L^p(Q)}\\
&\qquad + c_5 q^*\|\hat\sigma^1 z_t^1 - \hat\sigma^2 z_t^2\|_{L^p(Q)}\\
&\le (\tilde c(T) + cq^*)\|\hat\theta^1 - \hat\theta^2\|_{W_p^{2,1}(Q)}.
\end{aligned}$$

Thus, for T and q^* small enough, we have shown contractivity

$$\|\theta^1 - \theta^2\|_{W_p^{2,1}(Q)} \le \Lambda\|\hat\theta^1 - \hat\theta^2\|_{W_p^{2,1}(Q)}, \qquad 0 < \Lambda < 1,$$

of $\mathcal{P} : \mathcal{M} \to \mathcal{M}$ on the closed, nonempty subset $\mathcal{M}$ of the complete metric space $W_p^{2,1}(Q)$. The conditions for Banachs's fixed point theorem are fulfilled and system (3.81a) - (3.81h) possesses a unique solution.

By a bootstrapping argument, the solution is extended to larger time intervals.

Utilizing the same estimates that have shown the contractivity of $\mathcal{P}$ for solutions θ^i (that is $\hat\theta^i = \theta^i$) to varying data H^i, the H^i are not eliminated in the standard regularity estimate and

$$\|\theta^1 - \theta^2\|_{W_p^{2,1}(Q)} \le c\|H^1 - H^2\|_{L^p(Q)}. \tag{3.87}$$

We thereby achieve the continuous dependance of the solution on H. □

Utilizing the foregoing lemmas of this chapter, 3.18, 3.47, and 3.80, we are now in position to formulate the existence result for the whole coupled system.

Theorem 3.88 Existence and uniqueness of a solution to the complete system (3.2a) - (3.2h)
The system (3.2a) - (3.2h) possesses a unique solution.

Proof:
Let $(\tilde{\sigma}, \tilde{z})$ be the solution of the system given in Lemma 3.47 according to a given temperature profile $\tilde{\theta} \in W_p^{2,1}(Q)$ and θ the solution of (3.81a) - (3.81h) for $H(\tilde{\theta}) := \gamma(\tilde{\theta}, \tilde{z}, \tilde{z}_t)|\tilde{\sigma}^*|^2$ according to Lemma 3.80.
Thereby an operator $\mathcal{P} : W_p^{2,1}(Q) \to W_p^{2,1}(Q),\ \mathcal{P} : \tilde{\theta} \mapsto \theta,$ is defined,

$$W_p^{2,1}(Q) \ni \tilde{\theta} \to (\tilde{\sigma}, \tilde{z}) \to \gamma(\tilde{\theta}, \tilde{z}, \tilde{z}_t)|\tilde{\sigma}^*|^2 = H(\tilde{\theta}) \to \theta \in W_p^{2,1}(Q).$$

To proceed with a fixed point argumentation, we introduce the nonempty, closed, convex, and L^p-compact subset

$$\mathcal{M} = \{\eta \in W_p^{2,1} \ ; \ \|\eta\|_{W_p^{2,1}(Q)} \leq M\}, \qquad M \in \mathbb{R}_+. \tag{3.89}$$

Inequality (3.75) yields boundedness of H by $\tilde{\theta}$,

$$\begin{aligned} \|H(\tilde{\theta})\|_{L^p(Q)} &= \|\gamma(\tilde{\theta}, \tilde{z}, \tilde{z}_t)|\tilde{\sigma}^*|^2\|_{L^p(Q)} \leq c\|\tilde{\sigma}\|^2_{L^{2p}(Q)} \\ &\leq c_1(T)\|F\|^2_{L^{2p}(Q)} + c_2(T)\|\tilde{\theta}\|^2_{L^{2p}(Q)} \leq M \end{aligned} \tag{3.90}$$

as the estimate (3.75) is also valid for L^{2p} data F and $\tilde{\theta}$. By the boundedness of $H(\hat{\theta})$ by $\hat{\theta}$ and adjusting T and M (possibly largening M and correspondingly reducing T) in the Banach fixed point argumentation in Lemma 3.80 if necessary, we achieve as a corollary of the proof of Lemma 3.80 the self mapping property $\mathcal{P}(\mathcal{M}) \subset \mathcal{M}$ for the system considered here.
Let now $\tilde{\theta}^n, \tilde{\theta} \in \mathcal{M}$ with $\|\tilde{\theta}^n - \tilde{\theta}\|_{L^p(Q)} \xrightarrow{n\to\infty} 0$.

First we see that $\tilde{\theta} \to \gamma(\tilde{\theta}, \tilde{z}, \tilde{z}_t)|\tilde{\sigma}^*|$ is continuous in $L^p(Q)$. By Lemma 3.47 we know that $\tilde{\sigma}$ depends continuously on $\tilde{\theta}$ in $L^q(Q)$ for any $q \geq 1$, in particular for $q = 2p$ and also from Lemma 3.47 we know that $\gamma(\tilde{\theta}^n, \tilde{z}^n, \tilde{z}^n_t) \to \gamma(\tilde{\theta}, \tilde{z}, \tilde{z}_t)$ in $L^p(Q)$. Consequently,

$$\begin{aligned} &\|\gamma(\tilde{\theta}^n, \tilde{z}^n, \tilde{z}^n_t)|\tilde{\sigma}^{n*}|^2 - \gamma(\tilde{\theta}, \tilde{z}, \tilde{z}_t)|\tilde{\sigma}^*|^2\|_{L^p(Q)} \\ &\leq \|\gamma(\tilde{\theta}^n, \tilde{z}^n, \tilde{z}^n_t)(|\tilde{\sigma}^{n*}|^2 - |\tilde{\sigma}^*|^2)\|_{L^p(Q)} + \|(\gamma(\tilde{\theta}^n, \tilde{z}^n, \tilde{z}^n_t) - \gamma(\tilde{\theta}, \tilde{z}, \tilde{z}_t))|\tilde{\sigma}^*|^2\|_{L^p(Q)} \\ &\leq c_1\||\tilde{\sigma}^{n*}|^2 - |\tilde{\sigma}^*|^2\|_{L^p(Q)} + c_2\|\gamma(\tilde{\theta}^n, \tilde{z}^n, \tilde{z}^n_t) - \gamma(\tilde{\theta}, \tilde{z}, \tilde{z}_t)\|_{L^p(Q)} \to 0. \end{aligned}$$

The solution operator $\mathcal{S} : H \mapsto \theta$ is continuous by the foregoing Lemma 3.80. Therefore, $\mathcal{P} : \tilde{\theta} \mapsto \theta$ is a composition of continuous functions in $L^p \to L^p$ and thereby itself continuous in that sense and we have shown the existence of a solution to system (3.2a) - (3.2h).

All estimates are valid on any subinterval $[t_1, t_2] \subset [0, T]$ without changing the occuring constants, therefore the solution can be extended to the whole time interval $[0, T]$ by a bootstrapping argument.

We now compare two solutions θ^1 and θ^2 to show that this solution is unique. From (3.87) in Lemma 3.80 for the system with variable H we already have the estimate

$$\|\theta^1 - \theta^2\|_{W_p^{2,1}(Q)} \leq c\|\gamma(\theta^1, z^1, z_t^1)|\sigma^{1*}|^2 - \gamma(\theta^2, z^2, z_t^2)|\sigma^{2*}|^2\|_{L^p(Q)}, \tag{3.91}$$

where z^i, σ^i are the solutions to the system in Lemma 3.47 for θ^i, $i = 1, 2$, respectively. As in the continuity proof we have

$$\begin{aligned}
&\|\gamma(\theta^1, z^1, z_t^1)|\sigma^{1*}|^2 - \gamma(\theta^2, z^2, z_t^2)|\sigma^{2*}|^2\|_L^p(Q) \\
&\leq c_1\||\sigma^{1*}|^2 - |\sigma^{2*}|^2\|_{L^p(Q)} + c_2\|\gamma(\theta^1, z^1, z_t^1) - \gamma(\theta^2, z^2, z_t^2)\|_{L^p(Q)} \\
&\leq c_1\|\sigma^1 - \sigma^2\|_{L^p(Q)} + c_2\|\theta^1 - \theta^2\|_{L^p(Q} \\
&\leq c\|\theta^1 - \theta^2\|_{L^p(Q}
\end{aligned}$$

Since $\theta^1(0) = \theta^2(0)$ we can proceed by

$$c\|\theta^1 - \theta^2\|_{L^p(Q} = c\|\int_0^t \theta_s^1 - \theta_s^2\|_{L^p(Q} = cT^{\frac{1}{p}}\|\theta_s^1 - \theta_s^2\|_{L^p(Q)}.$$

Thereby we obtain from 3.91

$$\|\theta_s^1 - \theta_s^2\|_{L^p(Q)} \leq \|\theta^1 - \theta^2\|_{W_p^{2,1}(Q)} \leq cT^{\frac{1}{p}}\|\theta_s^1 - \theta_s^2\|_{L^p(Q)}, \tag{3.92}$$

that is,

$$(1 - cT^{\frac{1}{p}})\|\theta_s^1 - \theta_s^2\|_{L^p(Q)} \leq 0 \tag{3.93}$$

Choosing $T > 0$ small enough we have $(1 - cT^{\frac{1}{p}}) > 0$ and we achieve

$$\|\theta_s^1 - \theta_s^2\|_{L^p(Q)} \leq 0 \tag{3.94}$$

and therefore $\theta^1 = \theta^2$ almost everywhere. This procedure can be repeated for further time intervals as again $\theta^1(T-\varepsilon) = \theta^2(T-\varepsilon)$ for some infinitesimal $\varepsilon > 0$. There is no change in the occuring constants in the estimate, so the length of the continuation interval does not shorten. We obtain $\theta^1 = \theta^2$ almost everywhere for the whole time interval and uniqueness is proven.

□

3.4 Boundary conditions in the momentum balance

Throughout the statements in this section, pure Dirichlet boundary conditions were imposed. Those are convenient for the mathematical analysis but do not reproduce the physical reality well, because usually only parts of the workpiece are clamped. Unfortunately, piecewise clamping (that is, mixed Dirichlet-Neumann boundary conditions) is difficult for the mathematical theory, as they do not describe elliptic systems. But also pure Neumann conditions (more precisely: Dirichlet conditions only on a part of the boundary with measure zero) are of interest when one wants to investigate the effects of heating and phase transformations untroubled by the influence of the clamping. These boundary conditions are covered by the elliptic theory as in Agmon, Douglis, Nirenberg [3], [4] (again confronted with the issue that parts are proven only for scalar systems explicitly). Mathematically, this leads to ambiguous displacements, there is more than one solution to the elasticity system with pure Neumann conditions. One can get by this ambiguity by passing from V to the quotient space $\dot{V} = V \backslash \mathcal{R}$, where $\mathcal{R}$ denotes the set of *infinitesimal* rigid body motions,

$$\mathcal{R} := ker(\varepsilon) = \{v \ ; \ v(x) = a + b \wedge x, \ a, b \in \mathbb{R}^3\}. \tag{3.95}$$

Please bear in mind that this common notion of rigid body motions could collide with the intuitive understanding – in particular as some authors drop the word *infinitesimal* in front. For example, a (non-trivial) rotation in a 2D plane strain situation does not belong to this class of displacements, i.e. $\varepsilon(u) \neq 0$ for $u(x) = \begin{pmatrix} \cos(\alpha)x_1 - \sin(\alpha) - x_1 \\ \sin(\alpha)x_1 + \cos(\alpha)x_2 - x_2 \\ 0 \end{pmatrix}$, such a u does not describe an infinitesimal displacement if $\cos(\alpha) \neq 1$. Note furthermore, that $\tilde{\varepsilon}(u) = 0$ is very well fulfilled if we take u as above and $\tilde{\varepsilon}$ the nonlinear strain tensor in (2.11). This corresponds to the fact that, strictly speaking, *linear elasticity* is a little confusingly used term for *linearized elasticity*. We do not have a linear model but only approximately linear behaviour for small deformations. (Pure translations, however, may take arbitrarily large values, also in the linearized context.)

To have a consistent theory in the quotient space, one has to investigate the right hand side terms see (3.60) on page 119 in [25].

$$-div(K\varepsilon(u) - \eta) = F, \qquad (K\varepsilon(u) - \eta)n = 0 \tag{3.96}$$

is equivalent to

$$-div(K\varepsilon(u)) = F - div(\eta), \qquad (K\varepsilon(u))n = \eta n. \tag{3.97}$$

Simple manipulation of the right hand side terms yields

$$\int_\Omega (F - div(\eta))\varphi dx + \int_\Gamma \eta n \varphi da = \int_\Omega F\varphi dx + \int_\Omega \eta : \varepsilon(\varphi) dx.$$

So, using (3.60) on page 119 in [25], we end up with the condition

$$\int_\Omega F\varphi dx + \int_\Omega \eta : \varepsilon(\varphi) dx = 0 \qquad \forall \varphi \in \mathcal{R}.$$

Therefore another assumption on F is needed,

Assumption 3.98

$$\int_\Omega F\varphi dx = 0 \qquad \forall \varphi \in \mathcal{R}.$$

Concerning norms, we have

$$\|u\|_{\dot{V}} = \inf_{r \in \mathcal{R}(\Omega)} \|u + r\|_V, \tag{3.99}$$

in particular,

$$\|u\|_{\dot{W}^{k,p}(\Omega)} = \inf_{r \in \mathcal{R}(\Omega)} \|u + r\|_{W^{k,p}(\Omega)}. \tag{3.100}$$

The coupling terms in the complete system (3.2a) - (3.2h) which contain expressions in u (or σ) are invariant to rigid body motions, therefore the solution to the system (or their single equations) is not altered if translations or rotations are added. The analysis of the system can be accomplished in the usual setting using representatives in heat equation and phase rate laws.

3.5 Boundary conditions in the heat equation

The typical experimental or industrial heat treatment process includes the application of external cooling, e.g. nozzles emitting a liquid or gas onto the workpiece surface which raises its heat release. Therefore one would rather consider Newton type boundary conditions in the heat equation,

$$-k\frac{\partial \theta}{\partial n} = \alpha(x,t)(\theta - \theta_{\text{amb}}),$$

where α denotes the heat transfer coefficient and θ_{amb} the ambient temperature.

For reasons of simplicity, this case was not considered throughout the discussion of existence, but could be covered by analogous argumentation. According to chapter 4, §9, in the book of Ladyzhenskaya, Solonnikov, and Ural'ceva, [54], linear heat equation problems can be solved with both Dirichlet or Robin (mixed type, Newton

heat transfer) boundary conditions. The standard regularity result (3.85) for the solution carries over as well, only extended by a constant value coming from the heat transfer and the ambient temperature. Singular indices p vary for different boundary conditions, where for Dirichlet boundary condition $\frac{3}{2}$ is singular, for Robin boundary conditions it is $p = 3$. In any case, as we only consider integration indices $p > 4$, this does not affect the work presented in this thesis.

Chapter 4

Implementation

4.1 Model specifications

The complete model (3.1) has many coupling terms and rather complicated coefficient functions. For the numerical computations with inserted real world parameter values this large complexity is reduced. In particular, terms which turn out to be very small compared to the other occuring quantities are omitted. Volume forces like gravity were neglected. Coefficient functions of state derivatives are taken as constants to achieve a semilinear system. Furthermore, only those nonlinearities are included which behave linear in a context where only one respective state component is taken variable and the others as fixed data. That is, terms like $\gamma(\theta, z, z_t)|\sigma^*|^2$, which is quadratic in the single state component σ, are omitted, whereas $\beta(\theta, z) = q(z)\theta + q_r(z)$, which is linear with respect to z and θ, respectively, is still included. The terms linear in this sense are the ones which are intuitively relevant for the system behaviour and which are also found in thermomechanical phase transition models that were obtained without the formal approach presented in section 2.2.3. In the end, the restriction on such terms gives the opportunity to perform the semi-implicit iteration schemes which will be presented later on.

Accordingly, a numerical scheme for the following equation system was implemented:

Problem 4.1

$$-\operatorname{div}\sigma = 0 \quad in \quad Q \tag{4.2a}$$

$$\sigma = K\Big(\varepsilon(u) - \beta(\theta, z)I - \varepsilon^{tp}\Big) \tag{4.2b}$$

$$= \lambda tr(\varepsilon(u))I + 2\mu\varepsilon(u) - 3b\beta(\theta, z)I - 2\mu\varepsilon^{tp} \quad in \quad Q \tag{4.2c}$$

$$u_i = 0 \quad on \quad \Gamma_D^i \times (0,T), \quad \sigma n = 0 \quad on \quad \partial\Omega \times (0,T) \tag{4.2d}$$

$$\varepsilon_t^{tp} = \gamma(\theta, z, z_t)\sigma^* \quad in \quad Q \tag{4.2e}$$

$$\varepsilon^{tp}(0) = 0 \quad in \quad \Omega \tag{4.2f}$$

$$z_t = f(\theta, z, \sigma) \quad in \quad Q \tag{4.2g}$$

$$z(0) = 0 \quad in \quad \Omega \tag{4.2h}$$

$$\varrho c_p \theta_t - k\Delta\theta = h \quad in \quad Q \tag{4.2i}$$

$$-k\frac{\partial\theta}{\partial n} = \alpha(x,t)(\theta - \theta_{amb}) \quad on \quad \partial\Omega \times (0,T) \tag{4.2j}$$

$$\theta(0) = \theta_0 \quad in \ \Omega\,. \tag{4.2k}$$

The right hand side TrIP term $\int_0^t \gamma(\theta, z, z_s)\sigma^* ds$ is here replaced by a variable ε^{tp} which is determined by an additional ordinary differential equation. This equivalent formulation better reflects the numerical treatment. In the following we will have a closer look at the specific realizations of the parameter functions involved in the single equations.

We equip the heat equation with Newton type boundary conditions,

$$-k\frac{\partial\theta}{\partial n} = \alpha(x,t)(\theta - \theta_{\text{amb}}),$$

where θ_{amb} denotes the ambient temperature. θ_{amb} is taken as a constant. This might be a simplification of the physical reality, because changes in the ambient medium resulting from the workpieces heat release are neglected. But we have heat treatments in mind that include the application of a quenchant which is continously renewed during the quenching process, i.e. nozzles emitting gas coming from an attached inlet. This is unlike the use of a quenching container which in advance was filled with a liquid or a gas that remains in there and heatens up. Therefore this simple approach is reasonable. According to the typical quenching procedure employing cooling jets, the heat transfer coefficient α is in the following usually given by a time-variant spatially gaussian profile and depends in the experimental setup on the volume of spray water or gas hitting the workpiece surface. Again, this predefined shape of α is a simplification, see [2] and [20] for a discussion on the need of employing fluid dynamics to determine the heat transfer coefficient in (gas) quenching processes.

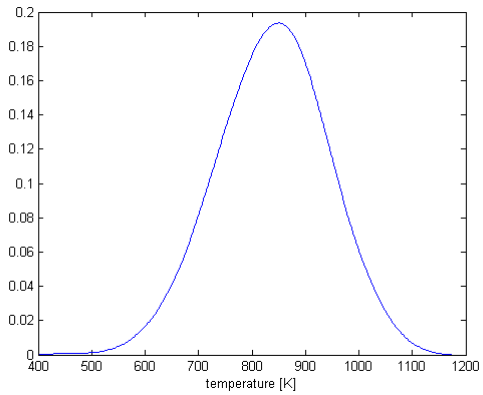

Figure 4.1: Sample data function $g_{11}(\theta)$.

In chapter 2 general phase evolution laws (2.5a) – (2.5c) for pearlite fraction z_1 and martensite fraction z_2 were introduced as

$$\begin{aligned} \dot{z}_1 &= f_1(\theta, z, \sigma) = (1 - z_1 - z_2) g_{11}(\theta) g_{12}(\sigma) \\ \dot{z}_2 &= f_2(\theta, z, \sigma) = [\min\{\bar{m}(\theta), 1 - z_1\} - z_2]_+ g_{21}(\theta) g_{22}(\sigma) \\ z_i(0) &= 0 \quad i = 1, 2. \end{aligned}$$

Typically, the data function $g_{11}(\theta)$, which describes the temperature dependency of the pearlite growth rate, is given as an interpolation of data obtained by Time-Temperature-Transformation diagrams (see (2.2.1) in the Appendix for details) and has a shape comparable to figure 4.1. Due to the fact that the martensite transformation happens almost instantaneously, the growth rate terms in the martensite equation are usually set to some large constant value. The important term in the martensite transformation law is $[\min\{\bar{m}(\theta), 1 - z_1\} - z_2]_+$ which is non-zero if both the amount $\bar{m}(\theta)$ is larger than the actual martensite fraction and there is still austenite left to transform. $\bar{m}$ is kind of a metastable equilibrium function and shaped like a backward S, i.e. antisigmoidal, see figure 4.2 for an easy example. M_f denotes the martensite finish temperature, at this and lower temperatures all remaining austenite is transformed into martensite. At martensite start temperature M_s and above no austenite is turned into martensite. During a cooling process, when M_s is reached, the martensite transformation starts and continues until M_f is reached. Inbetween, the maximal amount of martensite depends monotonously on temperature.

The remaining data function g_{12} was taken constant for the numerical computations within this thesis.

Regarding the equilibrium function in the trip term, we followed the approach

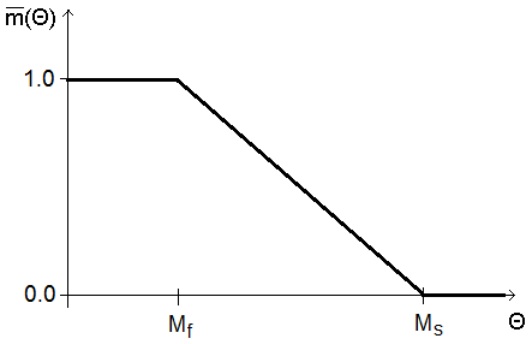

Figure 4.2: Sample data function $m_{eq}(\theta)$.

of Fischer, Sun, Tanaka ([32]) as cited in Wolff, Böhm [86] and considered functions

$$\gamma(\theta, z, z_t) = \frac{3}{2}\zeta \sum_i z_t^i \tag{4.3}$$

with a Greenwood-Johnson parameter ζ. Transformation induced plasticity, just like classical plasticity for pressure-resistant materials like steel, is assumed to be volume-preserving, see e.g. Wolff, Böhm [85], or Suhr, [77]. Therefore, it holds

$$tr(\varepsilon^{tp}) = 0. \tag{4.4}$$

Utilizing this condition, Hooke's law for the additive decomposition of the strain (2.28), and the bulk modulus $b = \frac{1}{3}(2\mu + 3\lambda)$, we achieve

$$\begin{aligned}\varepsilon^{tp} &= \frac{3}{2}\zeta \int_0^t (\sum_i z_t^i)\sigma^* ds = \frac{3}{2}\zeta \int_0^t (\sum_i z_t^i)(\lambda tr(\varepsilon)I + 2\mu\varepsilon - 3b\delta(z,\theta)I - 2\mu\varepsilon^{tp})^* ds \\ &= 3\zeta \int_0^t (\sum_i z_t^i)(\mu\varepsilon(u) - \frac{1}{3}\mu tr(\varepsilon(u))I - \mu\varepsilon^{tp}).\end{aligned}$$

This yields the following rule for the time derivative of ε^{tp},

$$\varepsilon_t^{tp} = \frac{3}{2}\zeta \sum_i z_t^i \sigma^* = -3\mu\zeta \sum_i z_t^i \varepsilon^{tp} + 3\mu\zeta \sum_i z_t^i \varepsilon^*, \tag{4.5}$$

$$\varepsilon^{tp}(0) = 0. \tag{4.6}$$

By the linear correspondence

$$\sigma^{tp} = -2\mu\varepsilon^{tp}$$

of TrIP stress and TrIP strain one can just as well formulate an ordinary differential

equation for the TrIP stress,

$$\begin{aligned}\sigma_t^{tp} &= -3\mu\zeta \sum_i z_t^i \sigma^* = -3\mu\zeta \sum_i z_t^i (\sigma^{el,*} + \sigma^{th,*} + \sigma^{tp,*}) \\ &= -3\mu\zeta \sum_i z_t^i (\sigma^{el,*} + \sigma^{tp}), \qquad (4.7)\end{aligned}$$

$$\sigma^{tp}(0) = 0. \qquad (4.8)$$

4.2 Discretization

At WIAS, the finite volume / finite element toolbox *WIAS-pdelib* (see [34]) is developped. Not being a black box commercial tool, pdelib enables the implementation of coupled physical models according to specific needs. The software package was used to set up and solve a numerical scheme based on linear finite elements. As a mechanical system is considered, quadratic finite elements would have been a better choice, but were not available in *pdelib* at the time of implementation. The numerical implementations in this thesis were done in collaboration with Wolf Weiss (WIAS Berlin) and benefits from fundamental components that were implemented during recent years by researchers from WIAS Berlin, among them Timo Streckenbach.

One purpose of the numerical computations is the solution of an optimal control problem, see chapter 5. This requires that the state equations are solved repeatedly, for example to obtain a optimal control by a gradient based method. The solution of the full 3D system ist too costly for repeated solving, therefore we want to consider 2D problems as well. The 2D model and the respective computations will be used as a first approximation to the real process. Unfortunately, the experiment we want to simulate does not allow an equivalent 2D representation. In 4.3 we will consider in how far an approximation by 2D computations could be given.

The system of partial and ordinary differential equations (4.2a) – (4.2k) is discretized solving the single state equations alternately where the state values of the other equations are treated as data. Concerning parabolic differential equations, we apply a semidiscretization approach, namely the horizontal method of lines (Rothe's method), see e.g. [67], [52]. Time derivatives are replaced by difference quotients to solve the parabolic state equation by using one-step procedures in time and the Finite Element Method to solve the stationary system that delivers the time increment.

The time interval $[0, T]$ is split equidistantly by discretization points

$$t_0,\ t_1,\ ..,t_{N_T}, \qquad \text{with } t_k = kh_T, \quad h_T = \frac{T}{N_T}.$$

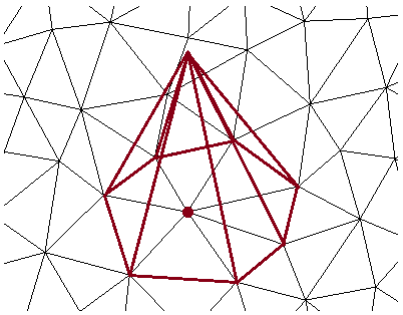

Figure 4.3: 2D linear shape function

For the sake of a stable method which is immune to oscillations, for the heat and TrIP equation implicit Euler schemes were applied. (Or rather *semi-implicit* schemes, in a sense, that the iteration scheme is implicit with respect to the single state variable under consideration but not with respect to the whole system. Coupling state variables may stem from the preceding time-step.) The discretization of the two- or three-dimensional workpiece geometry was done by triangulation tools, i.e. TetGen ([74]) for 3D and Triangle ([71]) for 2D geometries. Both mesh generators create irregular grids by default.

Furthermore, standard linear finite element shape and test functions were utilized. The according finite element space V_h is given as $\text{span}(\varphi_1, .., \varphi_n)$, where φ_i is the "hat function" belonging to mesh node i, see figure 4.3 and any of the following references for an explanation. A general overview on the numerical treatment of elliptic and parabolic partial differential equations including variant approaches besides the finite element method, namely finite difference and finite volume methods, can be found in the textbook by Knabner and Angermann, [52]. An extensive introduction into the finite element method with special emphasis on mechanical problems is given in the textbook by Braess, [13]. For a detailed description of finite element methods including hands-on implementation issues, also the book of Schmidt and Siebert about the finite element toolbox ALBERTA is recommended, [69]. Apart from the elaboration of finite element concepts, this book helps to understand many implementation aspects that are also relevant for working with the finite volume / finite element toolbox pdelib.

We will now focus on the discretization of the single equations, where coupling state variables are treated as data.

4.2.1 Heat equation

The spatially weak formulation of (4.2i)-(4.2k) reads $\forall\ \varphi \in H^1(\Omega),\ \forall\ t\dot{\in}[0,T]$

$$\int_\Omega \varrho c_p \theta_t \varphi dx dt + \int_\Omega k\nabla\theta\nabla\varphi dx dt = \int_\Gamma \alpha(x,t)(\theta - \theta_{\text{amb}})\varphi da dt$$
$$\theta(0) = \theta_0 \in L^2(\Omega).$$

($\forall\ t\dot{\in}[0,T]$ meaning "for almost every $t \in [0,T]$".)

It is first discretized with respect to time,

$$\int_\Omega \varrho c_p \frac{\theta^{k+1} - \theta^k}{h_T}\varphi dx + \int_\Omega k\nabla\theta^r\nabla\varphi dx = \int_\Gamma \alpha(x,t)(\theta^{k+1} - \theta_{\text{amb}})\varphi da,$$
$$\theta^0 = \theta_0 \quad \text{in } \Omega\,,$$

where θ_k denotes the temperature data point at time point t_k, $\theta_k \approx \theta(t_k)$. The indices r, r' could be chosen either as k or $k+1$ and were both taken as $k+1$ for the implicit time stepping scheme. For the finite element method, we use the same basis for the finite dimensional subspaces of both the test space and the trial space. This yields N_T linear equation systems

$$\left(\varrho c_p \left(\int_\Omega \varphi_i\varphi_j dx\right)_{j,i=1,..,n} + h_T\ k\left(\int_\Omega \nabla\varphi_i\nabla\varphi_j dx\right)_{j,i=1,..,n}\right.$$
$$\left. -h_T\left(\int_\Gamma \tilde{\alpha}(t_{k+1})\varphi_i\varphi_j da\right)_{j,i=1,..,n}\right)\vec{\theta}^{k+1}$$
$$= \varrho c_p \left(\int_\Omega \varphi_i\varphi_j dx\right)_{j,i=1,..,n}\vec{\theta}^{k} - h_T\left(\int_\Gamma \tilde{\alpha}(t_{k+1})\theta_{\text{amb}}\varphi_j da\right)_{j,i=1,..,n},\ k = 0,..,N_T-1,$$
$$\theta^0 = \theta_0,$$

in θ^{k+1}. Solving these equations iteratively with respect to k corresponds to an implicit time-stepping scheme, where in each time step a stationary problem is solved.

4.2.2 Phase equations

Several update rules for the phase transitions were applied, among them the explicit Euler scheme and the fourth-order-Runge-Kutta method. If one wants to apply an implicit scheme, one could proceed as follows. The pearlite fraction z_1 can be updated implicitly by

$$z_1^{k+1} = \frac{1}{1 + h_T g_{11}(\theta) g_{12}(\sigma)}(z_1^k + h_T(1-z_2)g_{11}(\theta)g_{12}(\sigma)). \tag{4.9}$$

The martensite evolution law (2.5b) is a little off-standard. Distinction of cases yields that the following implicit update rule for martensite makes sense.

$$z_2^{k+1} = \min\left(\frac{1}{1+h_T g_{21}(\theta)g_{22}(\sigma)}(z_2^k + h_T \min(\bar{m}(\theta), 1-z_1)g_{21}(\theta)g_{22}(\sigma)),\ \bar{m}(\theta),\ 1-z_1\right).$$

4.2.3 TrIP equation

Due to symmetry, the transformation induced plasticity stress tensor (or strain tensor, respectively) is determined for each spatial point x by six (3D) or four (2D plane strain, see end of section 4.3) non-trivial ordinary differential equations determined by (4.7) - (4.8).

Independent from the dimension, a component-wise implicit time stepping procedure for the TrIP stress is easily achieved by equation (4.7) as

$$\sigma_{k+1}^{tp} = \sigma_k^{tp} - h_T 3\mu\zeta \sum_i z_t^i \sigma^{el,*} - h_T 3\mu\zeta \sum_i z_t^i \sigma_{k+1}^{tp},$$

$$\text{that is,} \qquad \sigma_{k+1}^{tp} = \frac{1}{1 - h_T 3\mu\zeta \sum_i z_t^i}(\sigma_k^{tp} + h_T 3\mu\zeta \sum_i z_t^i \sigma^{el,*}).$$

4.2.4 Elasticity equations

Being quasi-stationary (not containing velocity terms / time derivatives), the elasticity equations are solved for each time step like a stationary problem. The displacement is only implicitly influenced by earlier displacements through the coupling terms ε^{th} and ε^{tp}. Considering the coupling state variables as data F (not to be confounded with F in chapter 2, equation (2.32); here in this chapter volume forces are omitted, therefore no confusion should occur), we have equations of the following kind for the conservation of momentum:

$$\begin{aligned} -div(\sigma) &= 0 \quad \text{in } \Omega, \\ \sigma &= K(\varepsilon^{el}(u)) = K(\varepsilon(u) - F), \\ \sigma n &= 0 \quad \text{on } \partial\Omega, \\ u_i &= 0 \quad \text{on } \Gamma_D^i. \end{aligned}$$

$F = \varepsilon^{th} + \varepsilon^{trip}$ stems from the additive decomposition of the strain,

$$\varepsilon(u) = \varepsilon^{el} + \varepsilon^{th} + \varepsilon^{trip}.$$

The according weak formulation reads

$$\int_\Omega \sigma : \varepsilon(v) = 0 \qquad \forall v \in H_D^1(\Omega)^d,$$

where $H^1_D(\Omega)^d = \{f \in H^1(\Omega)^d\,;\ f_i = 0 \ \text{ on } \ \Gamma^i_D\}$ and d denotes the spatial dimension in the numerical computations, i.e., $d = 3$ or $d = 2$ (plane strain). In the numerics, the Dirichlet boundary conditions are taken into account by manipulation of the node values, we do not modify the test space. Therefore, the test functions are simply chosen in $H^1(\Omega)^d$ in the following equations.

We will apply the pure displacement approach (see e.g. Braess, [13]; there you also find information about the mixed method approach), that means we will only treat u as a variable, the quantities stress and strain are not considered as independent variables.
By $K\varepsilon(u) = \lambda tr(\varepsilon(u))I + 2\mu\varepsilon(u)$ we achieve

$$\int_\Omega \lambda tr(\varepsilon(u))I : \varepsilon(v)dx + \int_\Omega 2\mu\varepsilon(u) : \varepsilon(v)dx = \int_\Omega F : \varepsilon(v)dx = \int_\Omega F : \nabla v dx, \quad (4.10)$$

where the last identity holds due to the symmetry of F. That is,

$$\begin{aligned}
&\int_\Omega \lambda div(u)div(v)dx + \int_\Omega \mu(\nabla u : \nabla v + \nabla^T u \nabla v)dx \\
&= 3b\int_\Omega q(\theta, z)I : \nabla v dx + 2\mu\int_\Omega \varepsilon^{tp} : \nabla v dx. \qquad (4.11)\\
&= 3b\int_\Omega q(\theta, z)div(v)dx + 2\mu\int_\Omega \varepsilon^{tp} : \nabla\varphi dx \qquad (4.12)
\end{aligned}$$

To achieve a finite-dimensional equation system for the numerical computation, all quantities will be described and tested in terms of the finite basis $\{\varphi_1, .., \varphi_n\} \subset H^1(\Omega)$. Let u and v be vector-valued functions $\in H^1(\Omega)^d$ represented by

$$\left(\begin{pmatrix} u^1_1 \\ u^1_2 \\ [u^1_3] \end{pmatrix}, .., \begin{pmatrix} u^n_1 \\ u^n_2 \\ [u^n_3] \end{pmatrix}\right) \qquad \text{and} \qquad \left(\begin{pmatrix} v^1_1 \\ v^1_2 \\ [v^1_3] \end{pmatrix}, .., \begin{pmatrix} v^n_1 \\ v^n_2 \\ [v^n_3] \end{pmatrix}\right) \quad (4.13)$$

with respect to $\{\varphi_1, .., \varphi_n\}$. The terms in square brackets $[\,\cdot\,]$ are only included in the 3D situation.

We will make use of the following identities where ∇_i denotes the partial derivative with respect to the i-th argument $\frac{\partial}{\partial x_r}$:

$$\int_\Omega div(u)\ div(v)dx = \sum_{i=1}^{d}\sum_{j=1}^{d}\sum_{k=1}^{n}\sum_{l=1}^{n} u^k_i v^l_j \int_\Omega \nabla_i\varphi_k\nabla_j\varphi_l dx, \quad (4.14)$$

$$\begin{aligned}
\int_\Omega \varepsilon(u)\varepsilon(v)dx &= \int_\Omega \frac{1}{2}(\nabla u + \nabla^T u) : \frac{1}{2}(\nabla v + \nabla^T v)dx \\
&= \int_\Omega \frac{1}{2}(\nabla u : \nabla v)dx + \int_\Omega \frac{1}{2}(\nabla u : \nabla v^T)dx, \qquad (4.15)
\end{aligned}$$

$$\int_\Omega \nabla u : \nabla v dx = \sum_{i=1}^{d}\sum_{r=1}^{d}\sum_{k=1}^{n}\sum_{l=1}^{n} u_i^k v_i^l \int_\Omega \nabla_r \varphi_k \nabla_r \varphi_l) dx, \tag{4.16}$$

$$\int_\Omega \nabla u : \nabla^T v dx = \sum_{i=1}^{d}\sum_{r=1}^{d}\sum_{k=1}^{n}\sum_{l=1}^{n} u_i^k v_r^l \int_\Omega \nabla_r \varphi_k \nabla_i \varphi_l) dx. \tag{4.17}$$

Furthermore, for matrix-valued $F = (F_{ir})_{i,r} = (\sum_{k=1}^{n} F_{ir}^k \varphi_k)_{i,r}$:

$$\int_\Omega F : \nabla v dx = \sum_{i=1}^{d}\sum_{r=1}^{d}\sum_{k=1}^{n}\sum_{l=1}^{n} \int_\Omega F_{ir}^k v_i^l \varphi_k \nabla_r \varphi_l dx. \tag{4.18}$$

Thereby the disretized equation (4.11) reads:

$$\begin{aligned}
&\lambda \sum_{i=1}^{d}\sum_{j=1}^{d}\sum_{k=1}^{n}\sum_{l=1}^{n} u_i^k v_j^l \int_\Omega \nabla_i \varphi_k \nabla_j \varphi_l dx \\
&\quad + \mu \sum_{i=1}^{d}\sum_{r=1}^{d}\sum_{k=1}^{n}\sum_{l=1}^{n} u_i^k v_i^l \int_\Omega \nabla_r \varphi_k \nabla_r \varphi_l dx + \mu \sum_{i=1}^{d}\sum_{r=1}^{d}\sum_{k=1}^{n}\sum_{l=1}^{n} u_i^k v_r^l \int_\Omega \nabla_r \varphi_k \nabla_i \varphi_l dx \\
&= \sum_{i=1}^{d}\sum_{r=1}^{d}\sum_{k=1}^{n}\sum_{l=1}^{n} \int_\Omega F_{ir}^k v_i^l \varphi_k \nabla_r \varphi_l dx \\
&= 3b \sum_{i=1}^{d}\sum_{k=1}^{n} v_i^k \int_\Omega q(\theta, z) \nabla_i \varphi_k dx + 2\mu \sum_{i=1}^{d}\sum_{r=1}^{d}\sum_{k=1}^{n} v_i^k \int_\Omega \varepsilon_{ir}^{tp} \nabla_r \varphi_k dx.
\end{aligned}$$

Variation of the test function v yields dn equations:

$$\begin{aligned}
&\forall i = 1, .., d,\ k = 1, ..n : \\
&\lambda \sum_{j=1}^{d}\sum_{l=1}^{n} u_j^l \int_\Omega \nabla_j \varphi_l \nabla_i \varphi_k dx \\
&\quad + \mu \sum_{r=1}^{d}\sum_{l=1}^{n} u_i^l \int_\Omega \nabla_r \varphi_l \nabla_r \varphi_k dx + \mu \sum_{r=1}^{d}\sum_{l=1}^{n} u_r^l \int_\Omega \nabla_i \varphi_l \nabla_r \varphi_k dx \\
&= \sum_{r=1}^{d}\sum_{l=1}^{n} \int_\Omega F_{ir}^l \varphi_l \nabla_r \varphi_k dx \\
&= 3b \int_\Omega q(\theta, z) \nabla_i \varphi_k dx + 2\mu \sum_{r=1}^{d} \int_\Omega \varepsilon_{ir}^{tp} \nabla_r \varphi_k dx.
\end{aligned}$$

In matrix notation for a "flattened" solution vector $\vec{u} = \begin{pmatrix} u_1^1 \\ u_2^1 \\ [u_3^1] \\ .. \\ u_1^n \\ u_2^n \\ [u_3^n] \end{pmatrix}$, one obtains using

$$d(\nu) := ((\nu + d - 1) \bmod d) + 1, \tag{4.19}$$

$$\text{i.e.,} \quad d(\nu) = \begin{cases} 1\ , & \nu \bmod 2 = 1 \\ 2\ , & \nu \bmod 2 = 0 \end{cases} \qquad \text{for } d = 2$$

$$\text{and} \quad d(\nu) = \begin{cases} 1\ , & \nu \bmod 3 = 1 \\ 2\ , & \nu \bmod 3 = 2 \\ 3\ , & \nu \bmod 3 = 0 \end{cases} \qquad \text{for } d = 3,$$

and

$$m(\nu) := \lfloor \frac{\nu - 1}{d} \rfloor + 1 = \begin{cases} 1\ , & \nu \in \{1, .., d\} \\ ..\ , & .. \\ n\ , & \nu \in \{d(n-1) + 1,\ ..,\ dn\} \end{cases} \tag{4.20}$$

the following equation system

$$\begin{aligned} &\left(\lambda \int_\Omega \nabla_{d(\nu)} \varphi_{m(\nu)} \nabla_{d(\iota)} \varphi_{m(\iota)} dx \right)_{\iota,\nu=1,..,dn} \vec{u} \\ &\quad + \left(\mu\ \delta_{d(\iota),d(\nu)} \int_\Omega \sum_{r=1}^{d} \nabla_r \varphi_{m(\nu)} \nabla_r \varphi_{m(\iota)} dx \right)_{\iota,\nu=1,..,dn} \vec{u} \\ &\quad + \left(\mu \int_\Omega \nabla_{d(\iota)} \varphi_{m(\nu)} \nabla_{d(\nu)} \varphi_{m(\iota)} dx \right)_{\iota,\nu=1,..,dn} \vec{u} \\ &= \left(\sum_{r=1}^{d} \sum_{l=1}^{n} \int_\Omega F^l_{d(\iota),r} \varphi_l \nabla_r \varphi_{m(\iota)} dx \right)_{\iota=1,..,dn} \\ &= \left(3b \int_\Omega q(\theta, z) \nabla_{d(\iota)} \varphi_{m(\iota)} dx \right)_{\iota=1,..,dn} + \left(2\mu \sum_{r=1}^{d} \int_\Omega \varepsilon^{tp}_{d(\iota),r} \nabla_r \varphi_{m(\iota)} dx \right)_{\iota=1,..,dn} \end{aligned}$$

where δ denotes the Kronecker symbol. Therefore, $dn \times dn$ system matrices are assembled to perform the numerical computations. The right hand side vectors could be assembled for each computation step by gauss quadrature or by application

of source matrices that only need to be assembled once. The latter variant avoids repeated integration loops and accelerates the computing. Here, this is achieved by

$$\left(\sum_{r=1}^{d}\sum_{l=1}^{n}\int_\Omega F^l_{d(\iota),r}\varphi_l\nabla_r\varphi_{m(\iota)}dx\right)_{\iota=1,..,dn}$$
$$\approx\sum_{i=1}^{d}\left(\left(\begin{array}{ll}\int_\Omega\varphi_{m(\nu)}\nabla_{d(\nu)}\varphi_{m(\iota)}dx\ , & \iota=i \mod d\\ 0\ , & else\end{array}\right)_{\iota,\nu=1,..,dn}\vec{F}_i\right)$$

with

$$\vec{F}_i:=\left(F^{m(\nu)}_{i,d(\nu)}\right)_{\nu=1,..,dn} \tag{4.21}$$

a vector of discretized values of F. Or, utilizing the specific structure of F,

$$\left(3b\int_\Omega q(\theta,z)\nabla_{d(\iota)}\varphi_{m(\iota)}dx\right)_{\iota=1,..,dn}+\left(2\mu\sum_{r=1}^{d}\int_\Omega\varepsilon^{tp}_{d(\iota),r}\nabla_r\varphi_{m(\iota)}dx\right)_{\iota=1,..,dn}$$
$$\approx\left(3bq^{m(\iota)}\int_\Omega\nabla_{d(\iota)}\varphi_{m(\iota)}dx\right)_{\iota=1,..,dn}+\left(2\mu\sum_{r=1}^{d}\varepsilon^{tp,m(\iota)}_{d(\iota),r}\int_\Omega\nabla_r\varphi_{m(\iota)}dx\right)_{\iota=1,..,dn},$$

it is sufficient to store the vectors

$$\left(3b\int_\Omega\nabla_{d(\iota)}\varphi_{m(\iota)}dx\right)_{\iota=1,..,dn}\quad\text{and}\quad\left(2\mu\int_\Omega\nabla_r\varphi_{m(\iota)}dx\right)_{\iota=1,..,dn},\ r=1,..,d,$$

and multiply discrete, changing values $q^{m(\iota)}$ and $\varepsilon^{tp,m(\iota)}_{d(\iota),r}$ componentwise when required.

4.2.5 Computation of stress

Throughout the last part, the issue of representing stress and strain in the finite dimensional, i.e., discretized, setting was not treated explicitly. In equation (4.18), we assumed the representation with respect to the underlying finite element basis $\{\varphi_1,..,\varphi_n\}$ which is actually not immediately given (see Schmidt, Wolff, Böhm, [70], Suhr [77], or the forthcoming explanation). The numerical implementations in this thesis were done using linear finite elements. After differentiation, elements of the space $\text{span}(\varphi_1,..,\varphi_n)$ are piecewise constant functions with jumps at cell boundaries and therefore discontinuous and themselves not members of the finite element space.

The first approach to determine ∇y by a formal differentiation of y's representation with respect to the shape functions $\{\varphi_1,..,\varphi_n\}$ (for simplicity consider scalar-valued y for the moment) would yield

$$\nabla\sum_{i=1}^{n}y_i\varphi_i=\sum_{i=1}^{n}y_i\nabla\varphi_i, \tag{4.22}$$

a discontinuous function. This situation occurs when stress-related quantities are concerned.

For the computation of transformation induced plasticity, ordinary differential equations are solved for the coefficients of the base representation belonging to the linear shape functions. One could also perform a time stepping update within a representation with respect to the gradients $\{\nabla\varphi_1, .., \nabla\varphi_n\}$ where cells instead of nodes are indexed. If one adapts the code to manage discrete data structures according to different finite representation schemes, e.g. introducing according data types, at first glance this is a possible treatment of the case. But right hand side data for the ordinary differential equations usually and in particular for the TrIP strain depend on a number of quantities, among them some that are expressed with respect to the shape functions in the finite element space. Therefore, for a pointwise evaluation of a time stepping scheme one has to adjust the discretizations of the different involved terms, a conversion of representation at some point is inevitable.

Usually one wants to express ∇u using the shape functions themselves, e.g., for exploiting existing assembly methods or visualization purposes. In this case, one has to find a vector v such that

$$\sum_i v_i\varphi_i \approx \sum_j u_j \nabla\varphi_j. \tag{4.23}$$

One possible heuristic and quite common approach is interpolation. To determine a function's gradient, one could take for each cell its discrete values at the cell nodes and then use these cell values to do for each node an averaging over neighbouring cells, i.e. for $C(i)$ the set of cells having i as node point and $N(c)$ the set of nodes belonging to cell c,

$$v_i = \frac{\sum_{c\in C(i)} |c| \sum_{k\in N(c)} u_k \nabla\varphi_k|_c}{\sum_{c\in C(i)} |c|} \tag{4.24}$$

A more rigorous approach is finding a representation within the finite element space that has a minimal distance to the given function $\sum_j u_j\nabla\varphi_j$. That means, that one solves a linear equation system to obtain a projection into the finite element space. In general, this equation system is derived as in the following. For given data f we want to minimize

$$\|f - f_h\|^2_{L^2(\Omega)} = \|f - \sum_i f_i\varphi_i\|^2_{L^2(\Omega)} = \int_\Omega (f(x) - \sum_i f_i\varphi_i)^2 dx \tag{4.25}$$

with respect to the f_k. This minimization problem has as neccessary optimality condition

$$\forall\ k = 1, .., n \qquad \int_\Omega \left(f(x) - \sum_i f_i\varphi_i(x) \right) \varphi_k(x) dx = 0, \tag{4.26}$$

that is

$$A_M \vec{f} = \int_\Omega \sum_i f_i \varphi_i(x) \varphi_k(x) dx = \left(\int_\Omega f(x) \varphi_k(x) dx \right)_k , \tag{4.27}$$

where A_M is the respective mass matrix. A projection $\vec{v}$ for $\sum_j u_j \nabla \varphi_j$ is therefore given as the solution to

$$A_M \vec{v} = \left(\int_\Omega \sum_j u_j \nabla \varphi_j(x) \varphi_k(x) dx \right)_k = \left(\int_\Omega \nabla \varphi_j(x) \varphi_k(x) dx \right)_{k,j} \vec{u}. \tag{4.28}$$

4.2.6 Algorithm

Based to the foregoing sections, we now formulate of the complete algorithm. The system matrices are given by:

- mass matrix:

$$A_M := \left(\int_\Omega \varphi_i \varphi_j dx \right)_{i,j=1,..,n} , \tag{4.29}$$

- stiffness (or flow) matrix:

$$A_S := \left(\int_\Omega \nabla \varphi_i \nabla \varphi_j dx \right)_{i,j=1,..,n} , \tag{4.30}$$

- boundary mass matrix for heat transfer coefficient α:

$$B_M(\alpha) := \left(\int_\Gamma \alpha \varphi_i \varphi_j da \right)_{i,j=1,..,n} , \tag{4.31}$$

- first system matrix for the "flattened" solution vector $\vec{u}$ for space dimension d, belonging to the volumetric part:

$$C_S^a := \left(\int_\Omega \nabla_{d(\nu)} \varphi_{m(\nu)} \nabla_{d(\iota)} \varphi_{m(\iota)} dx \right)_{\iota,\nu=1,..,dn} , \tag{4.32}$$

- second system matrix for the "flattened" solution vector $\vec{u}$ for space dimension d, belonging to shear:

$$C_S^b := \left(\delta_{d(\iota),d(\nu)} \int_\Omega \sum_{r=1}^{d} \nabla_r \varphi_{m(\nu)} \nabla_r \varphi_{m(\iota)} dx \right)_{\iota,\nu=1,..,dn} , \tag{4.33}$$

- third system matrix for the "flattened" solution vector $\vec{u}$ for space dimension d, belonging to shear:

$$C_S^c := \left(\int_\Omega \nabla_{d(\iota)} \varphi_{m(\nu)} \nabla_{d(\nu)} \varphi_{m(\iota)} dx \right)_{\iota,\nu=1,..,dn} , \tag{4.34}$$

- first source matrix for the momentum balance, belonging to thermal expansion:

$$D_{th}(q) := \left(\int_\Omega q \nabla_{d(\iota)} \varphi_{m(\iota)} dx \right)_{\iota=1,..,dn}, \tag{4.35}$$

- second source matrix for the momentum balance, belonging to TrIP:

$$D_{tp}(\varepsilon^{tp}) := \left(\sum_{r=1}^{d} \int_\Omega \varepsilon^{tp}_{d(\iota),r} \nabla_r \varphi_{m(\iota)} dx \right)_{\iota=1,..,dn}, \tag{4.36}$$

- source matrix for data represented with respect to $\{\nabla_d \varphi_1, .., \nabla_d \varphi_n\}$:

$$E^d_P := \left(\int_\Omega \nabla_d \varphi_j(x) \varphi_k(x) dx \right)_{k,j=1,..,n}, \tag{4.37}$$

- right hand side vector for weak formulation belonging to Neumann data f:

$$F(f) := \left(\int_\Gamma f \varphi_j da \right)_{j=1,..,n}. \tag{4.38}$$

With these matrices at hand the numerical algorithm reads:

- Initialize all state quantities according to the start values $\theta(0) = \theta_0$, $z(0) = 0$, $\varepsilon^{tp}(0) = 0$. The parameters are adapted to the initial values such that the solution of the quasi-stationary momentum balance for these values of θ, z, and ε^{tp} is $u = 0$, $\sigma = 0$.
- Iterate over the discrete time points t_k with distance h_T. The transition from t_k to t_{k+1} is performed by:
  - determine the temperature update by solving

$$\begin{aligned}(\varrho c_p A_M + h_T k A_S - h_T B_M(\alpha(t_{k+1}))) \, \vec{\theta}^{k+1} \\ = \varrho c_p A_M \vec{\theta}^k - h_T \theta_{\text{amb}} F(\alpha(t_{k+1}))\end{aligned}$$

  - update the phase values by a time stepping scheme, e.g. implicit Euler:

$$z_1^{k+1} = \frac{1}{1 + h_T g_{11}(\theta^{k+1}) g_{12}(\sigma^k)} (z_1^k + h_T (1 - z_2^k) g_{11}(\theta^{k+1}) g_{12}(\sigma))$$

$$z_2^{k+1} = \min\Big(\frac{(z_2^k + h_T \min(\bar{m}(\theta^{k+1}), 1 - z_1^{k+1}) g_{21}(\theta^{k+1}) g_{22}(\sigma^k))}{1 + h_T g_{21}(\theta^{k+1}) g_{22}(\sigma^k)}, \bar{m}(\theta^{k+1}),\ 1 - z_1^{k+1} \Big)$$

– `solve the quasi-stationary momentum balance for the "flattened" displacement vector` $\vec{u}^{k+1} \in \mathbb{R}$:

$$\left(\lambda C_S^a + \mu C_S^b + \mu C_S^c\right) \vec{u}^{k+1} = 3bD_{th}(q(\theta^{k+1}, z^{k+1})) + 2\mu D_{tp}(\varepsilon^{tp,k}),$$

– `compute presentations` v_{ij}^{k+1} `of` $\nabla_i u_j^{k+1}$ `by solving`

$$A_M \vec{v}_{ij}^{k+1} = E_P^i \vec{u}_j^{k+1}$$

`and compile the stress components`

$$\sigma_{ij}^{k+1} = \lambda \left(\sum_{r=1}^{d} v_{ij}^{k+1} \right) \delta_{ij} + \mu v_{ij}^{k+1} + \mu v_{ji}^{k+1} - 3bq(\theta^{k+1}, z^{k+1})\delta_i j - 2\mu \varepsilon_{ij}^{k}$$

– `update the TrIP term by the implicit Euler scheme:`

$$\sigma^{tp,k+1} = \frac{1}{1 - h_T 3\mu\zeta \sum_i \dot{z}_i^{k+1}} \left(\sigma^{tp,k+1} + h_T 3\mu\zeta \sum_i \dot{z}_i^{k+1} \sigma^{el,*,k+1} \right).$$

4.3 Approximation by a 2D model

Although the considered problem actually requires full 3D computations, for the sake of avoiding costly numerical computations, we want to consider a way to restrict it to two dimensions. First, we want to exploit the fact, that we deal with a symmetric system, i.e., the workpiece along with its material properties is symmetric and the surrounding system (boundary conditions) is symmetric as well. For simplicity, we assume a geometry orientation such that the symmetry plane is equal to the (x_1, x_2)-plane for $x_3 = 0$ as in figure 4.4.

Due to the symmetry conditions, it holds for any $h \in \mathbb{R}$ and $(x_1, x_2, h) \in \Omega$

$$\theta(x_1, x_2, h, t) = \theta(x_1, x_2, -h, t) \qquad \forall\ t \in [0, T], \tag{4.39}$$

$$z(x_1, x_2, h, t) = z(x_1, x_2, -h, t) \qquad \forall\ t \in [0, T], \tag{4.40}$$

and

$$u_i(x_1, x_2, h, t) = u_i(x_1, x_2, -h, t)\ ,\ i = 1, 2\ , \qquad \forall\ t \in [0, T], \tag{4.41}$$

$$u_3(x_1, x_2, h, t) = -u_i(x_1, x_2, -h, t)\ , \qquad \forall\ t \in [0, T]. \tag{4.42}$$

Furthermore, points $(x_1, x_2, 0)$ are only displaced along the symmetry plane, therefore

$$u_3(x_1, x_2, 0, t) = 0 \qquad \forall (x_1, x_2, 0, t) \in \Omega\ , \quad \forall\ t \in [0, T]. \tag{4.43}$$

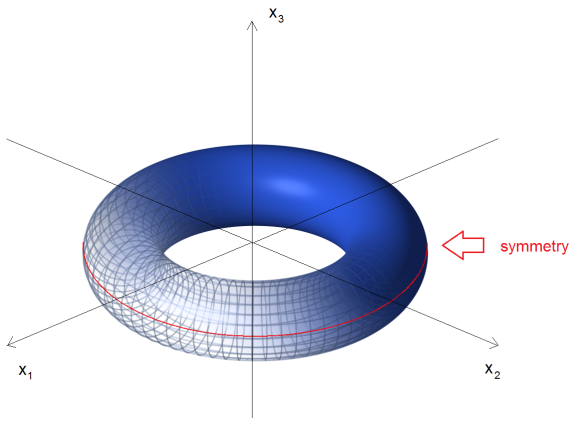

Figure 4.4: A geometry which is symmetric in x_3-direction

Equations (4.43), (4.42), and (4.41) together follow from the fact that also the displaced geometry $\tilde{\Omega} = (\mathrm{id} + u)(\Omega)$ is symmetric itself with respect to the same symmetry plane (at least for one representative solution if not unique, e.g. in the case of pure Neumann conditions). (4.39) and (4.40) yield

$$\frac{\partial \theta}{\partial x_3}(x_1, x_2, 0, t) = 0 \quad \text{and} \quad \frac{\partial z}{\partial x_3}(x_1, x_2, 0, t) = 0 \qquad \forall\ (x_1, x_2, 0) \in \Omega,\ t \in [0, T]. \tag{4.44}$$

For the displacements along the symmetry plane we achieve by (4.41)

$$\frac{\partial u_i}{\partial x_3}(x_1, x_2, 0, t) = 0\ , \quad i = 1, 2\ , \qquad \forall\ (x_1, x_2, 0) \in \Omega,\ t \in [0, T]. \tag{4.45}$$

Unfortunately, unlike in classical plane strain, where one has zero displacement u_3 for any slice $x_3 = a$, we do not have such a condition here. Therefore, the derivative of third displacement component u_3 with respect to x_3 is in general not equal to zero. Instead it holds a symmetry condition

$$\frac{\partial u_3}{\partial x_3}(x_1, x_2, h, t) = \frac{\partial u_3}{\partial x_3}(x_1, x_2, -h, t) \tag{4.46}$$

and therefore an elimination not until the second derivative,

$$\frac{\partial^2 u_3}{\partial x_3^2}(x_1, x_2, 0, t) = 0. \tag{4.47}$$

The shear components $\frac{\partial u_3}{\partial x_i}$ for $i = 1, 2$ are in general non-trivial. (An exception would be a completely symmetric workpiece structure like a ball or a cuboid with constant volumetric and boundary source terms. This does not apply for arbitrary inhomogenous cooling as we have in mind.) The strain tensor can then be computed

as

$$\varepsilon(u) = \begin{pmatrix} \partial_{x_1} u_1 & \frac{1}{2}(\partial_{x_1} u_2 + \partial_{x_2} u_1) & \frac{1}{2}\partial_{x_1} u_3 \\ \frac{1}{2}(\partial_{x_1} u_2 + \partial_{x_2} u_1) & \partial_{x_2} u_2 & \frac{1}{2}\partial_{x_2} u_3 \\ \frac{1}{2}\partial_{x_1} u_3 & \frac{1}{2}\partial_{x_2} u_3 & \partial_{x_3} u_3 \end{pmatrix}.$$

Neglecting internal forces (e.g. gravity) in the numerical computations, our aim is the investigation of the system

$$-\operatorname{div} \sigma = 0 \quad \text{in } \Omega.$$

Expressing σ by

$$\sigma = K\varepsilon^{el} = K(\varepsilon(u) - \varepsilon^{th} - \varepsilon^{tp})$$

demands to consider the divergence of the resulting three additive parts of $\sigma = \sigma^{el} + \sigma^{th} + \sigma^{tp}$,

$$\sigma^{el} = K\varepsilon(u), \qquad \sigma^{th} = -K\varepsilon^{th}, \qquad \sigma^{tp} = -K\varepsilon^{tp}.$$

The first part of the stress tensor reads

$$\sigma^{el} = \begin{pmatrix} 2\mu\partial_{x_1} u_1 + \lambda \sum_{i=1}^{3} \partial_{x_i} u_i & \mu(\partial_{x_1} u_2 + \partial_{x_2} u_1) & \mu\partial_{x_1} u_3 \\ \mu(\partial_{x_1} u_2 + \partial_{x_2} u_1) & 2\mu\partial_{x_2} u_2 + \lambda \sum_{i=1}^{3} \partial_{x_i} u_i & \mu\partial_{x_2} u_3 \\ \mu\partial_{x_1} u_3 & \mu\partial_{x_2} u_3 & 2\mu\partial_{x_3} u_3 + \lambda \sum_{i=1}^{3} \partial_{x_i} u_i \end{pmatrix}.$$

Its divergence is given by (inserting (4.47))

$$\operatorname{div} \sigma^{el} = \begin{pmatrix} 2\mu\partial_{x_1}^2 u_1 + \lambda \sum_{i=1}^{3} \partial_{x_1}\partial_{x_i} u_i + \mu\partial_{x_1}\partial_{x_2} u_2 + \mu\partial_{x_2}^2 u_1 + \mu\partial_{x_1}\partial_{x_3} u_3 \\ \mu\partial_{x_1}^2 u_2 + \mu\partial_{x_1}\partial_{x_2} u_1 + 2\mu\partial_{x_2}^2 u_2 + \lambda \sum_{i=1}^{3} \partial_{x_2}\partial_{x_i} u_i + \mu\partial_{x_2}\partial x_3 u_3 \\ \mu\partial_{x_1}^2 u_3 + \mu\partial_{x_2}^2 u_3 + \lambda\partial_{x_3}\partial_{x_1} u_1 + \lambda\partial_{x_3}\partial_{x_2} u_2 \end{pmatrix}.$$

The second part of the stress tensor, which refers to temperature dependent expansion, has only entries on the main axis,

$$\sigma^{th} = -3bq(\theta, z)I.$$

Here the divergence reads (using (4.44))

$$\operatorname{div} \sigma^{th} = 3b\nabla q(\theta, z) = \begin{pmatrix} 3b\partial_{x_1} q(\theta, z) \\ 3b\partial_{x_2} q(\theta, z) \\ 0 \end{pmatrix}.$$

As the workpiece is stress-free at initial time, $\sigma(0) = 0$, the ordinary differential equation for σ^{tp}, (4.2e),

$$\sigma^{tp} = -2\mu \int_0^t \gamma(\theta, z, z_\tau)\sigma^* d\tau.$$

gives that σ^{tp} and $(\sigma^{el}+\sigma^{th})^*$ have the same matrix structure. Both $\operatorname{div}\sigma^{el}$ and $\operatorname{div}\sigma^{tp}$ have non-trivial entries on the third component that also do not vanish if the sum is taken. Continuing this way it is not possible to simplify the 3D system. A remedy would be the imposition of the further condition $u_3 \equiv 0$ on the whole geometry Ω and that u_1 and u_2 do not depend on x_3 (as in plane strain), i.e.,

$$\partial_{x_3} u_i = 0, \quad i = 1,2,3,$$

everywhere and also

$$\partial_{x_j}\partial_{x_3} u_i = 0, \quad i = 1,2,3 \quad j = 1,2,3.$$

Then

$$\operatorname{div}\sigma^{el} = \begin{pmatrix} 2\mu\partial_{x_1}^2 u_1 + \lambda\sum_{i=1}^2 \partial_{x_1}\partial_{x_i} u_i + \mu\partial_{x_1}\partial_{x_2} u_2 + \mu\partial_{x_2}^2 u_1 \\ \mu\partial_{x_1}^2 u_2 + \mu\partial_{x_1}\partial_{x_2} u_1 + 2\mu\partial_{x_2}^2 u_2 + \lambda\sum_{i=1}^2 \partial_{x_2}\partial_{x_i} u_i \\ 0 \end{pmatrix}.$$

σ^{el} would then read

$$\sigma^{el} = \begin{pmatrix} 2\mu\partial_{x_1} u_1 + \lambda\sum_{i=1}^2 \partial_{x_i} u_i & \mu(\partial_{x_1} u_2 + \partial_{x_2} u_1) & 0 \\ \mu(\partial_{x_1} u_2 + \partial_{x_2} u_1) & 2\mu\partial_{x_2} u_2 + \lambda\sum_{i=1}^2 \partial_{x_i} u_i & 0 \\ 0 & 0 & \lambda\sum_{i=1}^2 \partial_{x_i} u_i \end{pmatrix}.$$

Correspondingly,

$$\sigma^{tp} = \begin{pmatrix} 2\mu \int_0^t (\partial_{x_1}(\gamma(\theta,z,z_\tau)\sigma_{11}^*) + \partial_{x_2}(\gamma(\theta,z,z_\tau)\sigma_{12}))d\tau \\ 2\mu \int_0^t (\partial_{x_1}(\gamma(\theta,z,z_\tau)\sigma_{12}) + \partial_{x_2}(\gamma(\theta,z,z_\tau)\sigma_{22}^*))d\tau \\ 2\mu \int_0^t \partial_{x_3}\gamma(\theta,z,z_\tau)\sigma_{33}^* d\tau \end{pmatrix}.$$

Accordingly, $\operatorname{div}\sigma = 0$ would read

$$\begin{aligned} &-\begin{pmatrix} (\lambda+2\mu)\partial_{x_1}^2 u_1 + \lambda\partial_{x_1}\partial_{x_2} u_2 + \mu\partial_{x_1}\partial_{x_2} u_2 + \mu\partial_{x_2}^2 u_1 \\ \mu\partial_{x_1}^2 u_2 + \mu\partial_{x_1}\partial_{x_2} u_1 + \lambda\partial_{x_1}\partial_{x_2} u_1 + (\lambda+2\mu)\partial_{x_2}^2 u_2 \\ \lambda\partial_{x_1}\partial_{x_3} u_1 + \lambda\partial_{x_2}\partial_{x_3} u_2 \end{pmatrix} + 3b\nabla q(\theta,z) \\ &+\begin{pmatrix} 2\mu \int_0^t (\partial_{x_1}(\gamma(\theta,z,z_\tau)\sigma_{11}^*) + \partial_{x_2}(\gamma(\theta,z,z_\tau)\sigma_{12}))d\tau \\ 2\mu \int_0^t (\partial_{x_1}(\gamma(\theta,z,z_\tau)\sigma_{12}) + \partial_{x_2}(\gamma(\theta,z,z_\tau)\sigma_{22}^*))d\tau \\ 2\mu \int_0^t \partial_{x_3}\gamma(\theta,z,z_\tau)\sigma_{33} d\tau \end{pmatrix} = \begin{pmatrix} 0 \\ 0 \\ 0 \end{pmatrix}. \end{aligned}$$

To achieve a plane strain formulation we consider the third component of $\operatorname{div}\sigma$ or rather the terms $\partial_{x_3}\sigma_{33}^{el}$, $\partial_{x_3}\sigma_{33}^{th}$, and $\partial_{x_3}\sigma_{33}^{tp}$. Due to $\partial_{x_3} u_i = 0$,

$$\partial_{x_3}\sigma_{33}^{el} = \lambda\partial_{x_1}\partial_{x_3} u_1 + \lambda\partial_{x_2}\partial_{x_3} u_2 = 0.$$

Furthermore, because of the invariance of temperature and phases with respect to x_3, also

$$\partial_{x_3}\sigma_{33}^{th} = 3b\partial_{x_3}q(\theta, z) = 0.$$

By the same argument

$$\partial_{x_3}\gamma(\theta, z, z_t) = 0$$

and therefore the differentiation of the ordinary differential equation for σ_{33}^{tp} with respect to x_3,

$$\partial_t\partial_{x_3}\sigma_{33}^{tp} = \partial_{x_3}(2\mu\gamma(\theta, z, z_\tau)\sigma_{33}^*) = 2\mu\gamma(\theta, z, z_\tau)\partial_{x_3}\sigma_{33}^* = 2\mu\gamma(\theta, z, z_\tau)\partial_{x_3}\sigma_{33}^{tp}$$

with initial condition $\partial_{x_3}\sigma_{33}^{tp}(0) = 0$, is solved by $\partial_{x_3}\sigma_{33}^{tp} \equiv 0$.

Altogether, the third of the elasticity equations $\operatorname{div}\sigma = 0$ is then satisfied trivially as $0 = 0$ and can be left out. We achieve a reduced system which can be solved as a 2D problem.

For the finite element method, the two non-trivial equations could then be formulated in terms of the 2D divergence operator,

$$\begin{aligned}
&- div_{(2D)} \begin{pmatrix} (\lambda + 2\mu)\partial_{x_1}u_1 + \lambda\partial_{x_2}u_2 \\ \mu(\partial_{x_1}u_2 + \partial_{x_2}u_1) \end{pmatrix} \\
&\qquad = -3b\partial_{x_1}q(\theta, z) - 2\mu \int_0^t (\partial_{x_1}(\gamma(\theta, z)\sigma_{11}^*) + \partial_{x_2}(\gamma(\theta, z)\sigma_{12}))d\tau, \\
&- div_{(2D)} \begin{pmatrix} \mu(\partial_{x_1}u_2 + \partial_{x_2}u_1) \\ \lambda\partial_{x_1}u_1 + (\lambda + 2\mu)\partial_{x_2}u_2 \end{pmatrix} \\
&\qquad = -3b\partial_{x_2}q(\theta, z) - 2\mu \int_0^t (\partial_{x_1}(\gamma(\theta, z)\sigma_{12}^*) + \partial_{x_2}(\gamma(\theta, z)\sigma_{22}^*))d\tau.
\end{aligned}$$

Although the elasticity equations could be solved in 2D if $u_3 \equiv 0$ is assumed, the stress tensor itself still has a non-vanishing entry σ_{33}. This has to be taken into account for the computation of the TrIP term under plane strain, which has the same structure as the overall stress under plane strain:

$$\begin{pmatrix} * & * & 0 \\ * & * & 0 \\ 0 & 0 & * \end{pmatrix}$$

For the calculation, ordinary differential equations for four scalar-valued components have to be solved. These are σ_{11}^{tp}, σ_{22}^{tp}, σ_{33}^{tp}, and σ_{12}^{tp} (or the corresponding TrIP strain components), the other entries are zero or redundant due to symmetry of the tensor. The storage of the component 33 is needed if one wants to achieve information about the stress in terms of a "post-processing". That is different for the case of systems

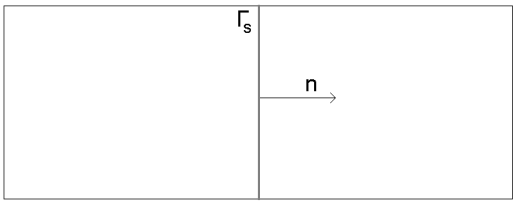

Figure 4.5: Symmetric geometry with symmetry axis Γ_S and according normal vector n.

without transformation induced plasticity (that is, without a deformation memory), where the stress can be computed in any timestep from 2D data. If the TrIP term is included, the stress can only be obtained by comprising all prior timesteps. Therefore, the storage of the TrIP stress component 33 is adjuvant. At least for the computation of von Mises stress, knowledge about the full stress tensor can turn out to be meaningful.

4.4 Exploitation of symmetries

There are experimental setups where numerical complexity can be reduced by making use of symmetric continuation. We will restrict ourselves to a presentation of the case of a symmetry axis within a 2D situation. A detailed description of the numerical treatment of (axial) symmetries within a finite element implementation of thermomechanics was elaborated in Suhr, [77].

Assume a symmetry axis Γ_S with normal vector n as in figure (4.5)

All occuring quantities, including boundary conditions, are mirrored along the symmetry axis which is given if one extends Γ_S to an infinite line. Then, problem complexity may be reduced by skipping half of the geometry and proper modification of the boundary conditions. Mere ordinary differential equations do not need any manipulation, they are simply evaluated on the reduced geometry as before. Also the scalar-valued temperature does not cause much trouble. The symmetry property yields

$$\theta(\bar{x} - hn) = \theta(\bar{x} + hn) \tag{4.48}$$

for any $\bar{x} \in \Gamma_S$ and $h \in \mathbb{R}$ with $\bar{x} - hn$ member of the geometry Ω (and thereby due to symmetry also $\bar{x} + hn \in \Omega$). Therefore,

$$\frac{\partial \theta}{\partial n}(\bar{x}) = 0 \qquad \forall\ \bar{x} \in \Gamma_S. \tag{4.49}$$

The symmetry condition for the scalar quantity temperature reads like insulation, it is simply a homogeneous Neumann boundary condition.

The non-scalar elasticity equations need more modification. First, the symmetry axis must not be displaced, this defines a Dirichlet condition

$$u \cdot n = 0 \qquad \text{on } \Gamma_S. \tag{4.50}$$

Here, boundary conditions are introduced that do not come from physical conditions. Thereby degrees of freedom are reduced and neccessary definiteness of the system matrix is introduced, while one remains with a physically underdetermined system. Circumstances that one does not want to consider (in this case clamping which would bring additional stresses into the workpiece) can be neglected while one still obtains a unique solution to the elasticity equations. A discussion within a quotient space modulo rotations as mentioned in section 3.4 is thereby superseded. Apart form the reduction of numerical complexity, one has gained an additional benefit from the symmetry conditions.

If one passes to the limit with the symmetry condition for the u_i, one obtains analogously as in the discussion of the temperature

$$\frac{\partial u_i}{\partial n}(\bar{x}) = 0 \qquad \forall\ \bar{x} \in \Gamma_S, \qquad i = 1, 2. \tag{4.51}$$

Instead of the natural boundary condition $\sigma n = 0$ on $\partial\Omega$, we get a differing boundary condition on Γ_S. This corresponds to the fact that the interior of the workpiece is generally speaking by no means stress-free, in particular not with respect to a symmetry plane.

Chapter 5

Application

5.1 Out-of-roundness of roller bearing rings

Plastic deformations, among them those caused by transformation induced plasticity, are investigated to large extent in the collaborative research center SFB 570 "Distortion Engineering" in Bremen. One of the participating institutions is the Institute for Material Science IWT Bremen, which provided experimental data for 100Cr6 bearing races. To investigate distortion (i.e., unwanted lasting deformation), samples of standard geometries as simplifications of common engineering objects are analyzed, i.e., rings representing bearing races, bars representing shafts and so forth. They go through usual production steps to make out in which way these steps influence distortion. To distinguish different effects, production conditions are varied. For the identification of distortion effects high precision measurement devices are utilized, among them contact requiring coordinate measurement machines that can only be applied to workpieces at room temperature as the measurement process lasts over several hours and should only be applied to non-changing geometries. For quick in-situ shape measurements during experiments less precise feelers are used.

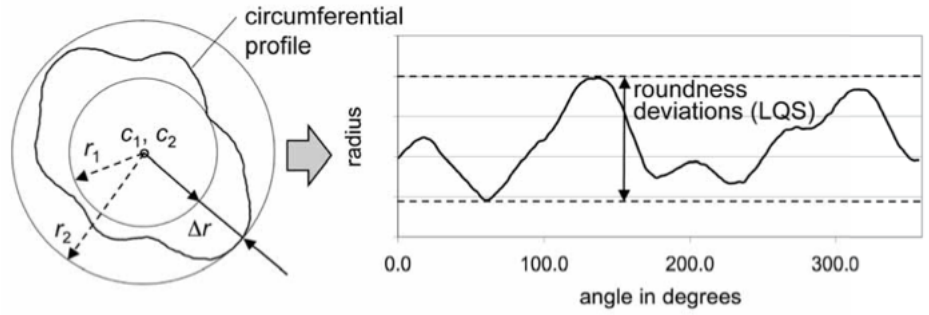

Figure 5.1: Schematic definition of (out-of-)roundness, taken from Dijkman, [23]

In this thesis, we are particularly interested in the radial effects that occur for (cylindrical) ring workpieces. (An examination of the influence of heat treatments on the inclination angle of conical rings can be found in Suhr, [77].) Radial distortion for rings is characterized by deviations from a single constant radius. To assign quantitative values to radial ring distortion, the notion "(out-of-)roundness" is utilized among engineers. It is defined for distorted circles via two concentric ideal circles, one enclosing from the outside and the other lying inside the distorted circle, with minimal radius difference, see figure 5.1. For the determination of these circles a least squares problem could be solved. If a single value is desired, some sources (e.g. [19], also [49]) refer to the radius difference of the two enclosing ideal circles as "out-of-roundness". If one wants to explore the roundness quality in more detail, one takes the distance of each point of the distorted circle to the center point of the two concentric circles (or only the offset to the inscribed circle) and gets a periodic deviation function which assigns to each angle a distorted radius (offset). Of course, this is only well-defined for moderate deformations that do not lead to drapery. In the following, we refer to "out-of-roundness" as a single value or a function depending on the context in accordance to considerations within SFB 570.

The out-of-roundness is investigated for the inner and outer boundary of two-dimensional horizontal cross-sections of the workpiece. For a deeper investigation, those roundness profiles as functions of the angle are subject to Fast Fourier Transformations. With respect to the radial distances, the Fourier terms of order zero and one are less interesting, they give a constant radius offset which does not affect roundness, just size, and eggshapedness that corresponds to mere translation. Order two and three, i.e., ovality and triangularity are relevant and occur quite often. They are among the out-of-roundness orders that can be linked to certain processing steps or can be traced back to specific production devices, e.g., the clamping device often consists of three chucks which leads to a triangular deformation. Another typical deformation is of order twelve and caused by the quenching device which is used late in the process chain, figure 5.2.

The considered distortion effects within SFB 570 are mainly caused by internal stresses accumulated during the process chain. In [18] the influence of the different production steps on the overall distortion was analyzed and compared. Whereas heating velocity has no significant impact on distortion, the quenchant choice is very important. Liquid (e.g., oil) quenchants cause problems because boiling and advective flows result in irregular heat transfer. Therefore, gas quenching is favorable although the cooling intensity is smaller (see [49]). A further factor is the machining strategy, in particular feed velocity and clamping. During machining, the workpiece is clamped which leaves its footprint on the geometry (in the case of a ring clamped by three jaw chucks a triangular deformation occurs). This effect is

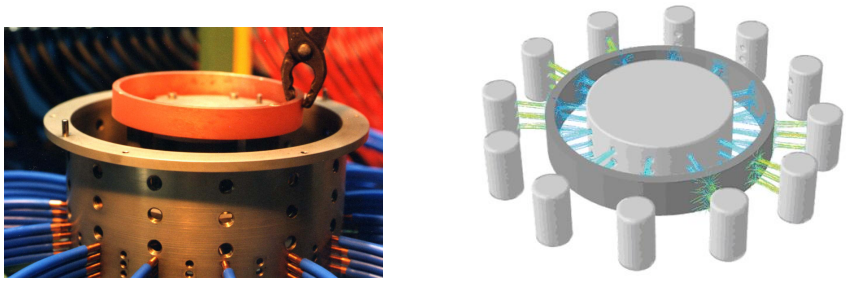

(a) Experiment (b) Schematic top view

Figure 5.2: Cylindrical gas quenching device, courtesy of IWT Bremen

partly rebalanced by a shift of clamping positions during the processing. This is an example for a compensation strategy: it is downright impossible to avoid unwanted deformations, therefore one adds compensating deformations that approximately restore the original shape.

However, shape alterations that still exist in the end of the process chain require costly postprocessing. This problem could be reduced if one focusses on further compensation of the remaining total distortion in the final production steps. A good opportunity for this is the hardening heat treatment. It takes place quite in the end of the process chain and the heat transfer profile during the quenching has a significant impact on the workpiece shape, [18]. Therefore, it is a good strategy to turn one's attention to distortion compensation by quenching. The model presented in (4.1) is capable to reproduce major effects observed in the experiments and will be utilized for the investigation of distortion compensation strategies. The model does not capture all details and solutions underlie quantitative deviations from measurements. For a more complete model that comes closer to measurement results, it is advisable to include more effects, in particular plasticity, and to be careful with the modeling of phase transitions for the particular steel type 100Cr6 (see again Suhr [77]). As we have the application of optimal control strategies in mind, models including plasticity would have been too complex and were not considered.

The heat treatment of interest is conducted within a gas nozzle field. A hot, austenitized steel ring is inserted into the cooling device depicted in figure 5.2. At each of the twelve positions $0°, 30°, 60°, .., 330°$ there are two times three vertically aligned jets that operate on the outside and on the inside of the ring, respectively. The outer gas nozzle triplets can be separately actuated to apply an inhomogenous cooling. It turns out in the experiments, see [49], that constant cooling from the inside and inhomogenous cooling from the outside evokes shape alterations. When nozzle triplets 1 to 3 and the opposed triplets 7 to 9 are active while the others are turned off as depicted in figure 5.3 c), an oval shape is produced with the bulge

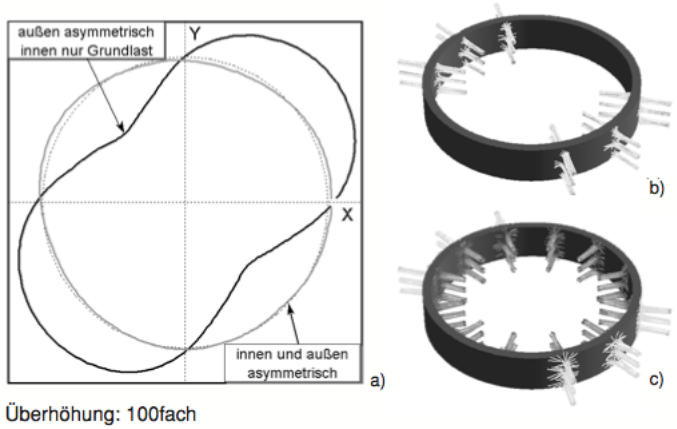

Figure 5.3: Ovality induced by inhomogenous cooling, taken from Hunkel et al., [49]

pointing inwards where the stronger cooling took place. (If the same inhomogenous setting is also applied for the inward nozzles as in part b), no deformation occurs.) Furthermore, an approximately linear correspondence of ovality degree and cooling intensity of the outer nozzles (heat transfer coefficient) could be identified. In SFB 570 it was further investigated if these phenomenons could be used to eliminate out-of-roundness, that is, to create a round ring out of a distorted workpiece.

5.2 Simulation

Employing the algorithm presented in chapter 4, we are in the position to compute deformation profiles according to varying heat transfer coefficients. Our code not being a black box commercial tool enables the adaption to specific needs emerging from the application. This is a good link to the works at IWT Bremen. Given their unroundness data, we want to determine (approximately) optimal heat transfer coefficient functions (see section 5.3). These in turn could be set at the quenching device.

For the optimization it is neccessary to solve the state equations repeatedly. This takes a lot of time if we consider the problem in 3D. Therefore, in a first approach we want to restrict ourselves to 2D computations although they cannot entirely reflect the physical reality of the experiments (see section 4.3). When the 2D optimization is working to complete satisfaction, one can switch to the 3D case without much difficulty.

For a reduction of dimensional complexity, we will confine ourselves to two space dimensions and furthermore to the case of symmetric workpieces and symmetric boundary conditions. For instance, for geometries exhibiting an out-of-roundnesses

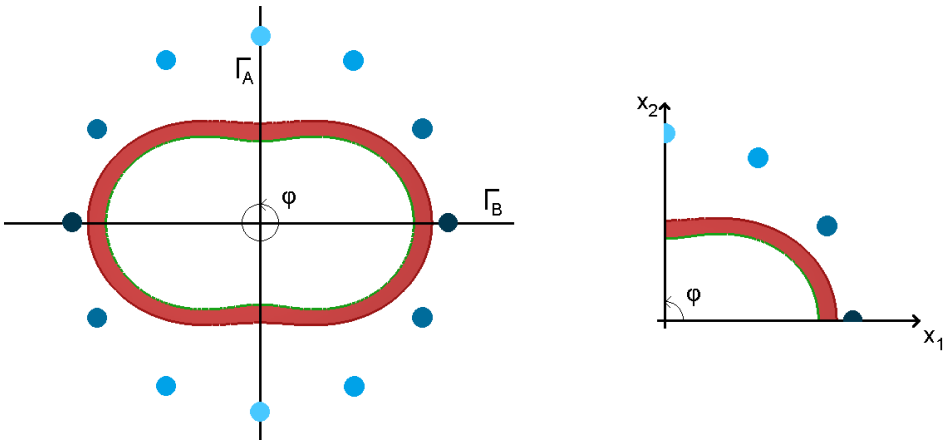

(a) Full geometry (b) Representative quarter

Figure 5.4: Symmetric geometry and boundary conditions

of even order and according periodic boundary conditions, the complete system has two symmetry axes and it suffices to consider quarter pieces of the ring (see figure (5.4) (a)). In this example, there is an oval deformation or unroundness of order two. The gas nozzles are set such that there is the same large heat transfer coefficient on the left and right at height of the x-axis which is declining if one moves along the ring boundary in equal measure down- and upwards,

$$\alpha(x_1, x_2, t) = \alpha(-x_1, x_2, t) \quad \text{and} \quad \alpha(x_1, x_2, t) = \alpha(x_1, -x_2, t). \tag{5.1}$$

As we assume constant (that is, in particular symmetric) material properties and initial conditions for the state variables, here we can restrict the representation of the ring to the first quadrant. The x- and the y-axis define the symmetry axes and the origin $(0, 0)$ corresponds to the center point of the ring.

The continuation in x_1 and x_2 direction for the quarter geometry (5.4) (b) is given by homogenous Neumann conditions for the temperature and Dirichlet boundary conditions for the single displacement components (as the symmetry axes are identical to the coordinate axes),

$$u_1(x) = 0 \ \text{ on } \ \Gamma_A, \qquad u_2(x) = 0 \ \text{ on } \ \Gamma_B. \tag{5.2}$$

Apart from the reduction of numerical complexity, this approach yields advantages as it introduces boundary conditions that do not come from physical conditions (as presented in more detail in section 4.4).

Furthermore, for this special setting, the out-of-roundness is determined easily because it is not required to solve a least squares problem. One knows in advance, that the center point of the ring defined by the initial geometry and also of the

ring defined by the set of displaced points $(id + u)(\Omega)$ lies on $(0, 0)$ and the out-of-roundness function is given by the distance of boundary points to the origin.

For the simulations, parameter data is mainly taken from the papers [1] and [2] where one can find detailed information and experimental results regarding steel 100Cr6.

(It has to be mentioned, that there have been new experimental results which suggest that also isothermal martensite formation occurs in steel 100Cr6 (see a remark on a conversation with Hunkel in [77]). As these are yet unpublished results and we do not aim at a model that reproduces experimental results for 100Cr6 in exact detail, these experimental results do not go into the model.)

The martensite finish temperature of 100Cr6 lies far below 0° C, therefore it is not possible to determine it without exceeding and costly experimental effort. It can be approximated by an extrapolation of measured data (see [1]). For our purposes it suffices to know the martensite fraction at room temperature, because we do not undergo 20°C in the simulations. The utilized data is achieved by table 4 in [2], oil-quenched 100Cr6 steel at room temperature consists of approximately 87 percent martensite and 13 percent retained austenite. Table 5 of the same article gives the martensite start temperature as 211 degree Celsius. Accordingly, we choose as martensite (metastable) equilibrium function $\bar{m}$ the following simple piecewise linear mapping defined for $\theta \geq \theta^a = 20$ depicted in figure (5.5),

$$\bar{m}(\theta) = \begin{cases} 0 \ , & \theta \geq 211 \\ 0.87(1 - \frac{\theta - 20}{211 - 20}) \ , & \theta \leq 211 \end{cases} \tag{5.3}$$

The formula would remain approximately correct for θ moderately lower than 20. But in our modeling approach, i.e., for Newton heat transfer boundary conditions, this does not come into play anyway.

We assume further that the quenching is rapid enough such that no pearlite or bainite is formed.

During gas quenching, the outlet of gas (e.g. air, nitrogen) is regulated by either opening or shutting valves, thereby emitting single pulses, [22]. These pulses come in very high frequencies, therefore one can set the desired gas volume as if the outlet could be regulated analogously. The heat transfer coefficient $\alpha(x, t)$ in (4.2j) was implemented as a sum where each addend is split into two factors, one depending only on time and the other only on the space variable,

$$\alpha(x, t) = \sum_i w^i_\Gamma(x) w^i_{[0,T]}(t). \tag{5.4}$$

The spatial parts are given by

$$w^i_\Gamma(x) = c_i + a_i \exp(-b_i d(x, x_i)^2) \tag{5.5}$$

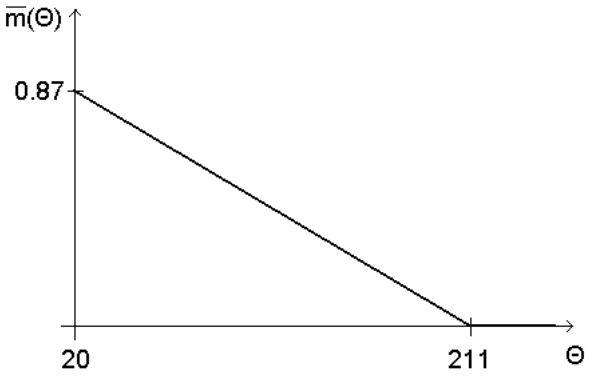

Figure 5.5: $\bar{m}(\theta)$ for steel 100Cr6 in the relevant range

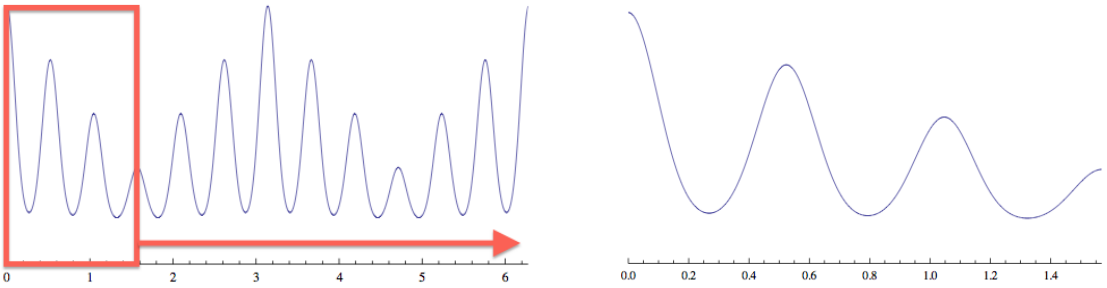

(a) Heat transfer coefficient for a full ring, parametrized over the angle $\varphi \in [0, 2\pi]$

(b) and the according restriction to a quarter ring, $\varphi \in [0, \frac{1}{2}\pi]$

Figure 5.6: Inhomogenous cooling profile

with some distance function d (e.g. $d(x, x_i) = |x - x_i|$ for straight geometries or $|\phi(x) - \phi(x_i)|$ where ϕ assigns angular coordinates for circular shapes), which map the space variable x to (piecewise) gaussian profiles, see e.g. figure 5.6 (a) for an example of 12 such summands that add to the heat transfer coefficient given by the cooling jets. The case $a_i \equiv 0 \ \forall \ i$ gives a spatially constant profile and is also of relevance.

In a first approach, the time variant heat transfer component $w_{[0,T]}$ corresponds to in situ steering of the quenching device and is well suited for being used as a control parameter in optimization.

5.2.1 Results

Although the 2D computation are not able to reproduce experimental results quantitatively, we want to check whether qualitative behaviour observed in the experiments is reflected. For this purpose, an inhomogenous cooling and the resulting

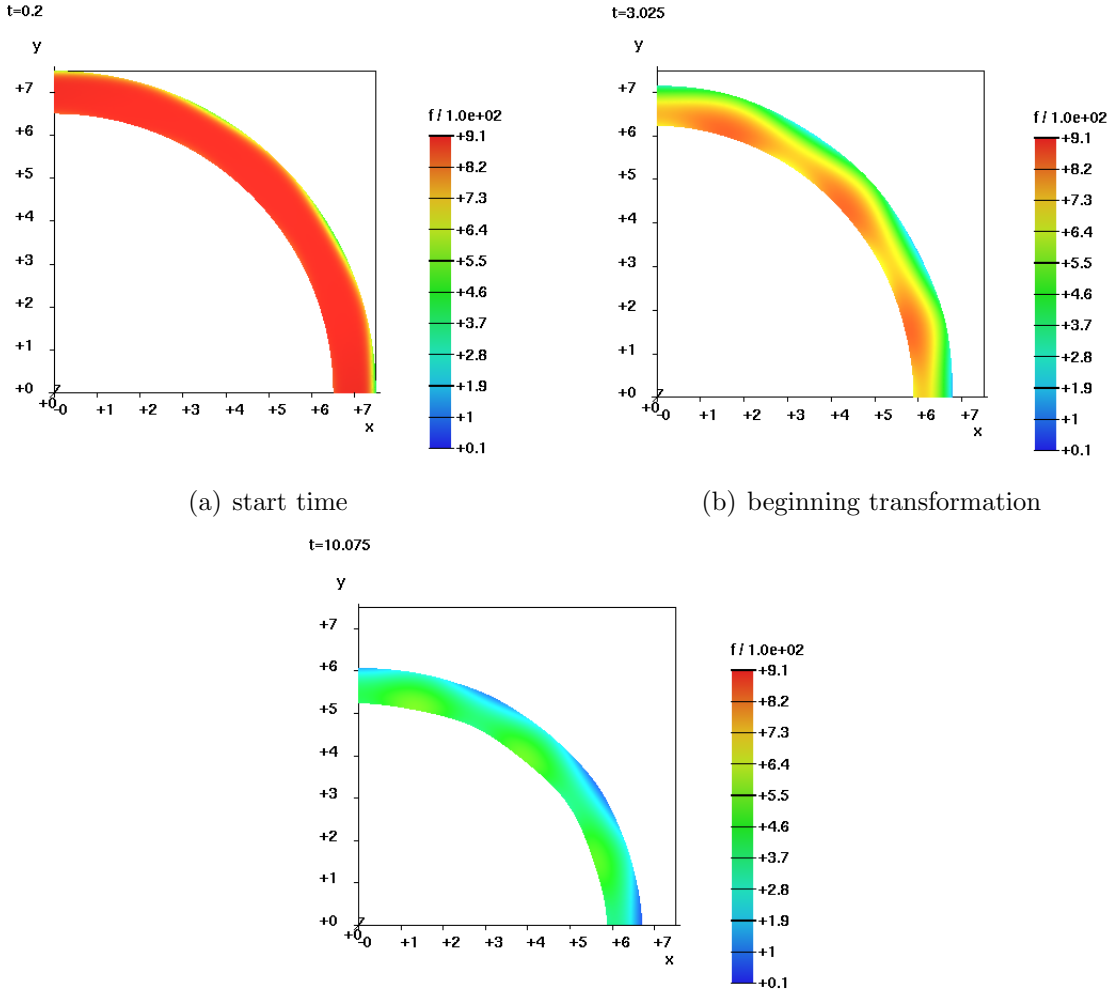

(a) start time

(b) beginning transformation

(c) ongoing transformation

Figure 5.7: Inhomogenous cooling of an initially round ring

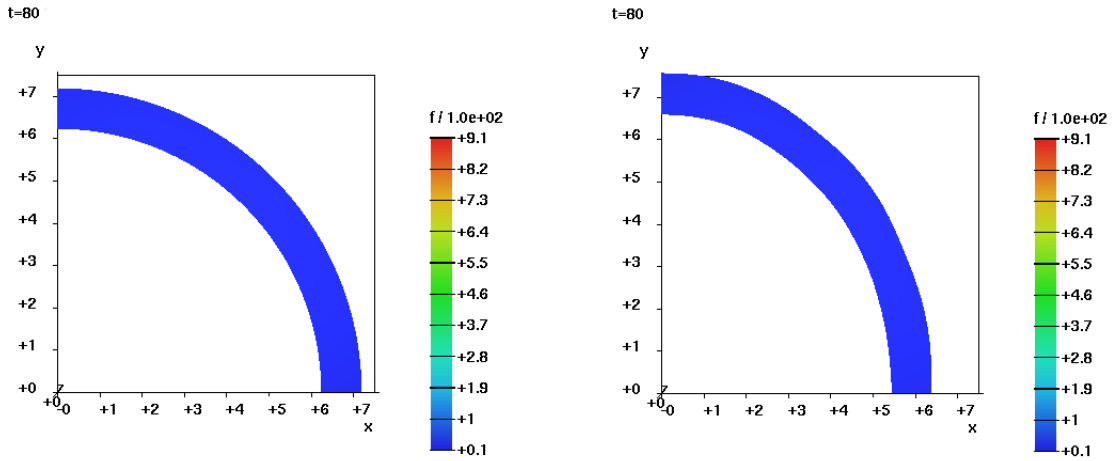

(a) end time without TrIP (b) end time including TrIP

Figure 5.8: Comparison of end time result of inhomogenous cooling with and without transformation induced plasticity

shape deformation is considered. The applied heat transfer coefficient is depicted in figure 5.6. A strong cooling is applied to the bottom right, the upper left is cooled more moderately. The sequence shown in figure 5.7 depicts what happens during cooling. In the beginning, the initally round workpiece (a) shrinks due to classical thermoelasticity. As the ring is colder at the right, it contracts more at this side leading to an ovality with higher expansion in vertical direction (b). After a while, the austenite-martensite-transformation sets in (c), beginning at the right side where temperature has already dropped below the martensite start temperature. Martensite has a lower density and thereby a larger volume than austenite, therefore the ring starts to expand in this area. Figure 5.8 shows the end time shape, when the ring is completely cooled such that the temperature field is again constant. To underline the effect of transformation induced plasticity, we show the end time shape for a simulation without TrIP (a) and including TrIP (b). In case a), when TrIP is not included into the model, the deformation is determined by the thermal strain which is constant for constant temperature and has no shear components. Therefore, in a) no shape alteration occurs. When TrIP is included into the model (b), the geometry at room temperature still exhibits a deviation from the initial shape. It has a bulge pointing inwards, where the stronger cooling was applied the radius is reduced. The initial thermoelastic shrinkage from stage b) was "frozen" by the TrIP effect. This corresponds to the observed behaviour in the experiments, see [49].

In figure 5.9, the outer radius of figure 5.8 b) is plotted against the angle. For an investigation of the deformation a Fourier transformation is carried out. The

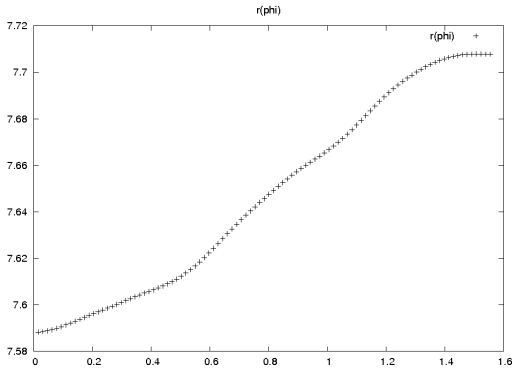

Figure 5.9: Radius $r(\varphi)$ over angle $\varphi \in [0, \frac{\pi}{2}]$

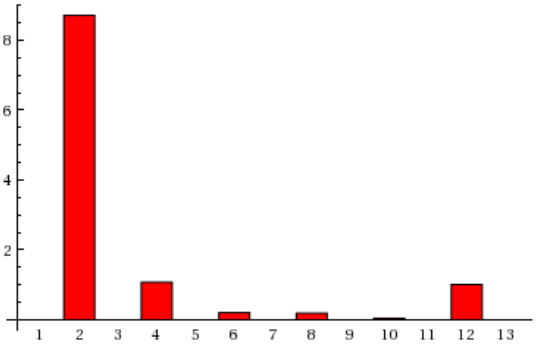

Figure 5.10: Fourier coefficients of out-of-roundness profile for inhomogenous cooling

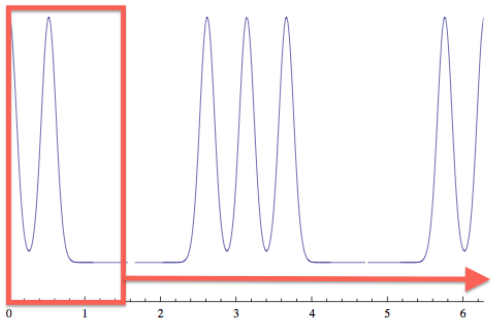

(a) Heat transfer coefficient for a full ring, parametrized over the angle $\varphi \in [0, 2\pi]$

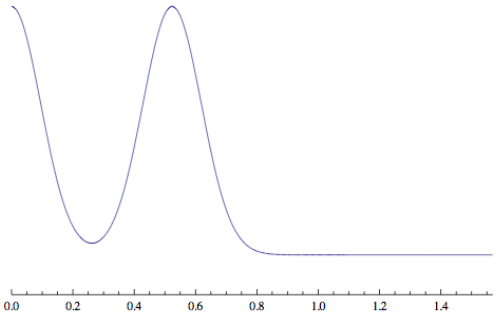

(b) and the according restriction to a quarter ring, $\varphi \in [0, \frac{1}{2}\pi]$

Figure 5.11: Inhomogenous cooling profile, alternatingly 3 jet triplets turned on or off

Fourier coefficients presented in figure 5.10 were obtained by the method `Fourier` within Mathematica®. If one mirrors the results for the quarter ring along the x- and y-axis according to the imposed symmetry, the Fourier Transformation for the radius function of the whole ring gives a dominating second order (ovality) and still remarkable values for the fourth and twelfth order. The order two stems from the two areas of strong cooling, the twelfth order from the twelve cooling jets (if talking of the complete ring). In all, this result coincides well with the measurements from the experiments.

For a better comparability to the inhomogenous cooling presented in [49], we also considered the case where single nozzles are active while the others are turned off as in figure 5.3.

The Fourier transformation in figure 5.13 gives the impression that when diffusion plays a bigger role in the cooling, the different order terms of the fourier series

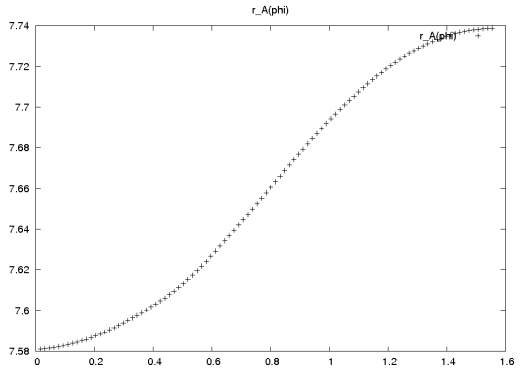

Figure 5.12: Radius $r(\varphi)$ over angle $\varphi \in [0, \frac{\pi}{2}]$

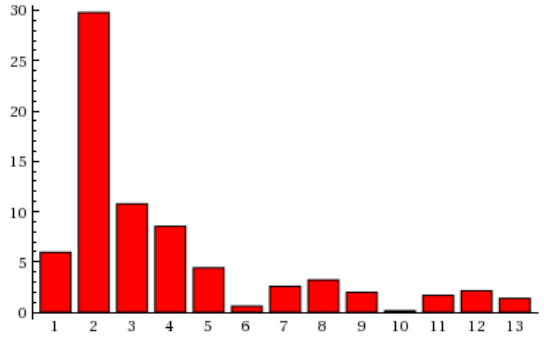

Figure 5.13: Fourier coefficients for inhomogenous cooling where nozzles are partly switched off

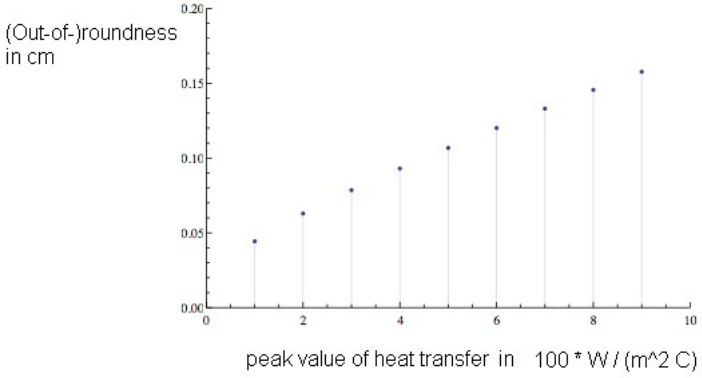

Figure 5.14: Linear Correspondence of out-of-roundness and heat transfer.

become less distinguishable. It is not surprising that the twelfth order plays a minor role when not all nozzles are active and parts of the ring are only cooled by heat diffusion.

Finally, linear variation of the heat transfer coefficients yields according variation of the out-of-roundness in terms of the single value $\max_{\varphi\in[0,2\pi]} r(\varphi) - \min_{\psi\in[0,2\pi]} r(\psi)$, they correspond linearly, see figure 5.14.

This reflects the fact that the heat transfer coefficient has linear influence in the model and it fits well with the observations in the experiments as presented in Hunkel et al. [49].

5.3 Optimal control problem

The application of the foregoing section naturally leads to the task of finding an optimal control for the jets or rather the heat transfer coefficients to achieve a desired deformation profile by influencing temperature. Given start geometries that exhibit "out-of-roundness", we want to use the TrIP effect to achieve a displacement function that annihilates this distortion and results in a circular ring shape (as far as possible).

Whereas in the field of engineering feedback controls are the first choice to optimize processes, mathematically there is a variety of approaches. The already mentioned process control as commonly applied in engineering is subject of many engineering and also mathematical articles e.g. by Alder, Hömberg, Weiss, [7], or Hömberg and Yamamoto, [48]. In [48], it was possible to show exact controllability of a laser heat treatment under observed temperature. Among many computer scientists and also engineers, neural network or fuzzy methods are popular, in particular as they can be applied like other process controls by means of an online-control that adapts to unpredicted physical circumstances. From a computational point of view, also other discrete optimization techniques are of relevance, (finite-dimensional) nonlinear optimization theory yields a large variety of mathematical knowledge and ways of numerical treatment, see e.g. [38].

If one is not primarily interested in numerical results but also likes to remain close with the physical modeling and the according existence theory, the theory of optimal control (of partial differential equations) is a fruitful field.

A very detailed and comprehensive introduction into the theory of optimal control problems governed by partial differential equations is given within the textbook of Tröltzsch, [78]. Here, only a very short sketch of the most important tools explained in [78] will be given.

The general form of an optimal control problem is

$$\min_{w \in W} J(y, w) \quad \text{subject to} \quad D(y, w) = 0,\ C(y, w) \in A. \tag{5.6}$$

One seeks an optimal control w, member of an admissible control set W, that determines a state y by solving the state equation system $D(y, w)$ and minimizes the objective functional $J(y, w)$ under the restriction $C(y, w) \in A$.

The restriction $C(y, w) \in A$ is often given by simple pointwise box constraints for the control, i.e., a condition

$$w \in [w_{\min}, w_{\max}].$$

The objective function is often specified to be of tracking type with respect to

the state, i.e., the state dependent part contains terms of the following kind,

$$\int_0^T \int_\Omega \lambda_y(x,t)(y(x,t)-y_d(x,t))^2 dxdt \quad \text{(tracking on the space-time-cylinder)},$$

$$\int_0^T \int_\Gamma \lambda_y(x,t)(y(x,t)-y_d(x,t))^2 dxdt \quad \text{(tracking on the spatial boundary of the space-time-cylinder)},$$

$$\int_\Omega \lambda_y(x)(y(T)-y_d(T))^2 dx \quad \text{(tracking of the end time state in space)},$$

$$\int_\Gamma \lambda_y(x)(y(T)-y_d(T))^2 dx \quad \text{(tracking of the end time state on the boundary)}.$$

Furthermore, a regularization term for the control can be included into the objective function,

$$\frac{1}{2}\int_0^T \lambda_w |w|^2 dt. \tag{5.7}$$

Apart from "adding convexity" and leading to a smoother optimal control, this term is physically meaningful as it penalizes effort, e.g., the amount of gas utilized for the quenching.

It is often useful to introduce the so-called *control-to-state-mapping* or *solution operator* $S : w \mapsto y$ which assigns each control u the solution y of the equation system $D(y,w) = 0$ in case that the equation system is uniquely solvable. This solution operator enables a reduced formulation of the objective,

$$f(w) := J(S(w), w), \tag{5.8}$$

and thereby of the control problem, i.e.,

$$\min_{w \in W} f(w) \quad \text{subject to} \quad C(S(w), w) \in A. \tag{5.9}$$

The main tool of optimal control theory is the utilization of adjoint variables that exist in function spaces. In the case of existence of an optimal control, there exists an adjoint variable which fulfills an adjoint equation system. Further exploiting a variational inequality in terms of the Fréchet derivative of $f(w)$ with respect to the control w, one obtains neccessary optimality conditions. The Fréchet derivative of $f(w)$ with respect to the control w can be determined by the state $S(w)$ and its adjoint variable. The neccessary optimality conditions may commit to optimization techniques in function spaces comparable to the finite dimensional case. In practice, a gradient (steepest descent) method derived from the theory of optimal controls in

function spaces consists of repeated solving of partial differential equations for the state and the adjoint state to generate control updates.

Basically, there are two major approaches to implement optimal control problems numerically, *First discretize then optimize* and *First optimize then discretize*.

In the first named case, one applies a discretization scheme on the state equations and the objective functional to obtain an optimization problem of finite dimension.

Nonlinear discrete optimization problems were subject to intense research during the last century and are well understood. There is a large number of available textbooks on this topic, particularly addressing mathematicians, economists, and engineers. Just to name two among this assortment, Alt, [8], and Großmann and Terno, [38], cover in their books both mathematical and numerical treatment of finite dimensional optimization problems.

Due to the well-established knowledge about nonlinear optimization, also a large variety of very capable solvers is availabe for this type of problems and there are a lot of helpful hints in literature how to implement such a solver by oneself if demanded. Unfortunately, discrete equations derived from (coupled, instationary) partial differential equations usually have an immense number of variables to approximate the continuous equations well enough. This leads to troubles as the solver routines for discrete optimization problems collapse under the large dimension.

The second approach *First optimize then discretize* relieves this curse of large dimension in so far as one is free to solve parts sequentially. The need for working memory does not increase too much even if one uses a simple algorithmic approach. In particular, the decoupling in single spatial problems with respect to only one state variable as presented in chapter 4 is compatible without further ado. A disadvantage is given by the fact that there are inconsistencies because the optimality conditions of the discrete system and the discretized optimality conditions of the continuous problem in general do not coincide. If the numerical error is rather large, adjoint computations already start with a serious error.

Alternatively, more sophisticated methods, for example receding horizon techniques (see e.g. [50]), could be applied.

5.4 Control problem under investigation

We will now set up an optimal control problem which models the distortion compensation application. The model is chosen as in the foregoing chapter 4. It remains to specify an objective function and conditions for the control. As already introduced in equation (5.4), the setup of the quenching device suggests that the control consists of twelve time dependent components that regulate the gas flow of the single

jets. The amount of gas that can be emitted is limited and is of course non-negative. That leads to box constraints

$$w_i \in W_{ad} = \{v \in L^2(0,T) \ ; \ 0 \leq v(t) \leq w_{max}\}.$$

The spatial distribution of the cooling impact on the boundary of the workpiece is given by coefficient functions $w^i_{\Gamma O}(x)$.

We take only the outer nozzles as controllable, the jets applied on the inner side of the ring have a fixed outlet.

The objective function is supposed to describe the desired roundness of the geometry $\tilde{\Omega}$ one obtains if the displacement u is applied to Ω,

$$\tilde{\Omega} = (\mathrm{id} + u)(\Omega).$$

We will not consider designated shape optimization techniques here (as introduced in e.g. [76]) but try to find a way to formulate a roundness condition in terms of mapping the state variables $(\theta, z, u, w) \mapsto J(\theta, z, u, w)$ as it is common in the theory of the control of partial differential equations.

A circle can be characterized by the property that, given a fixed volume, it possesses minimal boundary length. The volume of the workpiece at end time is known a priori because the temperature and the phase distribution are when the cooling process is complete. In our application a minimal heat transfer is given by the cooling jets that are applied on the interior boundary of the ring. They have a fixed positive outlet, therefore it is certain within the model that temperature reduces to room temperature provided the end time is chosen large enough. The according phase distribution is homogenous as well because there is only a single product phase in the model which forms immediately according to temperature. Furthermore, transformation induced plasticity does not influence the volume, only the shear. Therefore, the volume at end time is completely determined by the thermoelastic effect which is known a priori through the homogenous temperature and phase distribution. Accordingly, the roundness of a 100Cr6 disk under the model utilized here could be characterized just by minimal boundary length. This holds also true for rings because holes just expand as the surrounding material (see e.g. [36]). Therefore, (parts of) the objective function could be specified as

$$|\partial\tilde{\Omega}| = |\partial(\mathrm{id} + u)(\Omega)| = \int_{\partial((id+u)(\Omega))} 1 dx.$$

Whereas it is simple to describe roundness of $\tilde{\Omega}$ through this characterization by means of data points in a discretized context, the author sees difficulties in applying it in the infinite-dimensional context. The boundary $\partial\Omega$ or $\partial\tilde{\Omega}$ is a null set that can

not be treated with common transformation rules. A differentiation with respect to u of the operator $\int_{(id+u)(\Omega)} 1dx$ is nonstandard within the classical theory of optimal control of partial differential equations in the sense of [78] but would require shape optimization techniques.

Therefore, we introduce further restrictions on u and try a standard tracking type approach. Assuming that displacements occur only in radial directions, the a priori knowledge about the end time volume of the workpiece enables the computation of an optimal displacement function u_d via the following considerations. The hole circumscribed by the interior boundary of the ring and the disk traced by the outward boundary, respectively, contract from the hot initial state to the cooled end state by a factor $(1+\bar{\beta})$ which is determined by the homogenous temperature and phase distribution. Thereby, the interior radius r_I^f and the outer radius r_O^f of the ring at end time compute from the radius r_I^0 of a circle with an area equal to the hole of the initial geometry and the radiusr_O^0 of a circle with an area equal to the whole geometry including the hole to

$$r_I^f = \sqrt{1+\bar{\beta}}\, r_I^0, \qquad r_O^f = \sqrt{1+\bar{\beta}}\, r_O^0. \tag{5.10}$$

This radius change is implemented by

$$x \mapsto \frac{r_O^f - r_I^f}{|x_O(x)| - |x_I(x)|} x + \frac{r_I^f x_O(x) - r_O^f x_I(x)}{|x_0(x)| - |x_I(x)|} \tag{5.11}$$

where x_O and x_I are determined for each x or rather each angle separately as the point of largest and of smallest norm within Ω on the line connecting x and the origin, respectively,

$$x_O(x) = (\max_{a\in\mathbb{R},\ ax\in\Omega} a)x, \qquad x_I(x) = (\min_{a\in\mathbb{R},\ ax\in\Omega} a)x. \tag{5.12}$$

Then, $x_O(x)$ is mapped radially to the outer boundary, $x_I(x)$ to the interior boundary of the desired end time ring, i.e.,

$$x_O(x) \mapsto r_O^f \frac{x_O(x)}{|x_O(x)|}, \qquad x_I(x) \mapsto r_I^f \frac{x_I(x)}{|x_I(x)|},$$

and the points x inbetween congruently to a point on the middle segment. Thus, a radial displacement function which yields a circular ring reads

$$u_d(x) = \left(\frac{r_O^f - r_I^f}{|x_O(x)| - |x_I(x)|} - 1 \right) x + \frac{r_I^f x_O(x) - r_O^f x_I(x)}{|x_0(x)| - |x_I(x)|}. \tag{5.13}$$

The necessary data r_O^f, r_I^f, $x_O(x)$, and $x_I(x)$ can be obtained by a preprocessing step, see figure 5.15 for an illustration of their construction. For a treatment of typical

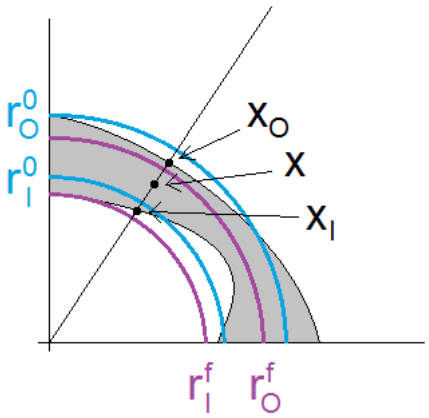

Figure 5.15: Construction of u_d

distortion profiles characterized by Fourier orders we focus on initial geometries with boundaries that can be parametrized with respect to the angle by a radius modulation

$$r(\varphi) = r_0 + a\cos(k\varphi), \tag{5.14}$$

where r_0 gives a base radius value, k the out-of-roundness order, and a the extent. Then u_d is such is taken such that the term $a\cos(k\varphi)$ is annihilated and such that shrinking due to temperature loss is taken into account,

$$u_d(x) = -(r_s + a\cos(k\arctan(\frac{x_2}{x_1})))\frac{x}{|x|}. \tag{5.15}$$

(We impose that computing is restricted to the quarter geometry, otherwise case distinctions have to be made to express the angle.) Employing a u_d, it is possible to choose a tracking type formulation for the objective function with respect to the displacement,

$$\frac{1}{2}\int_0^T \int_\Omega \lambda_u F(u)dxdt = \frac{1}{2}\int_0^T \int_\Omega \lambda_u (u-u_d)^2 dxdt. \tag{5.16}$$

As one maybe would want to apply a less restrictive characterization, we stay with

a general $F(u)$ in the following formulation of the full optimal control problem.

$$\text{Minimize} \quad J(u,\theta,w) = \frac{1}{2}\int_0^T \int_\Omega \lambda_u F(u) dx dt + \frac{\lambda_w}{2}\int_0^T |w|^2 dt$$

$$\text{s.t.} \qquad -div\ \sigma = 0, \qquad u_i = 0 \quad on\ \Gamma_D^i, \quad -\sigma n = 0 \quad on\ \Gamma_1$$

$$\sigma = K\left(\varepsilon(u) - \beta(z,\theta)I - \int_0^t \frac{3}{2}\zeta f(\theta,z)\sigma^* d\tau\right)$$

$$z_t = f(\theta,z), \qquad z(0) = 0$$

$$\varrho c_p \theta_t - k\Delta\theta = 0, \quad \theta(0) = \theta_0$$

$$-k\partial_n\theta = \begin{cases} \sum_i \alpha_i^I(x,t)(\theta - \theta_a) & \text{on } \Gamma_I \times (0,T) \\ \sum_i w_i^{\Gamma_O}(x) w_i(t)(\theta - \theta_a) & \text{on } \Gamma_O \times (0,T) \\ 0 & \text{on } \Gamma_S \times (0,T) \end{cases}$$

$$\text{where} \qquad w_i \in U_{ad} = \{v \in L^2(0,T)\ ;\ 0 \le v(t) \le w_{max}\}$$

where Γ_I denotes the interior and Γ_O the outward boundary, α^I gives fixed heat transfer coefficients for the interior boundary.

Of course the objective function could contain more terms, in particular a tracking term for the temperature such that a cooling to room temperature is achieved within an appropriate time. But as we consider a problem where a constant minimal cooling is given by the inner nozzles, we can do here without a temperature objective term.

By Lagrange formalism (see [78]) we achieve a time-reverse adjoint system in the variable p_θ for the heat equation, p_z for the phase equations, p^{tp} for the TrIP equation, p_σ and p_u for the elasticity equation,

$$\begin{aligned}\varrho c_p p^\theta - k\Delta p^\theta = {} & \partial_\theta f(\theta(T-t), z(T-t)) p^z + 3\kappa\partial_\theta q(\theta(T-t), z(T-t)) div(p^u) \\ & + 3\zeta\mu(\sum_i \partial_\theta h_i(\theta(T-t), z(T-t))(\varepsilon^*(u(T-t)) - \varepsilon^{trip}(T-t)) : p^{trip}\end{aligned}$$

$$-k\partial_n p^\theta = \begin{cases} \sum_i \alpha_i^I(x, T-t) p^\theta & \text{on } \Gamma_I \times (0,T) \\ \sum_i w_i^{\Gamma_O}(x) w_i(T-t) p^\theta & \text{on } \Gamma_O \times (0,T) \\ 0 & \text{on } \Gamma_S \times (0,T) \end{cases}$$

$$
\begin{aligned}
p^{\theta}(0) &= 0 \\
p_t^z &= \partial_z f(\theta(T-t), z(T-t))p^z + 3\kappa\partial_z q(\theta(T-t), z(T-t))div(p^u) \\
&\quad + 3\zeta\mu(\sum_i \partial_z h_i(\theta(T-t), z(T-t)))(\varepsilon^*(u(T-t)) - \varepsilon^{trip}(T-t)) : p^{trip} \\
p^z(0) &= 0 \\
-div(p^\sigma) &= \lambda_u \partial_u F(u(T-t)), \qquad p^{u_i} = 0 \text{ on } \Gamma_D^i, \qquad p^\sigma n = 0 \text{ on } \Gamma_1 \\
p^\sigma &:= K\varepsilon(p^u)) - 3\zeta\mu(\sum_i h_i(\theta(T-t), z(T-t)))p^{trip,*} \\
p_t^{trip} &= 2\mu\varepsilon(p^u) - 3\zeta\mu(\sum_i h_i(\theta(T-t), z(T-t)))p^{trip}, \qquad p^{trip}(0) = 0.
\end{aligned}
$$

With the help of the solution to the adjoint equations the i-th gradient component is determined as

$$\lambda_{w_i} w_i - \int_\Gamma w_i^{\Gamma_O}(\theta - \theta^a)p^\theta(T-t).$$

This system again requires the implementation of a numerical scheme as presented in chapter 4. Many system matrices can be reused but some coupling terms exhibit a different structure or differ regarding tensor rank from the matrices used so far. But as the assembly is very lengthy and obtained by similar approaches as in chapter 4 it will not be illustrated here.

Utilizing the adjoint equations and given a maximal step size $s_{\max}$ and a minimal step size $s_{\min}$, a simple gradient method for the optimal control problem is implemented by

- $k = 0$: Initialize the control such that $w^0 \in W$. Solve the state equations with w^0 to obtain state values $y^0 = (\theta^0, z^0, u^0, \varepsilon^{tp,0})$. Compute $J^0 = J(y^0, w^0)$. Initialize $J^d_{\min} = J^{k,0}$.
- Outer loop (gradient update) :
  - Increase k by 1.
  - Solve the adjoint equations where the right hand side is given by y^{k-1} to obtain p^k.
  - Compute the gradient d^k, $d_i^k = \lambda_{w_i} w_i - \int_\Gamma \alpha_i(x)(\theta - \theta_{amb})p^\theta(T-t)$.

- Set the initial step size for the line search method, $s_0 = s_{\max}$. Solve the state equations with $w^{k,0} = w^{k-1} + s_0 d^k$ to obtain $y^{k,0}$. Compute $J^{k,0} = J(y^{k,0}, w^{k,0})$. Initialize $J^s_{\min} = J^{k,0}$.
- Inner loop (step size iteration) :
  - Increase r by 1, set $s_r = \frac{s_{r-1}}{2} = \frac{1}{2^r} s_{\max}$.
  - Set $w^{k,r} = w^{k-1} + s_r d^k$. Solve the state equations for $w^{k,r}$ to obtain $y^{k,r}$. If $J(y^{k,r}, w^{k,r}) < J^s_{\min}$ set $J^s_{\min} = J(y^{k,r}, w^{k,r})$.
  - If $s_r \geq s_{\min}$ and the condition

    $$J^d_{\min} < J(y^{k,r}, w^{k,r}) \quad \text{or} \quad J(y^{k,r}, w^{k,r}) < J(y^{k,r-1}, w^{k,r-1})$$

    holds, proceed within the inner loop. Otherwise continue with the outer loop in k.
- If $J^s_{\min} + \varepsilon \leq J^d_{\min}$ set $J^d_{\min} = J^s_{\min}$ and continue with the outer loop. Otherwise, the line search did not result in a suitable descent and the iteration ends.

The investigation of the control problem and its implementation is still in process. Even in 2D, the mere state equations are numerically challenging due to the coupling with the deviatoric part of the stress. It requires a very fine discretization to reach an acceptable accuracy.

To relax the problem, we start with the investigation of a simpler objective

$$\frac{1}{2} \int_0^T \int_\Omega (\exp(at) - 1)\, \chi_{\{x_1 \leq b\}}(x)\, (u_2 - 1)^2 dx dt, \tag{5.17}$$

which is minimized for a displacement of the upper left segment in vertical direction. Whereas u_d defined as in (5.13) or (5.15) may procure ambiguous results, this simplified version produces a clearly traceable deformation of the work piece. Furthermore, we do not take the original experimental data but choose flatter Gaussian profiles for modeling the heat transfer coefficient produced by the cooling jets for a more immediate cooling.

In figures 5.16 and 5.17 the numerical results for this specific profile are presented. According to the algorithm above, for each gradient step the adjoint equation was

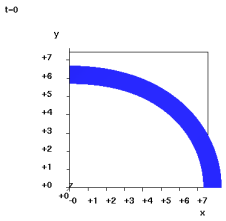

Figure 5.16: Martensite and deformation at initial time

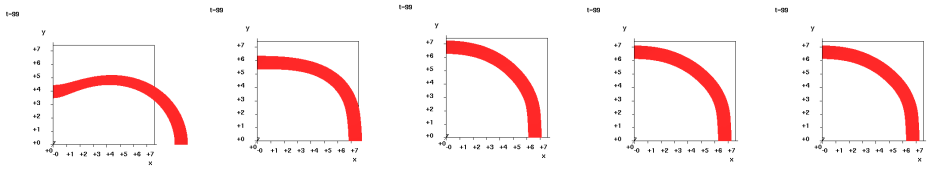

(a) step 0 (b) step 1 (c) step 2 (d) step 3 (e) step 4

Figure 5.17: Martensite and deformation at final time for the start control and the first four gradient steps

solved once and the state equations several times, each time for the whole time interval $[0, T]$. In every gradient step, the initial geometry and the initial values for the state variables remain the same, but the varying control leads to different displacements in the end time. Figure 5.16 shows the initial geometry (which is equal to the reference geometry, $u = 0$ for $t = 0$) and the colour indicates the initial martensite fraction (which is zero for the austenitized, hot steel). The geometry has an ovality in the sense of a larger horizontal expansion. The initial control for the gradient method is selected such that the cooling for φ close to $\frac{\pi}{2}$ is stronger, i.e., the jet at the twelve o'clock position emits more gas. Accordingly, at end time the bulge in horizontal direction gets even more distinct, see figure 5.17 (a). In gradient steps one to four the control is updated such that a stronger cooling is applied at the three o'clock position, i.e., for $\varphi = 0$. This creates a compensating displacement in vertical direction, figure 5.17 (b) - (e).

As it is usual for gradient methods, the first steps yield significant improvements by means of a reduction of the value of the objective function followed by only a minor descent rate in the ongoing method.

5.5 Outlook

The first results of the optimal control problem are encouraging but could be improved. We want to name some possible ways for further investigations.

The objective function of the control problem could be chosen to better model

the desired goal, possibly by employment of shape optimization techniques.

The numerical simulation based on chapter 4 is based on linear finite elements because higher order elements were not available at the time of implementation. By now, quadratic finite elments are implemented into the FE-toolbox of *pdelib*, enabling more accurate computions in particular of the stress.

Numerical errors in the computation of the state equations contribute to the coupling terms and the right hand side of the adoint equations. The error is then processed further, the descent direction is perturbed. When the code is adapted to utilize quadratic elements and the error in the stress computation is reduced, a more precise solution to the state equations probably yields more reliable results for the optimization algorithm.

Despite the longer computation time of the 3D optimal control problem, an application to the physically more realistic problem would be of interest.

Appendix

A.1 Notation

$\mathcal{L}^p(E)$:	seminormed vector space of p^{th} power integrable functions from E to $\mathbb{R}$ (or $\mathbb{C}$)
$L^p(E)$:	normed vector space given by the quotient space $\mathcal{L}^p(E)\backslash\mathcal{N}^p$ $\mathcal{N}^p := ker(\|\cdot\|_p)$
θ :	temperature
z :	phase vector
u :	displacement
ε :	strain tensor
σ :	(Cauchy) stress tensor
L :	latent heat vector
L_i :	latent heat for evolution of phase i
θ^i_{ref} :	constant reference temperature for the expansion of phase i
θ_{amb} :	ambient temperature
k :	heat conductivity (scalar constant)
c :	specific heat capacity (scalar constant)
I :	unit tensor
$\cdot^*$:	deviatoric part, i.e. $X^* = X - \frac{1}{d}tr(X)I$ for $X \in \mathbb{R}^{d\times d}$, $I \in \mathbb{R}^{d\times d}$ unit tensor
$tr(\cdot)$:	trace of a second-order tensor (i.e. a square matrix), $tr(A) = \sum_{i=1}^{d} a_{ii}$ for $A \in \mathbb{R}^{d\times d}$
K :	stiffness tensor
λ :	first Lamé parameter
μ :	second Lamé parameter
b :	bulk modulus $b = 3\lambda + 2\mu$
ϱ :	mass density
$\dot{\in}$:	"almost everywhere in"
$\forall\, x \dot{\in} X$:	"for almost every x in X"
$W^{k,p}(E)$:	set of all functions $f \in L^p(E)$ possessing weak derivatives up to the order k
$W^{k,r}_p(Q)$:	$L^p(0,T;W^{k,p}(\Omega)) \cap W^{r,p}(0,T;L^p(\Omega))$
$H^k(E)$:	$W^{k,2}(E)$, Sobolev spaces with integration order 2
e_k :	k-th unit vector
$\cdot^T$:	transposition
$[f]_+$:	positive part of f, $[f]_+ = \min\{0, f\}$
∇_r :	$\frac{\partial}{\partial x_r}$, derivative with respect to the r-th argument

A.2 Utilized definitions and theorems

Definition A.2.1 (Bochner Integral) *For $p \in [1, \infty)$ we denote by $L^p(0,T;X)$ the linear space of equivalence classes of Bochner integrable functions $u : [0,T] \to X$ satisfying*

$$\int_0^T \|u(t)\|_X^p dt < \infty. \tag{A.2.2}$$

$L^\infty(0,T;X)$ denotes the linear space of all equivalence classes of essentially bounded Bochner measurable functions.

Theorem A.2.3 (Rademacher) *Let u be locally Lipschitz continuous in U. Then u is differentiable almost everywhere in U.*
(See e.g. Evans [30].)

Theorem A.2.4 (Weyl) *Let $0 < p \leq \infty$.*
a) For every Cauchy sequence $(f_n)_{n\geq 1}$ in $\mathcal{L}^p$ there exists a subsequence $(f_{n_k})_{k\geq 1}$ and a $f \in \mathcal{L}^p$ such that $f_{n_k} \to f$ almost everywhere.
b) If $(f_n)_{n\geq 1}$ converges in $\mathcal{L}^p$ towards $f \in \mathcal{L}^p$, then it possesses a subsequence $(f_{n_k})_{k\geq 1}$ that converges towards f almost everywhere.
(See e.g. Elstrodt [28].)

Theorem A.2.5 (Hölder's inequality) *Let S be a measure space and let $1 \leq p, q \leq \infty$ with $\frac{1}{p} + \frac{1}{q} = 1$. Then, for all measurable real- or complex-valued functions f and g on S,*

$$\|fg\|_1 \leq \|f\|_p \|g\|_q. \tag{A.2.6}$$

Theorem A.2.7 (Sobolev embedding theorem 1) *Let $\Omega \subset \mathbb{R}^N$ be a bounded Lipschitz domain, $1 < p < \infty$, and m a non-negative integer. Then the following embeddings are defined and continuous:*

$$W^{m,p}(\Omega) \hookrightarrow \begin{cases} L^q(\Omega) \quad \text{for all } 1 \leq q \leq \frac{Np}{N-mp}, & \text{if } mp < N \\ L^q(\Omega) \quad \text{for all } 1 \leq q < \infty \quad , & \text{if } mp = N \\ C(\bar{\Omega}) \quad , & \text{if } mp > N \end{cases} \tag{A.2.8}$$

In particular, for $H^1(\Omega) = W^{1,2}(\Omega)$ we obtain

$$\text{if } \Omega \subset \mathbb{R}^2 : \quad H^1(\Omega) \hookrightarrow L^q(\Omega) \quad \text{for all } 1 \leq q < \infty \tag{A.2.9}$$

$$\text{if } \Omega \subset \mathbb{R}^3 : \quad H^1(\Omega) \hookrightarrow L^6(\Omega). \tag{A.2.10}$$

Theorem A.2.11 (Sobolev embedding theorem 2) *Let (0,T) be a bounded interval. Then $W^{1,p}(0,T;X)$ is contained in $C([0,T];X)$ and there exists a constant $C \geq 0$ such that*

$$\|u\|_{L^\infty} \leq C\|u\|_{W^{1,p}} \qquad \text{for every } u \in W^{1,p}(0,T;X). \tag{A.2.12}$$

Theorem A.2.13 (Rellich-Kondrachov Compactness Theorem) *Assume U is a bounded open subset of $\mathbb{R}^n$ and ∂U is C^1. Suppose $1 \leq p < n$. Then*

$$W^{1,p}(U) \Subset L^q(U) \qquad (\Subset \text{ denotes compact embedding}) \tag{A.2.14}$$

for each $1 \leq q < p^*$ where $p^* = \frac{np}{n-p}$ is the Sobolev conjugate of p.
Since $p^* > p$ and $p^* \to \infty$ as $p \to n$, we have in particular

$$W^{1,p}(U) \Subset L^p(U) \quad \text{for all } 1 \leq p \leq \infty. \tag{A.2.15}$$

(If $n < p \leq \infty$, this follows from Morrey's inequality and the Arzela-Ascoli compactness criterion.)
Even if ∂U is not assumed to be C^1 one achieves

$$W_0^{1,p}(U) \Subset L^p(U). \tag{A.2.16}$$

(See e.g. Evans [30].)

Theorem A.2.17 (Morrey's inequality) *Assume $n < p \leq \infty$. Then there exists a constant C, depending only on p and n, such that*

$$\|u\|_{C^{0,\gamma}(\mathbb{R}^n)} \leq C\|u\|_{W^{1,p}(\mathbb{R}^n} \tag{A.2.18}$$

for all $u \in C^1(\mathbb{R}^n)$ where $\gamma := 1 - \frac{n}{p}$.
(See e.g. [30].)

Theorem A.2.19 (Arzela-Ascoli's compactness criterion for uniform convergence)
Suppose that $\{f_k\}_{k=1}^{\infty}$ is a sequence of real-valued functions defined on $\mathbb{R}^n$, such that

$$|f_k(x)| \leq M \qquad (k = 1, .. \,, \quad x \in \mathbb{R}^n) \tag{A.2.20}$$

for some constant M and the $\{f_k\}_{k=1}^{\infty}$ are uniformly equicontinuous. Then there exists a subsequence $\{f_{k_j}\}_{j=1}^{\infty} \subseteq \{f_k\}_{k=1}^{\infty}$ and a continuous function f such that

$$f_{k_j} \to f \quad \text{uniformly on compact subsets of } \mathbb{R}^n. \tag{A.2.21}$$

To say the $\{f_k\}_{k=1}^{\infty}$ are uniformly equicontinuous means that for each $\varepsilon > 0$ there exists $\delta > 0$ such that $|x - y| < \delta$ implies $|f_k(x) - f_k(y)| < \varepsilon$ for $x, y \in \mathbb{R}^n$, $k = 1, ...$
(See e.g. Evans [30].)

Theorem A.2.22 (Korn inequality) *Let $1 < p < \infty$, $\Omega \subset \mathbb{R}^n$ be a domain with smooth boundary, and $\Gamma_D \subset \partial\Omega$, $|\Gamma_D| \neq 0$. Then there is a constant $C_K = C_K(p, \Omega)$ such that for any $v \in W^{1,p}_D(\Omega) = \{u \in W^{1,p}(\Omega)\ ;\ u = 0 \text{ on } \Gamma_D\}$ it holds that*

$$\|v\|_{W^{1,p}_D(\Omega;\mathbb{R}^n)} \leq C_K \|\varepsilon(v)\|_{L^p(\Omega;\mathbb{R}^n)} \quad \text{where } \varepsilon(v) = \frac{1}{2}\left(\nabla v + (\nabla v)^T\right).$$

(This variant e.g. in Herzog, Meyer, Wachsmuth [40].)

Theorem A.2.23 (Product Rule) *Suppose $\Omega \subset \mathbb{R}^n$ open, $1 \leq p \leq \infty$, and $\frac{1}{p} + \frac{1}{p'} = 1$. If $f \in W^{m,p}(\Omega)$ and $g \in W^{m,p'}(\Omega)$ then $f \cdot g \in W^{m,1}(\Omega)$ and the weak derivatives of $f \cdot g$ are given by Leibniz product rule.*

Theorem A.2.24 (Carathéodory's Theorem) *Let $I = [0, T]$ for fixed $T > 0$ and $f : I \times \mathbb{R}^k \to \mathbb{R}^k$ satisfying the following conditions:*
(Carathéodory mapping)

$$f(\cdot, \zeta) \quad \text{is measurable for all } \ \zeta \in \mathbb{R}^k \tag{A.2.25}$$

$$f(t, \cdot) \quad \text{is continuous for almost all } \ t \in I \tag{A.2.26}$$

(Growth condition)

$$|f(t, z)| \leq \gamma(t) + C|z| \quad \text{with some } \ \gamma \in L^1(I). \tag{A.2.27}$$

Then :

(i) The initial-value problem

$$\frac{dz}{dt} = f(t, z(t)) \quad \text{for almost all } t \in I, \qquad z(0) = z_0 \tag{A.2.28}$$

has a solution $z \in W^{1,1}(I; \mathbb{R}^k)$ on the interval $I = [0, T]$

(ii) If $f(t, \cdot)$ is also Lipschitz continuous in the sense

$$|f(t, z_1) - f(t, z_2)| \leq L(t)|z_1 - z_2| \tag{A.2.29}$$

with some $L \in L^1(I)$, then the solution is unique.

(This variant e.g. in Roubíček [67].)

Theorem A.2.30 (Gronwall's Lemma) *Let $c \in L^\infty(0, t_E)$ and $a \in L^1(0, t_E)$ denote non-negative functions. If a function $u \in L^\infty(0, t_E)$ satisfies*

$$0 \leq u(t) \leq c(t) + \int_0^t a(s)u(s)ds, \quad t\dot{\in}(0, t_E), \tag{A.2.31}$$

then

$$0 \leq u(t) \leq c(t) + \int_0^t c(s)a(s) \exp\left(\int_s^t a(\tau)d\tau\right) ds, \quad t\dot{\in}(0, t_E). \tag{A.2.32}$$

In particular, if $c(t) = c$ *and* $a(t) = a$ *for almost every* $t \in (0, t_E)$*, then*

$$0 \leq u(t) \leq c \exp(at), \quad t\dot{\in}(0, t_E). \tag{A.2.33}$$

(This variant e.g. in Brokate, Sprekels [14].)

Theorem A.2.34 *Consider the Dirichlet problem*

$$\begin{aligned} -divL(Du) &= f \quad in\ \Omega, \\ u &= g \quad on \partial\Omega, \end{aligned}$$

where $f : \Omega \to \mathbb{R}^n$ *and* $g : \partial\Omega \to \mathbb{R}^n$ *are given functions,* $L = (l_{ijhk})$*. The differential operators* D *and* div *may as well be understood in a weak sense. Suppose* $l_{ijhk} \in L^\infty(\Omega)$ $(i, j, h, k = 1, .., n)$*, then the operator*

$$u \mapsto divL(Du) \tag{A.2.35}$$

maps $W^{1,p}(\Omega)$ *into* $W^{-1,p}(\Omega) \simeq (W_0^{1,q})^*$ *with* $1 < p < \infty$*,* $\frac{1}{p} + \frac{1}{q} = 1$*. Let*

$$b(v, u) = \int_\Omega l(x, Du(x))Dvdx \tag{A.2.36}$$

be $W_0^{1,2}(\Omega)$*-elliptic (coercive),*

$$\exists\ c > 0\ :\ |b(v, v)| \geq c\|v\|^2_{W^{1,2}(\Omega)}\ , \quad \forall\ v \in W_0^{1,2}(\Omega). \tag{A.2.37}$$

Then (A.2.35) is a (linear) homeomorphism of $W_0^{1,2}(\Omega)$ *onto* $W^{-1,2}(\Omega)$*. Moreover, (using Simader's methods, [73]) (A.2.35) is a homeomorphism of* $W_0^{1,p}(\Omega)$ *onto* $W^{-1,p}(\Omega)$ *with* p *any real number* > 1*, provided the functions* l_{ijhk} *are continuous on* $\bar{\Omega}$ *and* Ω *is of class* C^1*.*
(See Valent [80].)

Theorem A.2.38 (Banach's Fixed Point Theorem) *Consider the nonlinear equation*

$$x = Tx, \qquad x \in M. \tag{*}$$

Suppose that

1. $T : M \subseteq X \to M$*, i.e., M is mapped into itself by an operator T;*
2. *M is a closed nonempty set in a complete metric space* (X, d)*;*

3. T is k-contractive, i.e.,

$$d(Tx, Ty) \leq kd(x, y)$$

for all $x, y \in M$ and for a fixed k, $0 \leq k < 1$.

Then we may conclude the following:

- *Existence and uniqueness: Equation (*) has exactly one solution, i.e., T has exactly one fixed point on M;*
- *Convergence of the iteration: The sequence (x_n) of successive approximations converge to the solution, x, for an arbitrary choice of initial point x_0 in M;*
- *Error estimates: For all $n = 0, 1, 2, ..$ we have the a priori error estimate*

$$d(x_n, x) \leq k^n(1-k)^{-1}d(x_0, x_1),$$

and the a posteriori error estimate

$$d(x_{n+1}, x) \leq k(1-k)^{-1}d(x_n, x_{n+1});$$

- *Rate of convergence: For all $n = 0, 1, 2, ..$ we have*

$$d(x_{n+1}, x) \leq kd(x_n, x).$$

(See e.g. [93].)

Definition A.2.39 (Compact operator) *Let X and Y be Banach spaces and $T : D(T) \subseteq X \to Y$ an operator. T is called compact iff:*
(i) T is continuous,
(ii) T maps bounded sets into relatively compact sets.

Theorem A.2.40 (Schauder's Fixed Point Theorem – Version 1) *Let M be a nonempty, closed, bounded, convex subset of a Banach space X, and suppose $T : M \to M$ is a compact operator. Then T has a fixed point.*

Theorem A.2.41 (Schauder's Fixed Point Theorem – Version 2) *Let M be a nonempty, closed, convex, and compact subset of a Banach space X, and suppose $T : M \to M$ is a continuous operator. Then T has a fixed point.*

Theorem A.2.42 (Dominated Convergence Theorem (Lebesgue)) *Assume the functions $(f_k)_{k=1}^{\infty}$ are integrable and*

$$f_k \to f \quad a.e. \qquad and \qquad |f_k| \leq g \quad a.e. \tag{A.2.43}$$

for some summable function g. Then

$$\int_{\mathbb{R}^n} f_k \, dx \to \int_{\mathbb{R}^n} f \, dx. \tag{A.2.44}$$

In particular, for $1 \leq p < \infty$ and $\Omega \subset \mathbb{R}^n$

$$\|f_k - f\|_{L^p(\Omega)} \to 0 \tag{A.2.45}$$

can be achieved by application of the foregoing statement on $h_k = |f_k - f|^p$.
(See e.g. Evans [30].)

Bibliography

[1] C. Acht, M. Dalgic, F. Frerichs, M. Hunkel, A. Irretier, T. Lübben, H. Surm *Ermittlung der Materialdaten zur Simulation des Durchhärtens von Komponenten aus 100Cr6. Teil 1: Einleitung – Charakterisierung des Werkstoffs und der Wärmebehandlung – Grundsätzliche Überlegungen – Beschreibung von Abhängigkeiten – Thermo-physikalische Kennwerte – Thermomechanische Kennwerte*, HTM J. Heat Treatm. Mat. 63, vol. 5, pp. 234-244 (2008)

[2] C. Acht, M. Dalgic, F. Frerichs, M. Hunkel, A. Irretier, T. Lübben, H. Surm *Ermittlung der Materialdaten zur Simulation des Durchhärtens von Komponenten aus 100Cr6. Teil 2: Parameter zum Umwandlungsverhalten – Beurteilung des Datensatzes anhand von Bauteilversuchen – Diskussion – Ausblick*, HTM J. Heat Treatm. Mat. 63, vol. 6, pp. 362-371 (2008)

[3] S. Agmon, A. Douglis, L. Nirenberg *Estimates near the boundary for solutions of elliptic partial differential equations satisfying general boundary conditions I*, Communications on pure and applied mathematics 12, pp. 623-727 (1959)

[4] S. Agmon, A. Douglis, L. Nirenberg *Estimates near the boundary for solutions of elliptic partial differential equations satisfying general boundary conditions II*, Communications on pure and applied mathematics 17, pp. 35-92 (1964)

[5] H.D. Alber *Mathematische Theorie des inelastischen Materialverhaltens von Metallen*, Mitteilungen der Gesellschaft für Angewandte Mathematik und Mechanik 18, pp. 9-38 (1995)

[6] H.D. Alber, K. Chełmiński *Quasistatic problems in viscoplasticity theory*, Preprint 2190, Fachbereich Mathematik, Technische Universität Darmstadt (2002)

[7] H. Alder, D. Hömberg, W. Weiss *Simulationsbasierte Regelung der Laserhärtung von Stahl*, HTM Z. Werkst. Waermebeh. Fertigung 61 (2), pp. 103-107 (2006)

[8] W. Alt *Nichtlineare Optimierung: Eine Einführung in Theorie, Verfahren und Anwendungen*, Vieweg + Teubner, Wiesbaden (2002)

[9] ASM *ASM Handbook: volume 4: Heat Treating* ASM International (1991)

[10] J.-P. Aubin *Variational principles for differential equations of elliptic, parabolic and hyperbolic type*, Math. Techniques of Optimization, Control and Decision, Eds. J.-P. Aubin, A. Bensoussan, I. Ekeland, pp. 31-45, Birkhäuser, Boston (1981)

[11] A. Bertram *An alternative approach to finite plasticity*, Report IFME 98/3 (1998)

[12] M Böhm, S. Dashkovskiy, M. Hunkel, T. Lübben, M. Wolff *Übersicht über einige makroskopische Modelle für Phasenumwandlungen im Stahl*, Universität Bremen, Berichte aus der Technomathematik, Report 03-09 (2003)

[13] D. Braess *Finite Elemente, Theorie, schnelle Löser und Anwendungen in der Elastizitätstheorie*, Springer, Berlin (2003)

[14] M. Brokate, J. Sprekels *Hysteresis and Phase Transitions*, Springer, Berlin (1996)

[15] K. Chełmiński, D. Hömberg, D. Kern *Analysis of a thermomechanical phase transition model*, Sixth International Congress on Industrial Applied Mathematics (ICIAM07) and GAMM Annual Meeting, Zürich 2007, vol. 7 of Proceedings in Applied Mathematics and Analysis, pp. 115080/5-115080/6, Wiley-VCH Verlag GmbH & Co. KGaA (2008)

[16] K. Chełmiński, D. Hömberg, D. Kern *On a thermomechanical model of phase transitions in steel*, Adv. Math. Sci. Appl. 18(1), pp. 119-140 (2008)

[17] P.G. Ciarlet, P. Ciarlet Jr. *Another approach to linearized elasticity and Korn's inequality*, C. R. Acad. Sci. Paris, Ser. I 339 (2004)

[18] B. Clausen, F. Frerichs, G. Goch, D. Klein, Th. Lübben, L. Nowag, C. Prinz, T. Sackmann, D. Stöbener, H. Surm, H.-W. Zoch *Verzugsentstehung von Wälzlagerringen*, HTM Z. Werkst. Wärmebeh. Fertigung 61 (2006)

[19] W. H. Cubberly, R. Bakerjian *Tool and manufacturing engineers handbook*, Society of Manufacturing Engineers (1989)

[20] M. Dalgic, G. Löwisch *Transformation plasticity at different phase transformations of bearing steel*, Proc. 1st Int. Conf. on Distortion Engineering, IDE2005, 14-16.09.05, Bremen, H.-W. Zoch, Th. Lübben (Eds.), pp. 347-356 (2005)

[21] S. Denis, S. Sjöström, A. Simon *Coupled temperature, stress, phase transformation calculation model numerical illustration of the internal stresses evolution during cooling of an eutectoid carbon steel cylinder*, Met. Trans. 18A, pp. 1203-1212 (1987)

[22] M. Dijkman, M. Hunkel, G. Goch *Automatische Qualitätsregelung für die Gasabschreckung von Wälzlagerringen*, HTM Z. Werkst. Wärmebeh. Fertigung 62 (2007)

[23] M. Dijkman *Automated Compensation of Distortion in the Production Process of Bearing Rings*, Dissertation am Fachbereich Produktionstechnik der Universität Bremen (2009)

[24] W. Dreyer, D. Hömberg, T. Petzold *A model for the austenite-ferrite phase transition in steel including misfit stress*, Weierstrass Institute for Applied Analysis and Stochastics, WIAS preprint 1310 (2008)

[25] G. Duvaut, J.L. Lions *Inequalities in mechanics and physics*, Die Grundlehren der mathematischen Wissenschaften 219, Springer, Berlin (1976)

[26] J. Elschner, H.C. Kaiser, J. Rehberg, G. Schmidt *$W^{1,q}$-regularity results for elliptic transmission problems on heterogeneous polyhedra*, Math. Models Methods Appl. Sci. 17, vol. 4, pp. 593–615 (2007)

[27] J. Elschner, J. Rehberg, G. Schmidt *Optimal regularity for elliptic transmission problems including C^1-interfaces*, Interfaces Free Bound. 9, pp. 233–252 (2007)

[28] J. Elstrodt *Maß- und Integrationstheorie*, Springer, Berlin (2005)

[29] E. Emmrich *Gewöhnliche und Operator-Differentialgleichungen*, Vieweg, Wiesbaden (2004)

[30] L. C. Evans *Partial Differential Equations*, Graduate Studies in Mathematics 19, AMS (1998)

[31] F.D. Fischer, G. Reisner, E. Werner, K. Tanaka, G. Cailletaud, T. Antretter *A new view on transformation induced plasticity (TRIP)*, Int. J. Plasticity 16, pp. 723-748 (2000)

[32] F.D. Fischer, Q.-P. Sun, K. Tanaka *Transformation induced plasticity (TRIP)*, Appl. Mech. Rev. 49, pp. 317–364 (1996)

[33] K.O. Friedrichs *On the boundary-value problems of the theory of elasticity and Korn's inequality*, The Annals of Mathematics, Second Series 48, No. 2, pp. 441-471 (1947)

[34] J. Fuhrmann et al. *pdelib*, http://www.wias-berlin.de/software/pdelib/

[35] J. Fuhrmann, D. Hömberg *Numerical simulation of the surface hardening of steel*, Internat. J. Numr. Methods Heat Fluid Flow, 9, pp. 705-724 (1999)

[36] D. Giancoli *Physics for Scientists and Engineers*, Prentice Hall, 3rd edition (2000)

[37] R. Griesse and C. Meyer *Optimal control of static plasticity with linear kinematic hardening*, ZAMM, to appear (2010), Weierstrass Institute for Applied Analysis and Stochastics, WIAS preprint 1370 (2009)

[38] Ch. Grossmann, J. Terno *Numerik der Optimierung*, Teubner Studienbücher Mathematik, Stuttgart (1997)

[39] R. Haller-Dintelmann *L^p-Regularity Theory for Linear Elliptic and Parabolic Equations*, Habilitationsschrift, TU Darmstadt (2008)

[40] R. Herzog, C. Meyer, G. Wachsmuth *Regularity of Displacement and Stresses in Linear and Nonlinear Elasticity with Mixed Boundary Conditions*, Preprint SPP1253-093 (2010)

[41] D. Hömberg *A mathematical model for the phase transitions in eutectoid carbon steel*, IMA J. Appl. Math. 54, pp. 31-57 (1995)

[42] D. Hömberg *A numerical simulation of the Jominy end–quench test*, Acta Mater. 44, pp. 4375-4385 (1996)

[43] D. Hömberg *Irreversible phase transitions in steel*, Math. Meth. Appl. Sc., 20, pp. 59-77 (1997)

[44] D. Hömberg *A mathematical model for induction hardening including mechanical effects*, Nonlinear Anal. Real World Appl. 5(1), pp. 55-90 (2004)

[45] D. Hömberg, D. Kern, W. Weiss *Die Wärmebehandlung von Stahl — ein Optimierungsproblem*, Distortion Engineering – Verzugsbeherrschung in der Fertigung III – vol. 3 of Sonderforschungsbereich 570, Universität Bremen, Kolloquium, pp. 39-55 (2006)

[46] D. Hömberg, Ch. Meyer, J. Rehberg, W. Ring *Optimal control for the thermistor problem*, SIAM J. Control Optim. 45(5), pp. 3449-3481 (2010)

[47] D. Hömberg, W. Weiss *PID Control of Laser Surface Hardening of Steel*, IEEE Trans. Control Syst. Technol. 14, pp. 896-904 (2006)

[48] D. Hömberg, M. Yamamoto *On an inverse problem related to laser material treatments*, Inverse Problems 22, pp. 1855 - 1867 (2006)

[49] M. Hunkel, S. Schüttenberg, F. Frerichs, U. Fritsching, H.-W. Zoch *Verzugskompensation mittels Gasabschreckung in flexiblen Düsenfeldern*, HTM Z. Werkst. Wärmebeh. Fertigung 59 (2004)

[50] K. Ito, K. Kunisch *Receding horizon optimal control for inifinite dimensional systems*, ESAIM: Control, Optimisation and Calculus of Variations 8, pp. 741-760 (2002)

[51] W. Johnson, R. Mehl *Reaction Kinetics in Processes of Nucleation and Growth*, AIME Technical Publication No. 1089 (1939)

[52] P. Knabner, L. Angermann *Numerik partieller Differentialgleichungen: eine anwendungsorientierte Einführung*, Springer Berlin (2000)

[53] A. Korn *Sur les équations d'élasticité*, Ann. École Norm. 24 (1907)

[54] O. Ladyzhenskaya, V. Solonnikov, N. Ural'ceva *Linear and Quasilinear Equations of Parabolic Type*, Translations of Mathematical Monographs 23, AMS (1968)

[55] J. Leblond, J. Devaux *A new kinetic model for anisothermal metallurgical transformations in steels including effect of austenite grain size*, Acta Met., 32, p.137-146 (1984)

[56] J. Lemaitre *Handbook of Materials Behavior Models*, Academic Press, San Diego, USA (2001)

[57] D. Lüdecke, C. Lüdecke *Thermodynamik. Physikalisch-chemische Grundlagen der thermischen Verfahrenstechnik*, Springer Berlin (2000)

[58] J.E. Marsden, T.J.R. Hughes *Mathematical foundations of elasticity*, Dover (1994)

[59] Max-Planck-Institut für Eisenforschung und der Werkstoffausschuss des Vereins Deutscher Eisenhüttenleute *Atlas zur Wärmebehandlung der Stähle* (1961)

[60] W.G. Mazja, S.A. Nasarow, B.A. Plamenewski *Asymptotische Theorie elliptischer Randwertaufgaben in singulär gestörten Gebieten, volume 1: Störungen isolierter Randsingularitäten*, Mathematische Lehrbücher und Monographien, 2. Abteilung: Mathematische Monographien, 82, Akademie-Verlag, Berlin, (1991)

[61] I. Müller *Thermodynamics*, Pitman Publishing (1985)

[62] L. Panizzi *On a mathematical model for case hardening of steel*, PhD thesis, Scuola Normale Superiore in Pisa and Technische Universität Berlin (2009)

[63] H. Parisch *Festkörperkontinuumsmechnanik – Von den Grundgleichungen zur Lösung mit Finiten Elementen*, Vieweg+Teubner (2003)

[64] H. Petryk *Thermodynamic Conditions for Stability in Materials with Rate-Independent Dissipation*, Philosophical Transactions: Mathematical, Physical and Engineering Sciences 363, No. 1836, Thermodynamics in solids mechanics, pp. 2479–2515 (2005)

[65] W. Piersig *Die sieben Metalle der Antike: Gold, Silber, Kupfer, Zinn, Blei, Eisen, Quecksilber*, Beiträge zur Technikgeschichte (5), Grin Verlag (2009)

[66] R. Qin, H. Bhadeshia *Phase field method*, Materials Science and Technology 26 (2010)

[67] R. Roubíček *Nonlinear Partial Differential Equations with Applications*, Birkhäuser (2005)

[68] A. Schmidt *A Multi-mesh Finite Element Method for 3D Phase Field Simulations*, Free boundary problems: theory and applications, P. Colli, C. Verdi, A. Visintin eds. (2003)

[69] A. Schmidt, K.G. Siebert *Design of Adaptive Finite Element Software. The Finite Element Toolbox ALBERTA (Lecture Notes)*, Springer Berlin (2004)

[70] A. Schmidt, M. Wolff, M. Böhm *Numerische Untersuchungen für ein Modell des Materialverhaltens mit Umwandlungsplastizität und Phasenumwandlungen beim Stahl 100Cr6 (Teil 1)*, Universität Bremen, Berichte aus der Technomathematik, Report 03-13 (2003)

[71] J.R. Shewchuk *Triangle: Engineering a 2D quality mesh generator and Delaunay triangulator*, Applied Computational Geometry: Towards Geometric Engineering (M. C. Lin, D. Manocha, eds.), Lecture Notes in Computer Science 1148, pp. 203-222, Springer Berlin (1996)

[72] M. Seibold *Optimale Steuerung von Phasenübergängen in Stahl*, diploma thesis, University of Karlsruhe (2004)

[73] C. G. Simader *On Dirichlet's Boundary Value Problems*, Lecture Notes in Mathematics 268, Springer Berlin (1972)

[74] H. Si *TetGen, a quality tetrahedral mesh generator and three-dimensional delaunay triangulator, v1.3, User"s manual*, WIAS Technical Report No. 9 (2004)

[75] J. Simon *Compact sets in the space $L^p(0,T;B)$*, Annali di Mat. Pura Applic. 146, pp. 65–96 (1987)

[76] J. Sokolowski, J. Zolesio *Introduction to Shape Optimization – Shape Sensitivity Analysis*, Springer Berlin (1992)

[77] B. Suhr *Simulation of steel quenching with interaction of classical plasticity and TRIP – numerical methods and model comparison*, PhD thesis, Logos Berlin (2010)

[78] F. Tröltzsch *Optimale Steuerung partieller Differentialgleichungen – Theorie, Verfahren und Anwendungen*, Vieweg, Wiesbaden (2005)

[79] C. Truesdell, W. Noll *The Non-Linear Field Theories of Mechanics*, Springer Berlin (2004)

[80] T. Valent *Boundary Value Problems of Finite Elasticity. Local Theorems on Existence, Uniqueness, and Analytic Dependence on Data*, Springer Tracts in Natural Philosophy, 31, Springer New York (1988)

[81] C. Verdi, A. Visintin *A mathematical model of the austenite-pearlite transformation in plain steel based on the Scheil's additivity rule*, Acta Metall. 35, pp. 2711-2717 (1987)

[82] Verein Deutscher Eisenhüttenleute *Steel, a Handbook for Materials Research and Engineering*, Vol. 1-2, Springer Berlin (1993)

[83] A. Visintin *Mathematical models of solid-solid phase transitions in steel*, IMA J. Appl. Math. 39, pp. 143-157 (1987)

[84] M. Wolff *Zur Modellierung des Materialverhaltens von Stahl unter Berücksichtigung von Phasenumwandlungen und Umwandlungsplastizität*, Habilitationsschrift, Universität Bremen (2008)

[85] M. Wolff, M. Böhm *On the Singularity of the Leblond Model for TRIP and Its Influence on Numerical Calculations*, Journal of Materials Engineering and Performance 14, pp. 119-122, Springer New York (2005)

[86] M. Wolff, M. Böhm *Transformation-induced plasticity in steel – general modelling, analysis and parameter identification*, Universität Bremen, Berichte aus der Technomathematik, Report 06-02 (2006)

[87] M. Wolff, M. Böhm, S. Dashkovskiy *Volumenanteile versus Massenanteile – der Dilatometerversuch aus der Sicht der Kontinuumsmechanik*, Universität Bremen, Berichte aus der Technomathematik, Report 03-01 (2003)

[88] M. Wolff, M. Böhm, D. Helm *Material behaviour of steel – Modeling of complex phenomena and thermodynamic consistency*, International Journal of Plasticity 24, pp. 746-774 (2008)

[89] M. Wolff, M. Böhm, G. Löwisch, A. Schmidt *Modelling and testing of transformation-induced plasticity and stress-dependent phase transformations in steel via simple experiments*, Comput. Materials Sci. 32, pp. 604-610 (2005)

[90] M. Wolff, S. Boettcher, M. Böhm *Phase transformations in steel in the multi-phase case – general modelling and parameter identification*, Universität Bremen, Berichte aus der Technomathematik, Report 07-02 (2007)

[91] M. Wolff, S. Boettcher, M. Böhm, I. Loresch *Vergleichende Bewertung von makroskopischen Modellen für die austenitisch-perlitische Phasenumwandlung im Stahl 100Cr6*, Universität Bremen, Berichte aus der Technomathematik, Report 07-03 (2007)

[92] M. Wolff, F. Frerichs, N. Lysenko *Bewerten von Modellen der Martensitbildung bei nichtmonotoner Abkühlung für den Stahl 100Cr6*, Universität Bremen, Berichte aus der Technomathematik, Report 07-01 (2007)

[93] E. Zeidler *Nonlinear Functional Analysis and its Applications I, Fixed Point Theorems*, Springer Berlin (1986)

[94] E. Zeidler *Nonlinear Functional Analysis and its Applications II/b, Nonlinear Monotone Operators*, Springer Berlin (1989)